



**Politecnico
di Torino**

POLITECNICO DI TORINO

Master of Science in Biomedical Engineering

Development of an organ-on-chip model to mimic exocrine pancreas

Supervisors

Prof. Gianluca Ciardelli

Prof. Matteo Cocuzza

Prof. Chiara Tonda Turo

Dr. Simone Luigi Marasso

Candidate

Matilde Aronne 278513

A.Y. 2021/2022

July 2022

Table of contents

Abstract	3
1 Introduction	5
1.1 <i>Pancreatic tissue's overview</i>	5
1.1.1 Exocrine pancreas	6
1.2 <i>Pancreatic cancer: PDAC</i>	7
1.2.1 PDAC tumorigenesis	11
1.2.2 Precursor lesions	11
1.2.3 Genetic alterations	13
1.2.4 Tumour microenvironment	15
1.2.5 Pancreatic stellate cells	16
1.3 <i>In vitro and in vivo models: an overview</i>	20
1.4 <i>In vivo models</i>	21
1.4.1 Animal models	21
1.5 <i>In vitro models</i>	22
1.5.1 2D culture	24
1.5.2 3D culture	25
1.6 <i>Organ-on-chip technology: a brief description</i>	31
1.6.1 Fabrication techniques	31
2 Materials and methods	35
2.1 <i>Microfluidic devices</i>	35
2.1.1 Materials: PDMS	35
2.1.2 Bottom layer design	36
2.1.3 Bottom layer mould realization method: mask realization	38
2.1.4 Bottom layer mould realization method: SU-8 lithography	39
2.1.5 Top layer design	44
2.1.6 Reservoir design	44
2.1.7 Top layer and reservoir mould realization method: 3D printing	45
2.1.8 Bottom, top, reservoir layers realization method: replica molding	46
2.1.9 Microfluidic device assembly technique: plasma oxygen	47
2.1.10 Microfluidic device assembly technique: interlayer bonding	48
2.2 <i>Microfluidic devices characterization</i>	48
2.2.1 Digital microscope analysis	48

2.2.2	Microfluidic test	49
2.2.3	Permeability test	49
2.3	<i>Membrane</i>	50
2.3.1	Materials: PCL	50
2.3.2	Materials: gelatin	51
2.3.3	PCL/gelatin solution	52
2.3.4	Membrane realization methods: electrospinning	52
2.4	<i>Membrane characterization</i>	54
2.4.1	Scanning Electron Microscope (SEM)	54
2.5	<i>Cellular components</i>	55
2.5.1	Material: collagen	55
2.5.2	Human Foreskin Fibroblasts cells	56
2.5.3	Human Pancreatic Duct Epithelial cells	58
2.5.4	Assembled device	60
2.5.5	Fluorescence imaging	61
2.5.6	Live/Dead (L/D) assay for cell viability	62
3	Results and discussion	63
3.1	<i>Microfluidic devices characterization</i>	63
3.1.1	Digital microscope analysis	63
3.1.2	Microfluidic test	67
3.1.3	Permeability test	68
3.2	<i>Membrane characterization</i>	70
3.2.1	Scanning Electron Microscope (SEM)	70
3.3	<i>Cellular components</i>	70
3.3.1	Fluorescence imaging	70
3.3.2	Live/Dead (L/D) assay for cell viability	74
4	Conclusion and future perspectives	76
5	Bibliography	78
6	Addendum	I
6.1	<i>CAD bottom layer</i>	<i>I</i>
6.2	<i>SU-8 soft lithographic process optimization</i>	<i>IV</i>
6.3	<i>Bottom layer PDMS master</i>	<i>VII</i>
6.4	<i>Kapton</i>	<i>VIII</i>

Abstract

Pancreatic ductal adenocarcinoma (PDAC) is the fourth major leading causes of cancer-related deaths worldwide; it is the more lethal type of pancreatic cancer because of PDAC's high resistance to treatments (due also to tumour microenvironment), late diagnosis, metastasis fast diffusion. To study tumour microenvironment, its influence on therapies and tumoral growth, to develop safe and effective drugs, to understand cellular components crosstalk in the tumor, in vitro models result helpful and powerful tools.

In this thesis work, organ-on-chip model has been implemented to recreate the pancreatic acino-ductal unit in vitro; the PDMS microfluidic device realized presents three-layer structure: a reservoir, for the culture media, a top layer, used for human pancreatic duct epithelial (HPDE) cells seeding, and a bottom layer, for human foreskin fibroblast (HFF-1) cells seeding. The PDMS layers have been realized using replica molding technique, and a mould has been designed for each layer; the production method used has been different for each mould: for bottom layer, soft lithographic process, using SU-8 resist, has been chosen, while for top and reservoir layer, 3D printing technique has been used. Bottom and top layers have been separated through an electrospun microporous membrane, made by polycaprolactone and gelatin (PCL/Gel), that divide the bottom central channel, loaded with collagen hydrogel that mimics the stromal component, and the top channel, where seeded cells reproduce the tumor cellular component.

Every microfluidic device component has been characterized through several tests: for PDMS replicas morphological characterization, optical microscopy has been performed, while for membrane morphological characterization Field Emission Scanning Electron Microscopy (FESEM) has been chosen; for studying membrane diffusion, permeability test has been performed using fluorescein isothiocyanate-dextran (FICT-dextran) and phosphate buffered saline (PBS), then the read values have been analysed using Excel. Cell proliferation and vitality on the microfluidic chip have been tested using different cell lines and different culture conditions: HPDE cells have been seeded on the top layer alone, and the vitality has been tested using cellular staining and fluorescence microscopy, while HFF-1 cells have been seeded on

the bottom layer alone, suspending them into the collagen hydrogel, and vitality test have been using live/dead assay and cellular staining and fluorescence microscopy. The assembled device has been tested using HFF-1 and HPDE cells co-culture, and the vitality has been evaluated using a cellular dye, for HFF-1, and cellular staining and fluorescence microscopy, for HPDE. Also, optical microscopy has been used to observe cells before and after seeding.

Results suggest that HFF-1 cells are vital into the collagen hydrogel for the whole culture period, and that they present the characteristic active elongated shape; the HPDE cells can adhere on the PCL/Gel membrane, and they can also proliferate on it. The electrospun membrane presents absence of defects, and the morphology results unaltered by the usage of interlayer bonding for its positioning. The membrane shows a high diffusion of molecules, that takes place in the first few minutes.

1 Introduction

1.1 Pancreatic tissue's overview

Pancreas is a glandular organ, located in the abdomen, that takes part to different processes of digestive system and others. It can accomplish all these functions thanks to its anatomy as it is composed by an exocrine part and an endocrine part. The position of pancreas, in the left abdomen and behind the stomach (fig. 1), makes difficult to diagnose problems affecting this organ.

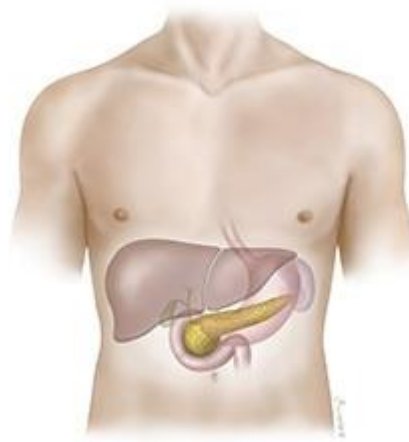


Figure 1 Position of pancreas into abdomen[1]

Pancreas is a parenchymal organ, that appears flat shaped. It is divided into three regions (fig. 2):

- the head, positioned in the centre of abdomen[1];
- the body, that is the central part;
- the tail, that is the thinner part.

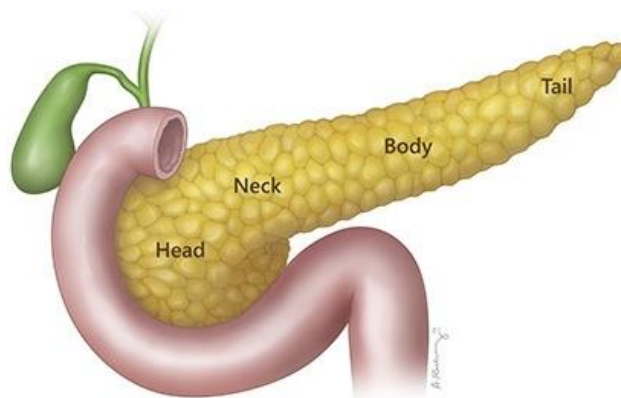


Figure 2 Parts of pancreas[1]

Pancreas is well irrigated by many of the major blood vessels, like the superior mesenteric artery, the superior mesenteric vein, the portal vein, and the celiac axis. A huge part of pancreas, around 95%, is exocrine tissue producing enzymes that take part to digestive processes. The 5% parts is the endocrine tissue, that produces and releases hormones.

1.1.1 Exocrine pancreas

Exocrine pancreas is responsible for the enzymes production, in particular trypsin and chymotrypsin for proteins digestion, amylase for carbohydrates digestion and lipase for fats. These enzymes are released from the pancreatic duct into the bile duct, which spills this digestive juice into duodenum.

The structure of exocrine pancreas is the reason of exocrine gland behaviour: the functional unit is made by an acinus and a ductal system.

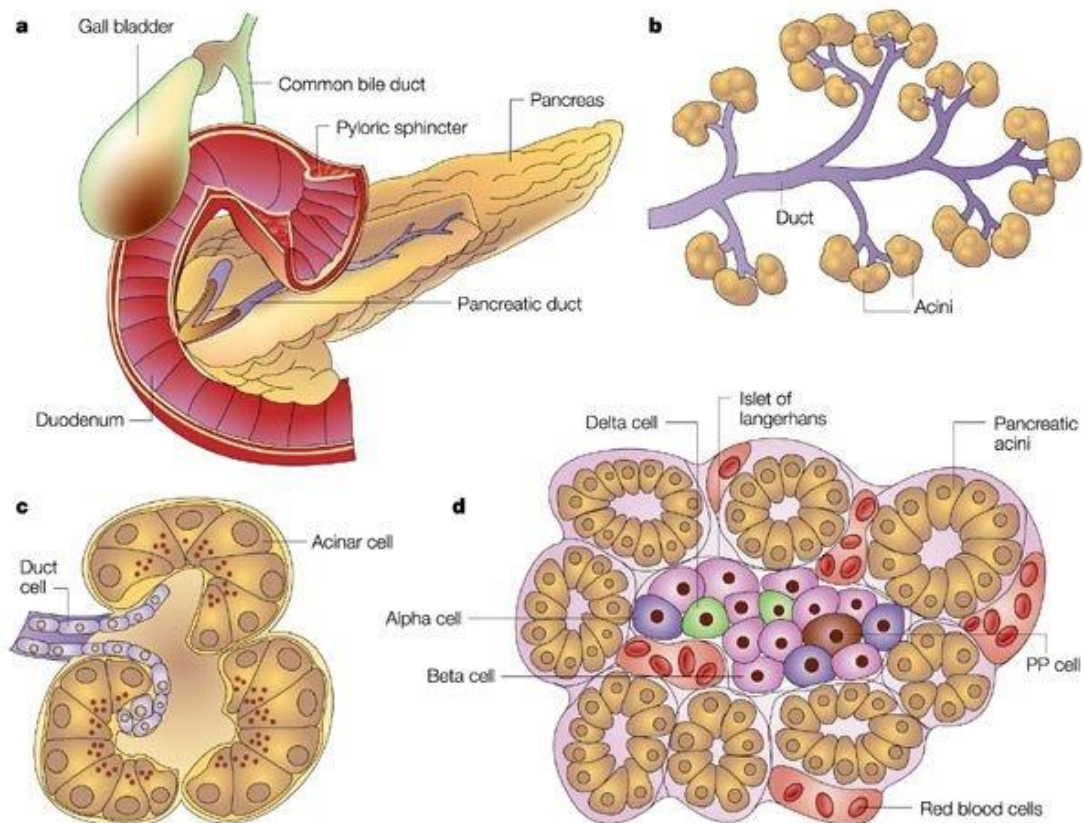


Figure 3 Pancreas position (A), pancreatic acino-ducts structures (B), acinus organization (C), exocrine pancreatic cells (D)[2]

The acinus is a spherical or tubular cluster of cells, the acinar cells, specialized into synthesis, storage and secretion of digestive enzymes[3]. Acinar cells are parenchymal cells, that present a pyramidal geometry. They have receptors for

hormones and neurotransmitters on their basolateral membrane, which regulate enzymes secretion. The acinar cells basal region presents nucleus and a large amount of rough endoplasmic reticulum, because it is the protein synthesis site[3], and it is also responsible for exocrine secretions, together with Golgi's apparatus. The apical part of acinus is where enzymes are stored; on the apical surface, acinar cells expose microvilli, involved in exocytosis of stored granuli. The acinar lumen is connected to the ducts end part, developing the so called acino-ductal unit, showed in the fig. 3C. It is possible to observe two different types of intercellular connection between acinar cells: the tight and gap junctions. Tight junctions are established in the apical regions of acinar cells, in order to obtain a sort of barrier that prevent passage of large molecules, like enzymes. Gap junctions, instead, allow small molecules passage, providing the chemical and electrical communication between cells[1].

The ductal system starts from acinus lumen and finishes into duodenum; these ducts are composed by epithelial cells, cuboidal or pyramidal shaped, that are responsible for ions transport. To guarantee this mechanism of transport, ductal cells have a great number of mitochondria, that produce energy for ions exchange.

The meeting point for acinus and ductal system is characterised by the presence of another cell type, the centroacinar cells, that have ductal cells features but, at the same time, they are presumably progenitors for many type of pancreatic cells[1].

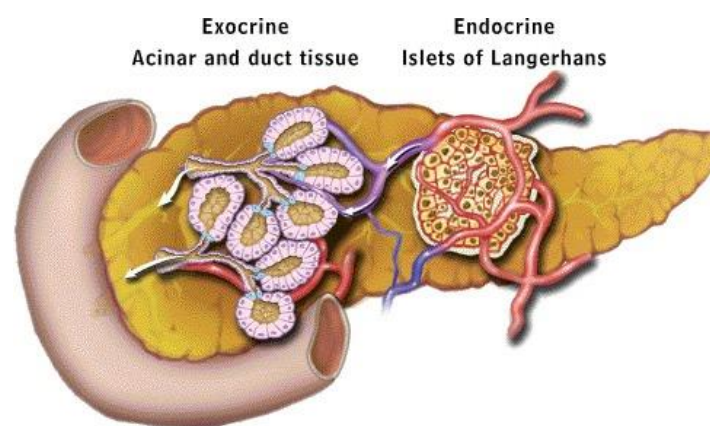


Figure 4 Endocrine and exocrine pancreas structures[3]

1.2 Pancreatic cancer: PDAC

Pancreatic ductal adenocarcinoma (PDAC) is becoming one of the major leading causes of cancer-related deaths worldwide, currently representing the fourth one.

PDAC is the most common type of pancreatic cancer and the more lethal too, in fact, the averaged 5-years survival rate is less than 10%[4]. This poor outcome is related to late diagnosis, metastasis fast diffusion, PDAC's high resistance to treatments[5]. The PDAC incidence rate changes between regions, for examples there is a higher incidence rate in developed countries, in particular Western world, while in undeveloped ones the incidence is lower. There is also an enormous difference in age of symptoms appearance: it is higher in Europe and North America; it is lower in Africa and South-Central Asia[6].

The big gap in incidence rate between world regions seems to suggest that environmental factors are involved into cancer onset as risk factor. There are also other risk factors to consider, that can be divided into two categories.

Non-modifiable risk factors

- Age, which means acquired genetic defects arisen over years. They are the reason why the median age of onset is 71 years, with the 75% of patients diagnosed between 55 and 84 years old[7].
- Sex, because the incidence of PDAC is higher in males than females, with 5.5 males averaged incidence rate despite 4.0 females averaged incidence rate. The gap appears bigger in developed countries, as in fig. 5[6].
- A familial PDAC, because people with 1 affected first-degree relatives (FDR) at least have 6% of possibilities to develop the pathology. The percentage raises if there are 2 or 3 (or even more) FDR: it becomes 10% for 2 FDR and 40% for 3 FDR[7].
- Diabetes, in particular type one but similar for type two, influences the risk of pancreatic cancer, that becomes twice for diabetic patients. It is also known that diabetes is a consequence of PDAC, so it gets foothold the interest for HbA1c as a biomarker for PDAC early detection[6].

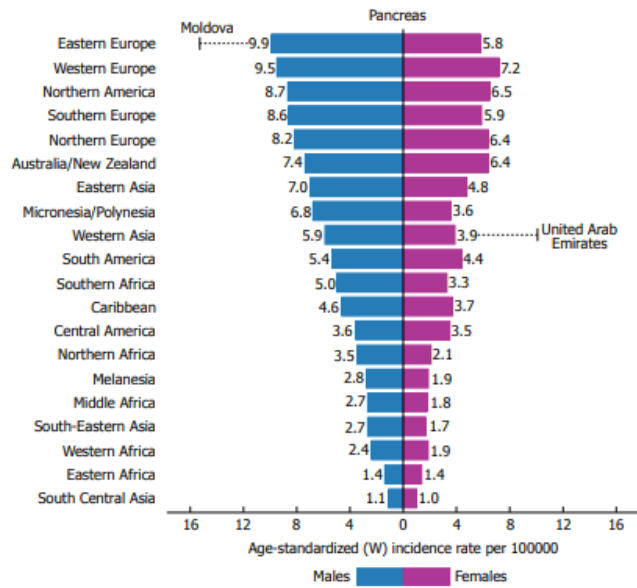


Figure 5 Average distribution of PDAC incidence worldwide for both sex[6]

Modifiable risk factors

- Smoking is considered the best validated and depicted environmental risk factor, so active smokers run a higher relative risk (1.74 times more), that is also directly influenced by the number of daily smoked cigarettes. The risk decreased when smokers quit smoking, and it returns to base level after 20 years[7].
- Alcohol large consumption seems to be related to PDAC development, it has been observed an increased risk in patients who consumed, daily, more than 30g of alcohol; those people show a 15% increased risk of PDAC development. Furthermore, alcohol abuse causes chronic pancreatitis, a well-known PDAC risk factor[6].
- Obesity is another major risk factor for PDAC development, with no distinction between males and females. It is linked to dietary factors, other important modifiable PDAC risk factor. In the Table 1 a summary of evidence about obesity and dietary factors as risk factors[6].

Table 1 Obesity and dietary PDAC risk factors[6]

		DECREASES RISK	INCREASES RISK
STRONG EVIDENCE	Convincing		Body fatness
	Probable		Adult attained height
LIMITED EVIDENCE	Limited – suggestive		Red meat, processed meat; alcoholic drinks (heavier drinking); foods and beverages containing fructose; foods containing saturated fatty acids
	Limited – no conclusion	Physical activity; fruits; vegetables; folate; fish; eggs; tea; soft drinks; coffee; carbohydrates; sucrose; glycaemic index; glycaemic load; total fat; monounsaturated fat; polyunsaturated fats; dietary cholesterol; vitamin C; and multivitamin/mineral supplements	

Early detection strategies do not exist, even for high-risk patients, but it is important to turn to traditional screening methods, like whole-body computed tomography, for healthy patients; endoscopic ultrasonography or magnetic resonance imaging can be useful for high-risk patients, and this type of surveillance should be annual for them. This mentioned early detection results fundamental for the outcomes of this disease, because even “early” disease patients can hide micrometastatic diseases that can become relevant few years later the first treatments.

As mentioned above, the survival rate for PDAC patients after 5 year is extremely low, under 10%, mainly because of tumour stage at the diagnosis’ time. Indeed, only 20% of patients present a surgically resectable cancer, and the 5-years survival rate is 27% for them[6].

It seems to be clear that is necessary to understand which early detection is required and how to achieve this objective. The PDAC pathogenesis can help in the understanding of early detection definition.

1.2.1 PDAC tumorigenesis

90% of all pancreatic carcinomas are pancreatic adenocarcinomas, and 60%-70% of them start in the head of pancreas, while the remaining 30% of PDAC is equally divided between body and tail as point of origin. This disease, that originates in ductal epithelium, becomes an invasive cancer briefly and it shows the cited therapeutic resistance[8].

The PDAC strength lies in its morphological variants and in a series of stepwise mutations of mucosa, that make PDAC invasive. A significant contribution to PDAC resistance is recognised to tumour microenvironment, as described below.

Tumorigenic phases can be summarized as described in the follow flow chart (fig. 6):

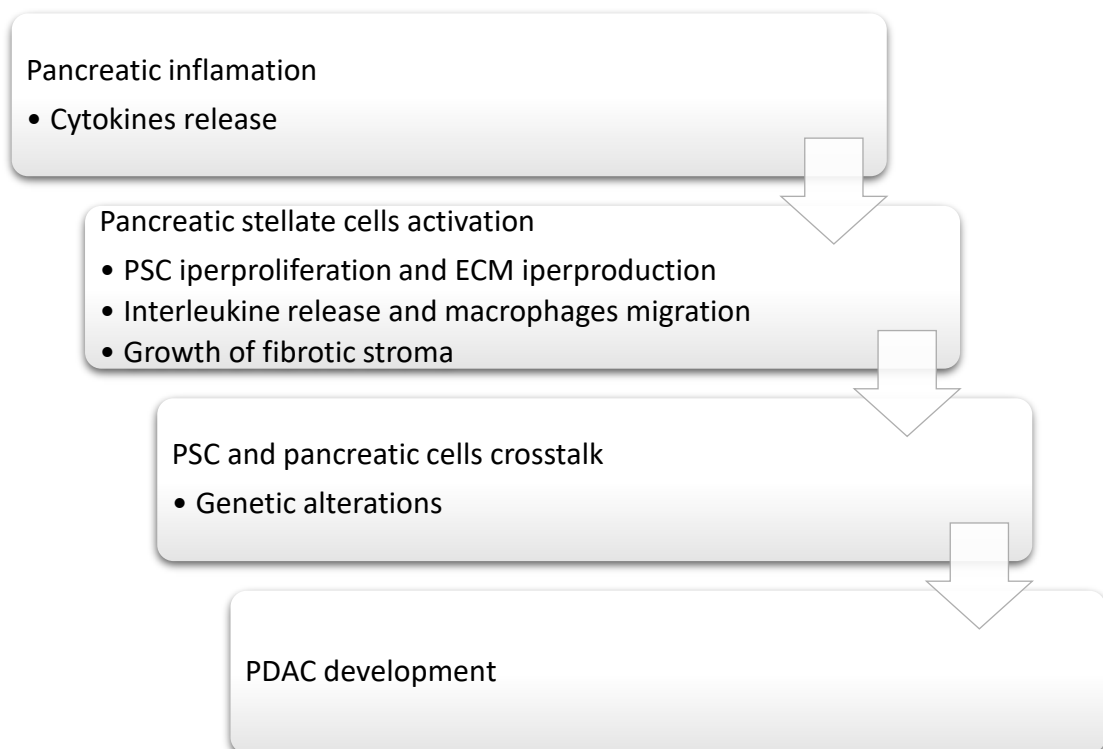


Figure 6 Flow chart of PDAC tumorigenesis

1.2.2 Precursor lesions

Nowadays, three precursor lesions have been described as characteristic of PDAC development: pancreatic intraepithelial neoplasia (PanIN), intraductal papillary mucinous neoplasms (IPMN) and mucinous cystic neoplasms (MCN).

PanIN

Pancreatic intraepithelial neoplasia is a non-invasive microscopic lesion (less than 0.5 cm), which appears in pancreatic ducts. It seems to provoke localised pancreatitis, that cause epithelial injuries and, during their repair cycle, the spread of neoplasia. PanIN's lesions can be classified for their progressive morphological changes in low grade PanIN, that includes grades 1a/b and 2, (fig. 7, A and B) and high grade PanIN, that includes grade 3 (fig. 7 C).

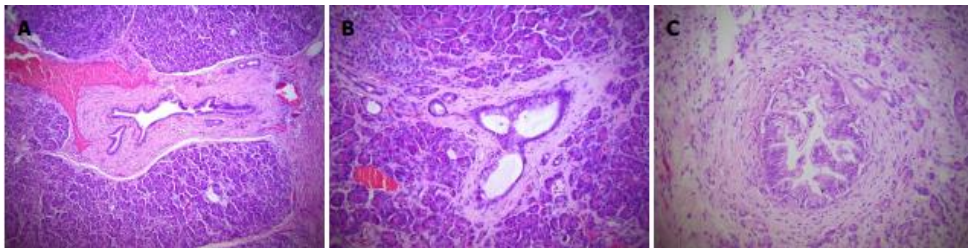


Figure 7 PanIN lesions' grades: A) low grade PanIN, B) grade 2 PanIN, C) high grade PanIN[6]

Scientists have estimated that a PanIN 3 will take 11.3 years for men and 12.3 years for women to transform into pancreatic adenocarcinoma[6], so that period can be a possible screening window to catch an invasive malignancy.

IPMN

IPMNs are other well established precursor lesions for pancreatic cancer. IPMNs form a group of pathology that arise from the main pancreatic duct or one of the lateral branches. This distinction is important because around 70% of main duct IPMNs can be resected, while only the 25% of side branch lesions can be resected[6].

MCN

Mucinous cyst neoplasms represent the third group of premalignant lesions. They represent the 25% of pancreatic cysts that are removed, and a high percentage of them, around 17.5%, show malignancy, especially in those of them resected by women[6]. Only 1% of pancreatic cysts can be identified with CT, and there are not clear guidelines on how to manage these potential premalignant lesions.

1.2.3 Genetic alterations

As mentioned above, PanIN is the most common PDAC precursor lesion, which shows genetic abnormalities typical of pancreatic adenocarcinomas. In low grade PanIN, K-RAS oncogene is one of these common mutations, together with telomeres shortening, two changes at the base of invasive malignancy. In higher grade PanIN, there are mutations in p16, CDKN27, p53 and SMAD4, supported by an increase in the rate of K-RAS mutations. Recurrent mutated genes have been analysed, 4 subgroups have been identified with unique genomic signature, histopathological findings, and prognosis: squamous, pancreatic progenitor, immunogenic and aberrantly differentiated endocrine exocrine[6].

The squamous type is associated with adenosquamous pancreatic adenocarcinoma, and it leads to a poor prognosis.

The pancreatic progenitor group shows transcription factors for determining pancreatic cell lineage.

Immunogenic refers to tumours with a significant immune infiltration.

Aberrantly differentiated endocrine exocrine tumours are all those tumours that involve acinar cell.

It is now clear that, ideally, PDAC should be diagnosed and treated maximum at the PanIN 3 stage, whose incidence is similar to adenocarcinoma; PanIN 3 stage can be the best moment to maximize the effective treatments and minimize unnecessary therapies. However, current technologies offer little success in early detection of this type of lesion.

As arisen above, pancreatic lesions are challenging to detect, especially if they are under 2 cm in dimension, but invasive injury are often smaller than 2 cm, so they result only in alteration in ducts diameter[7].

Treatments of PDAC lesions are based on the type and extension of diseases, for example resection is chosen for patients with local disease, in stage 1 and/or 2, while chemotherapy is chosen for patients with locally advanced disease.

Genetic alterations, jointly with epigenetic one, give origin to cancer heterogeneity, and several studies agree that K-RAS alteration is the most influential genetic modification, that causes other alterations that limit tumour suppressors genes. Together with these common features, there are sporadic mutations. These are the

80% of abnormalities occurred during PDAC development, as showed in fig. 8[9], and they can change from one patient to another, contributing to the increase of the heterogeneity level of biological alterations in any patient[10].

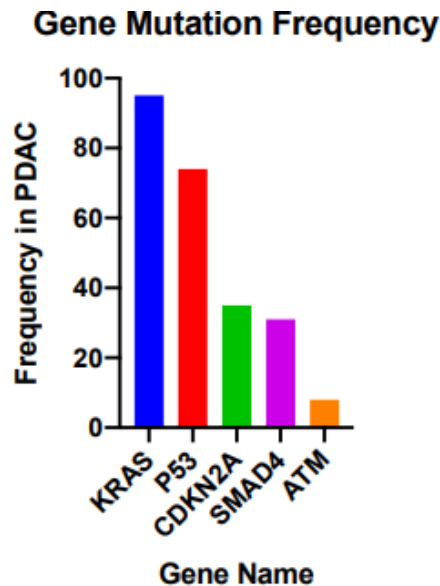


Figure 8 PDAC genetic alterations' frequency[9]

However, genetic instability is a consolidate fingerprint of cancer cells, and the responsible for this genetic variability that makes difficult modelling cancer features with one *in vitro* model. Because of this effort, genetic studies are hard to realize, and all genetic features are not so far well known. In present day, there are information about common genetic alterations only, like K-RAS modification, which occurs in around 94% of tumours.

Punctual mutation in K-RAS provokes its activation; it operates as a molecular switch that regulates cell proliferation, differentiation, apoptosis, and cell signalling. K-RAS mutation itself is not enough for carcinogenesis, but other genes activation, like Raf-1, Rac, Rho or PI3K are concomitant[9]. Surely K-RAS mutation allows gene to be independent from external stimuli and regulation, and to stimulate proliferation of stroma. Next to K-RAS mutated PDAC patients, there is a little part of PDAC patients who do not show this genetic alteration, but with a progression of the pathology not completely understood[11].

1.2.4 Tumour microenvironment

As mentioned before, tumour microenvironment (TME) has a substantial impact on treatments outcomes, so it is necessary to shed light on TME.

Tumour microenvironment is composed by a fibrotic stroma, several non-cellular components (around the 70%-90% of tumour mass), like hyaluronic acid, and cellular components (the 10-30% of tumour mass), like cancer-associated fibroblasts (CAF), pancreatic stellate cells (PSC), immune cells and muscle cells[3].

This fibrotic stroma is mainly synthesised by CAFs and PSCs, and it is composed by high amount of ECM proteins, like collagen, fibronectin and periostin, that show an autocrine loop which promotes ECM synthesis and cell growth under hypoxia and starvation, also maintaining PSCs activation[12]. This involves vessels collapse and reduction, disorganized vessel networks and aberrations[5]. The efficient vessels lack is the reason of hypoxia in TME and poor drug delivery in tumour. This hypoxic microenvironment stimulates stroma deposition by tumour associated fibroblasts, supports increased PSCs migration (thank to 2-oxoglutarate 5-dioxygenase 2 production) and endothelial cells proliferation and migration[12].

CAFs are stromal cells that contribute to also regulate cytokines, growth factors, immune infiltration levels into TME. CAFs have a tumour supportive role into PDAC, because they enhance proliferative ability of cancer cells, and they recruit also immune cells[13].

Fibrosis acts as a rigid barrier for drug delivery, because common antitumoral medicines cannot cross the thick and protein rich PDAC stroma, and it provokes an increase in tumour pressure. This elevated pressure causes a negative regulation in substances diffusion[4].

In the heterogeneous mix of cells which populate PDAC's TME there are also immune cells, that interact with microenvironment and contribute to alter immunotherapies effect. These cells are regulatory T cells (Treg), myeloid-derived suppressor cells (MDSC) and macrophages; T cells tend to accumulate in TME, so they lose their immune skills and intensify immunosuppressive TME's feature. T cells are not able anymore to recognise cancer antigens exposed by cancer cells, because there is a degradation of major histocompatibility complex -I (MHC-I). The degree of T cell infiltration is used to classify tumours in "hot" and "cold": hot tumours present a

variation in CD8+ and Treg cells when attacked by immunotherapeutic drugs, while cold tumours have a 20%-40% response to inhibitors of immune checkpoints[4], especially in early stages.

In fibrotic ECM, a variety of cellular molecules can be also observed, like osteopontin and osteonectin, expressed in TME of many cancer types. All these stromal components contribute to cancer cells radicalisation and protection[8].

1.2.5 Pancreatic stellate cells

Pancreatic stellate cells are star-shaped cells that surround the acino-ductal structures. They are specialized myofibroblasts that represent the 4% of the total cellular population[8]. Their function is to store vitamin A when they are in a quiescent state, throughout lipid droplets into cytoplasm, and to direct the formation of epithelial structures[3]. These quiescent PSCs contribute also to maintain the physiological ECM turnover thanks to the expression of matrix metalloproteinases (MMPs) and tissue inhibitors of metalloproteinases (TIMPs). Additionally, PSCs help ductal and vascular regulation, but also exocrine function because they release acetylcholine, an intermediate for pancreatic exocrine secretion that are mediated by cholecystokinin[12]. When the tissue is exposed to an injury or an inflammation, PSCs are activated, changing their morphology and their function; they become spindle shaped, and they dysregulate the ECM production. The activation process is influenced by autocrine and paracrine factor, as shown in the fig. 9.

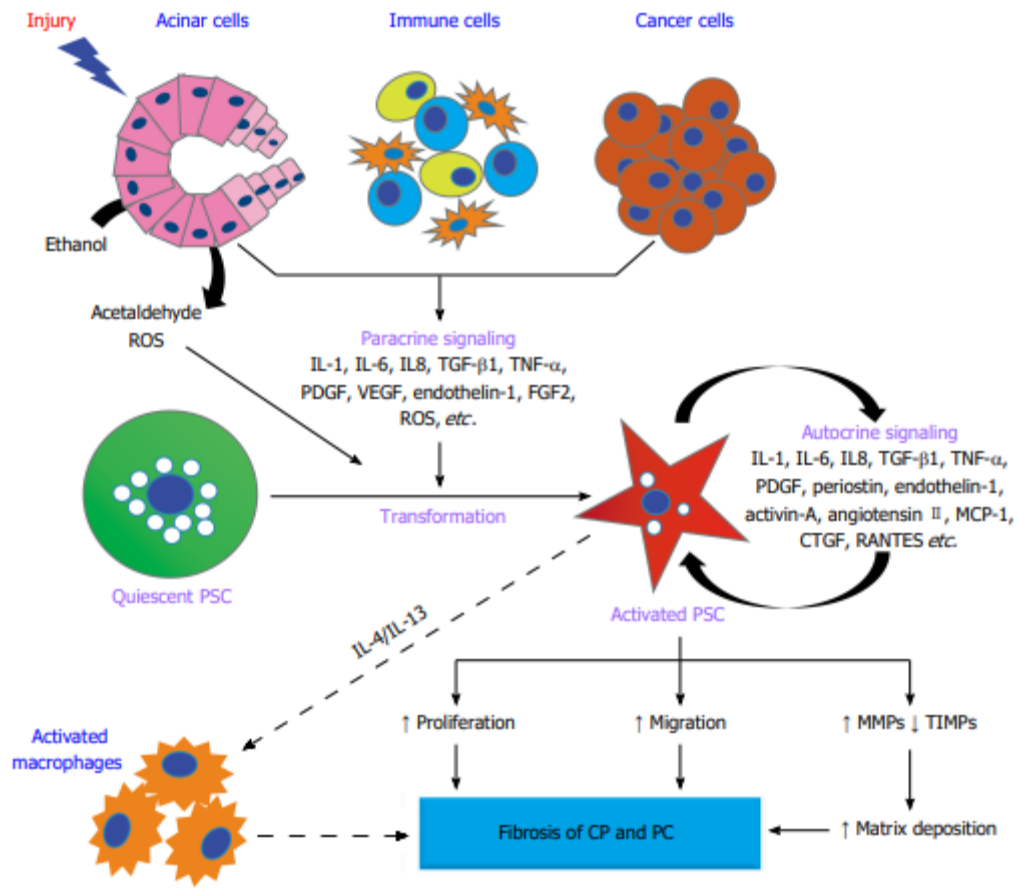


Figure 9 Activation process of PSCs[12]

Characteristic features of activated PSCs are the lack of lipid droplets, the secretion of α -smooth muscle actin (α -SMA), a mark of the quiescent PSCs transdifferentiation to the active phenotype[12]. Moreover, there is an excessive ECM deposition, with the overproduction of protein like collagen type I, fibronectin, etc., that takes at excessive contraction and fibrotic stroma previously described[8]. Activated PSCs secrete also proinflammatory cytokines and growth factors, which influence the cancer rate of growth and chemotherapy resistance[3]; cytokines also promote self-proliferation, migration and fibrogenesis[12].

An unsolved question is the fate of activated PSCs, described into fig. 10. Different explanations exist today, one is that inflammation sustains PSC activation, carrying to fibrosis; another one is that PSCs go to apoptosis or revert to quiescence stopping the inflammation.

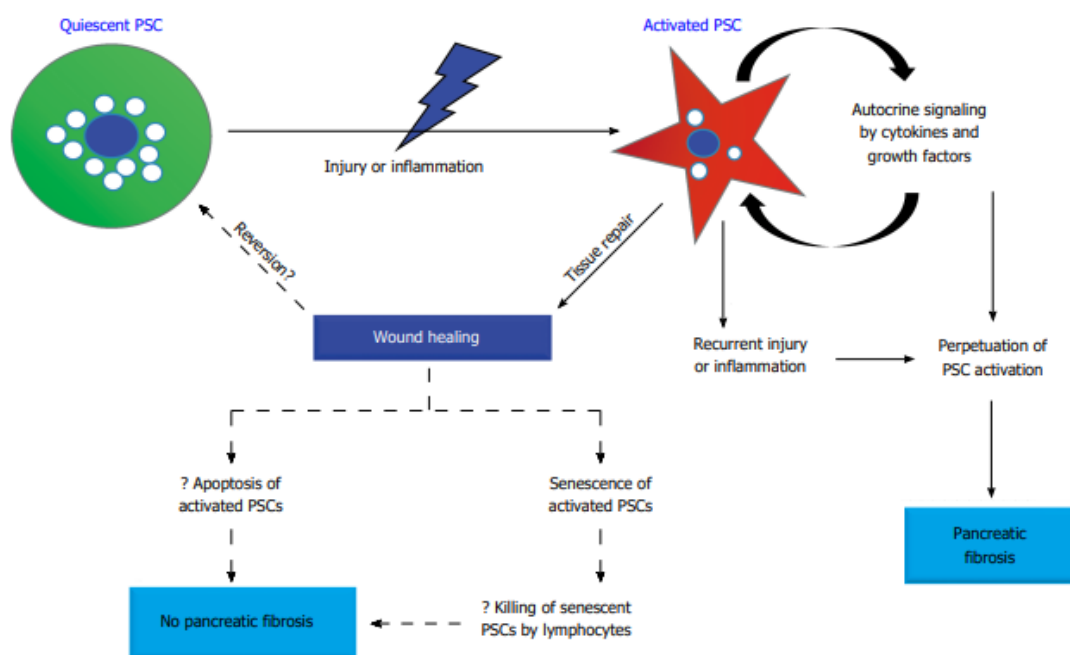


Figure 10 Active PSCs fate[12]

Another essential information about PSCs is their role in metastasis and invasion of PDAC, that seems driven by Galectin-3, thrombospondin-2, stromal cell derived factor and nerve growth factor (NGF)[12] secreted by active stellate cells. PSCs can facilitate tumour growth and metastasis after a brief exposure to cancer cells, because they acquire a tumour inductive property[12].

It is clear that pancreatic tumour models should present PSCs together with cancer cells, in order to completely reproduce interactions between cells which occur in situ.

Pancreatic stellate cells-PDAC crosstalk

As mentioned in the paragraph above, PSCs influence pancreatic cancer cells behaviour.

A large part of PDAC volume (50%-80%) is composed by the fibrotic stroma, produced by PSCs and pancreatic fibroblasts. Studies have revealed the existence of two types of interaction between stromal components and cancer cells. As explained before, stroma is mainly composed by ECM proteins, like collagen type I, non-ECM proteins, like growth factors, immune cells, and endothelial cells. All these components can mediate PSCs and cancer cells crosstalk, but also influence treatments outcomes.

Other stromal components that affect PDAC-PSCs crosstalk are fibroblast growth factor (FGF) and fibroblast growth factor receptor (FGFR), that induce the development of invasive phenotype in cancer cells. There is also the galectin family member of β -galactoside binding proteins, expressed by pancreatic cancer cells, that promotes proliferation of PDAC cells and PSCs.

Fibrotic stroma results a protection for tumour, permitting its development. This interaction seems to be dynamic and stage dependent, resulting in cancer growth, while the interaction between PSCs and stromal cells helps the immune invasion, metastasis, hypoxia, and therapeutic resistance, as already seen.

The PDAC-PSCs interaction is bipolar, with the acceleration of proliferation and the inhibition of apoptosis. It also observed the so called epithelial mesenchymal transition (EMT), associated with the PSCs capability to trigger pancreatic cancer cells metastasis and consequent cells migration[12]. PSCs are responsible for PDAC relapse, because they regulate cancer stem cell niches genesis.

Pancreatic cancer cells release some factors like PDGF, trefoil factor 1 and COX-2, which stimulate PSC proliferation, and that are expressed also in PanINs and activated PSCs[12].

These considerations are summarized in the fig. 11 below.

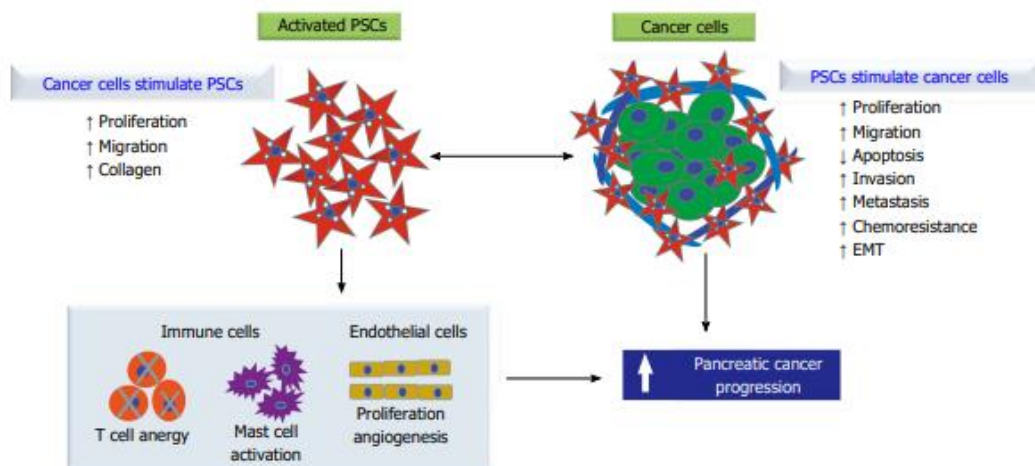
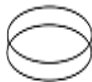
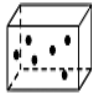




Figure 11 Interaction between cancer cells and active PSCs[12]

1.3 *In vitro* and *in vivo* models: an overview

Experimental biological models are essential for: studying basic biology, understanding diseases development, investigating tissues and organs, developing new therapies. These recapitulatory models of human tissues and organs can be *in vitro* or *in vivo* models: *in vitro* models use cell culture, 2D or 3D, to recreate biological characteristics, while *in vivo* models rely on animals to mimic human organism. All models have advantages and limitations, due to the impossibility to fully reproduce human organism complexity, both with *in vitro* and *in vivo* models. For example, 2D *in vitro* models are simple to realize and easy to manipulate, but they are inadequate to reproduce cell-cell and cell-ECM interactions. On the other hand, *in vivo* models show a physiological microenvironment and similarity with human genetics, on the other hand are expensive and unable to mimic some human characteristic features. In the table 2 below there is a summary of *in vitro* and *in vivo* models' applications, advantages, and disadvantages.

Table 2 Summary of *in vitro* models' advantages and disadvantages[14]

Models	Complexity	Biological relevance ^a	Model subtype	Application	Advantage	Limitation
2D <i>in vitro</i> 	+	+/++	1) Petri dish 2) Flask 3) Multiwell plate	1–3) Migration; proliferation; tumor growth; cell signaling; drug screening; gene expression.	1–3) Simple; low cost; easy to manipulate; highly accessible; reproducible. 3) High-throughput.	1–3) Oversimplified; extreme cell phenotypes; cell-cell and cell-ECM interaction not reproduced; lack of vasculature; no predictive power. 1–2) No high-throughput.
3D <i>in vitro</i> 	++	++/+++	1) Transwell 2) Hydrogel ^b , scaffold, matrix ^c 3) Micro-carrier culture 4) Spheroid ^d 5) Biopsy	1) Migration; drug screening; invasion; intra/extravasation; trans-endothelial. 2) Invasion; migration; drug discovery and screening; matrix remodeling; apoptosis; angiogenesis; tumor growth; gene expression. 3) Cell function; tumor growth; proliferation; invasion; intra/extravasation; drug discovery and screening; immune cell response; gene expression. 4) Cell function; tumor growth; proliferation; invasion; intra/extravasation; drug discovery and screening; apoptosis; angiogenesis; immune cell response; gene expression; tumor hypoxia. 5) Drug screening; tumor growth; invasion; drug penetration; culture-drug sensitivity test; gene expression; apoptosis.	1) Easy; low-cost; high-throughput. 2) Mimic <i>in vivo</i> scenario; Preservation cell phenotype; rich basement membrane-like matrix Cell-cell and cell-ECM interactions; high control on mechanical properties; co-culture; compatible with microfluidics; can incorporate growth factors. 3) Support aggregation of cells; preservation of cell phenotype; co-culture; cell-cell and cell-ECM interactions; different bead coatings; cell produce own matrix; high-throughput. 4) Maintain the heterogeneity of tumor cells; cell-cell and cell-ECM interactions; hypoxic core; high-throughput. 5) Simple; preservation cell phenotype, genotype, and architecture; high-throughput; size-control; co-culture compatible; preserve cell-cell and cell-ECM interactions.	1) Oversimplified; only single cell motility studies; no perfusion; no shear stress. 2) Lack of vasculature; no perfusion; no shear stress; collecting cells for analysis may be difficult; Large-scale production is expensive. 3) No perfusion; no shear stress; in general, lack of vasculature. 4) No perfusion; no shear stress; collecting cells for analysis is difficult; requires assay development; in general, lack of vasculature. 5) No perfusion; no shear stress; control of necrotic core is difficult; highly invasive.
Organ-on-chip 	+++	+++/ ++++	Microfluidic devices ^e	Cell morphology; invasion; intra/extravasation; transvascular migration; colonization; drug screening and discovery; matrix remodeling; immune interaction; angiogenesis; tumor growth; chemotaxis; ratchetaxis; hydrodynamics; tumor cell dormancy; gene expression.	Co-culture; preservation cell phenotype; customized design; control on physical (geometry, size) and biochemical properties of the tumor microenvironment; well-defined vessel endothelium; gradient compatible; dynamic system, control on hydrodynamic parameters (e.g. shear stress); real-time measurement; microscopy compatible.	Complex compared to static; limited range of dimensions due to microfabrication limitations; planar geometry; difficulty in collecting cells for analysis; specialized – expensive – equipment is typically required.
Model animal 	++++	+++	Mouse Rabbit Pig ^f	Tumor growth and dissemination; gene expression; drug discovery and screening	More physiological; genetic similarity; moderate prediction of drug behavior; physiological microenvironment; enable mutation studies.	Highly expensive; requires specialized personnel and facilities; low-throughput; no predictive to humans; inability to mimic human-specific features (e.g. immune system, stem cell differentiation); long-term culture; ethical issues.

1.4 *In vivo* models

In vivo models rely on animals to recapitulate living systems complexity and dynamic interaction between cells into a physiological environment. There are many *in vivo* models that have been used as tumour models, starting from simple animals to complex ones, depending on their genetic similarity with human genome. Many times, animals are used to transplant *in vitro* models and study their interaction with the organism, but they are also used to provoke a selected pathology, through genetic modification. There are many problems with animal models, both ethical and economical, but not only: these models are often not predictive about human organism and human drug response[14].

1.4.1 Animal models

Most common animal model used to model human organism is mouse model. This model shares a large part of human genome, even if there are important differences between mice and humans' physiology[10]. There are many mouse models used for cancer research:

- **Immunocompromised mouse models**, where mouse immune system is compromised to avoid rejection during human cells transplant. Mice deficient in T cells are called **nude mice**, and they can support human cancer cells. Mice with a lack of B and T cells are called **severe combined immune deficient (SCID) mice**, and their mutation happens spontaneously. If they are crossed with **non-obese diabetic mice (NOD)**, the resulting **NOD/SCID mice** are deficient in also innate immunity.
- **Humanized mouse models**, where immunocompromised mice are treated with human immune cells, to mimic human antitumoral immune response.
- **Patient derived xenografts (PDXs)**, where human cancer cells are transplanted into immunocompromised mice. Cancer cell lines are collected by patients in order to preserve genetic and disease features. A big problem with xenografts is their heterogeneity, that reduce their reliability, together with their genetic instability. There is also another problem that affect reliability, the *in vivo* microenvironment is different in mice than in humans, in particular stroma and the lack of immune cells. Cancer cells are first

cultured *in vitro*, then they are transplanted, and this also introduces variability.

- **Immunocompetent mouse models**, where mice keep their immune system. **Syngeneic mouse models** are obtained by transplanting cancer cells from mice with an identical genetic background to the receiving. Through this, immune rejections are avoided without the need for immunocompromised mice, so an immune reaction can be considered in a mouse cancer model.
- **Genetic mouse models (GEMMs)**, where mice are genetically modified to induce tumour development, with correct histology, preneoplastic stages and metastasis. Some problems of GEMMs are due to the lack of gradual development of tumoral heterogeneity, affecting model ability to predict human outcomes[10].

Even if animal models seem to be promising, they present many drawbacks that make them poorly reliable. Firstly, immunocompromised mouse models cannot reproduce an immune reaction, show a reduction in animal life span, and stroma and infiltrating cells are of animal origin, creating an unpredictable response to drugs. Then, animal models are expensive and difficult to manage, not to mention the ethical concern about animal usage in research[15]. Moreover, these models are resource intensive and time consuming, with poor results about clinical outcomes of the pathology, for the genetic differences between animals and humans[16].

1.5 *In vitro* models

As mentioned in the previous paragraph, *in vitro* models are cellular systems that recapitulate human tissues and organ biology. These models can be 2D or 3D, and the use of cells is employed. The cell type depends on the experiment and the model, but in general, it is possible to distinguish two main cell categories, based on their origin:

- Primary cells, isolated by donor's living organism;
- Established cell lines, from biobanks.

Primary cells can mimic the genetic features of interest because they come from a human organism, but they are difficult to isolate, and they have a short lifespan *in vitro*.

Established cell lines are routinely used in research because they allow to realize reproducible and long-term experiments, thanks to their long lifespan. They are often used for preclinical studies, cancer research and genetic studies.

In vitro studies can be performed under adherent conditions or in suspension, depending on the situation[17]. For example, 2D models are commonly monolayer culture where cells are adhered on a surface. Instead, 3D models are often suspension cell cultures, in order to obtain model like spheroids or organoids, where cells can self-organize. These models can mimic *in vivo* tissue's characteristics like cell-cell interactions, cell-ECM interactions, or tumour tissue's niche.

It is also true that there are some 3D models where cells are adhered on substrates, like biomimetic scaffolds, that resemble physiological tissues, to reproduce biological environment[5]. In the following fig. 12, there is a summary about the current *in vitro* models, 2D or 3D, used in research. In the next paragraphs they are analysed in detail.

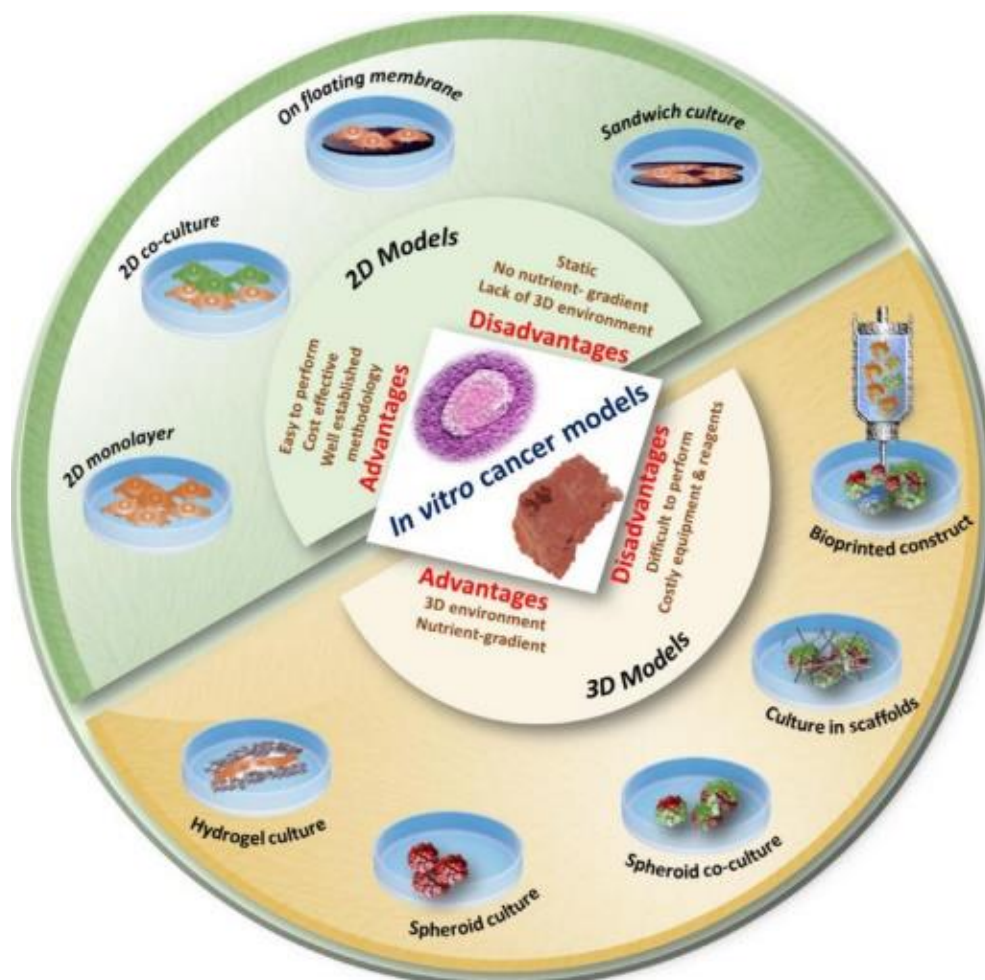


Figure 12 Images of *in vitro* 2D and 3D models[18]

1.5.1 2D culture

2D monoculture

2D monocultures are easy to maintain, to modify and to perform long-term analysis, these are the reason they are so used in research. They are also highly reproducible, low cost and quick to expand. They allow to study tumorigenesis and cancer cells evolution, to characterize malignant cells, with a simple accessible *in vitro* model[13], so they are used to understand genetic alteration or cancer cells biochemistry, but they present a lot of drawbacks. Firstly, 2D cultured cells tend to undergo a phenotypic selection, taking to culture alteration[15], together with changes in morphology[17]. Then, monocultures lack of tissue architecture and cellular heterogeneity representation, making them unreliable for tumour origin studies and drug evaluating[16]. Additionally, tumour microenvironment presents soluble factors and ECM molecules carried by vessel, that is not possible to replicate in 2D models[15]. Another limitation is that 2D monocultures guarantee a limited access to medium's components, creating a wrong gradient of nutrients[17]. Last, there are the cell-cell and cell-ECM interactions that are not represented into 2D monocultures, but they are important for differentiation, proliferation and vitality of cultured cells, but also for genes and proteins expression, stimuli-related cellular responses and other cellular mechanisms[17].

2D Co-culture

A commonly used tool in biological research, especially for cancer modelling, is co-culture, which allows the implementation of cancer heterogeneity and cell-cell communication. Into co-culture models, there is always a target type of cells, on which culture is focused, and assisting cell type, which support target cells. However, both cell types have a beneficial effect through co-culture. How to realize the co-culture depends on the need; it is possible to realize the two types of co-culture described here.

Direct co-culture

In this case, there are two or more cell types mixed and cultured together. These mixed cells form a monolayer on dishes or flasks, and they are used to study specific cellular behaviour and interactions. Cell-cell interaction can be achieved through

paracrine signalling or cell adhesion, that take place thanks to cell junctions. An explicative image of direct co-culture is the fig. 13A.

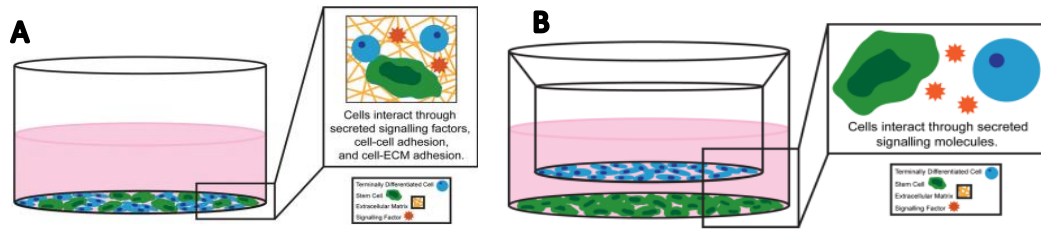


Figure 13 A) direct co-culture; B) indirect co-culture[19]

Indirect co-culture

In this case, there are two or more cell types cultured in the same support but physically separated. A well insert is used to separate two cellular monolayers, to reproduce cell-cell communication by paracrine signals. These soluble factors from local environment can influence cell fate and behaviour. The system outcomes are profoundly affected by the interaction realized in the co-culture model, in different ways depending on the chosen model[19]. Next to advantages of co-cultures, there are some problems, like the number of variables to consider and that are necessary to optimize for the culture[17]. However, it is a powerful tool for cancer models, because cancer tissues present a considerable number of cell types beside cancer cells, like cancer associated fibroblasts (CAF), immune infiltrate cells, stromal cells, that influence each other behaviour and support tumour growth, proliferation, and metastasis[13].

1.5.2 3D culture

Spheroids

Spheroids are 3D models where cells are organized into a spheroidal shape. These structures can mimic physiological microenvironment, cellular interactions, and tissue typical multi-level organization. They are realized using cell lines embedded into an artificial matrix, like Matrigel®, or natural matrix, like collagen; cells tend to self-organize and coalesce together[13], forming spheres of 20–1,000 μm in diameter[20]. Using spheroid as tumour model permits to: recreate some tumour cells characteristics, such as cell-cell interaction, cell-microenvironment interaction; preserve cell polarity; maintain cells morphology. Cells embedded into spheroid show similarity with those one grown in vivo, in terms not only of morphology but also of

gene expression, signalling and metabolism[15]. Spheroids are used a lot for biological research and for drug testing, because of their low costs, their simple realization, and their biological response to drugs. They are also used for studying cells migration, cancer tissue architecture, metastasis, and angiogenesis. Studying different spheroids, it is arisen a possible categorization of them into 3 separate groups, based on the spheroid architecture[15]:

- tight spheroids;
- compact aggregates;
- loose aggregates.

There are some disadvantages about the spheroid to take in mind using them:

- the time necessary to establish a line[13], and the constant necessity to resuspend cells after a certain period[5];
- the necrotic core, consequence of a high diffusion gradients inside the spheroid[5];
- difficulties in control shape and size of spheroid[5];
- mechanical weakness, that results in poor long-term maintenance[5];
- single cells separation through proteolysis for cellular evaluations[17];
- lack of accuracy due to the usage of Matrigel®, that is originated from animal[15].

Organoids

The term organoid refers to 3D model originated from cells, derived by tissues biopsy or resection, embedded into a matrix, like spheroid[13], or 3D model originated from human stem cells, which self-organizes into a spheroidal shape. Organoids are complex structure that mimic architectural and cellular features of existing organs, so they can be used for resume organogenesis, tissue morphology, cellular behaviour in an in vivo like environment[21]. This model is useful also because organoids can be cryopreserved, established so called “biobanks”, where 3D models are stored long term into liquid nitrogen[13]. As said before, organoid’s cells can be collected by patients’ tissue, realizing the patient-derived organoids (PDOs), that can be used for personalized medicine, drug testing, or research. Organoids can be used for long time because they can be passaged indefinitely, and they can be also influenced in their phenotype using supplements, like growth factors, to achieve the desired changes.

Furthermore, using organoids for cancer research can help the evaluation of gene expression, transcriptional regulation, epigenetics, metabolisms of cancer cells, because the 3D architecture of this model can recapitulate the 3D structure and heterogeneity of tumour microenvironment. As for other *in vitro* models, organoids present some drawbacks; first, the average time to complete organoid establishment is about 2 month, and complete maturation of cells is not always assured, if they are stem cells. Then, Matrigel or other matrices can introduce variability because there is a batch-to-batch variation, so the experimental consistency and the possibility to compare data between laboratories fail[13].

Scaffold based models

Another 3D *in vitro* model is based on scaffolds, structure for culturing cells. Scaffolds can influence cell fate through its composition, architecture, and surface that give signals to guide cell. Scaffold architecture must remark native tissue topography and mechanical strength, to guarantee cell adhesion, migration, and differentiation, if it is necessary[15]. To reach this goal, control of pore size is fundamental, because porosity dimension mediates cellular response, cell-ECM interaction, and all the other elements described above[22]. The distinct types of porosity are resumed into the table 3 below, together with their fabrication methods and cellular responses.

Scaffolds can be realized with different composition, natural polymers or synthetic ones, or they can be also decellularized matrix. They can be added with proteins to enhance cells adhesion, or soluble factors that influence cellular behaviour[16]. In conclusion, polymeric scaffold-based models can overcome limitation of other only cellular 3D models, present tuneable properties, allow long-term cultures, recapitulate spatial organization of cells[5]. However, there are some limitations to consider: large scale production is time-expensive and costly, assure the correct perfusion and generated nutrient gradient is important to permit cells survivor, there is a lack of vasculature, so the model needs some adjustments to be predictive[14].

Table 3 Influence of scaffold pores dimensions on cell response, with the fabrication methods that can be used to realized them[22]

Pore size scale	Fabrication methods	Cell response
NANO <300 nm	Bottom-up hydrothermal method	Cell type: MSCs <ul style="list-style-type: none"> • Adhesion • Osteogenic differentiation
	Thermally induced crosslinking	Cell type: Human ITSCs <ul style="list-style-type: none"> • Osteogenic differentiation
	Electrochemical anodization + etching	Cell type: N2a <ul style="list-style-type: none"> • Adhesion • Neuronal differentiation
	Oxidative nanopatterning; Electron beam lithography (EB);	Cell type: MC3T3-E; HOS; hMSCs <ul style="list-style-type: none"> • Adhesion • Migration • Proliferation • Mineralization
MICRO 0.3–100 μm	Electrospinning	Cell type: BMMC <ul style="list-style-type: none"> • Proliferation
	Electrospinning	Cell type: Human ITSCs <ul style="list-style-type: none"> • Inflammatory response • Angiogenesis
	Melt electrospinning	Cell type: hSSC <ul style="list-style-type: none"> • Adhesion • Osteogenic differentiation
MACRO >100 μm	Salt leaching	Cell type: hMSCs <ul style="list-style-type: none"> • Proliferation • Osteogenic differentiation
	Solvent casting + particle leaching method	Cell type: hMSCs <ul style="list-style-type: none"> • Proliferation • Osteogenic and chondrogenic differentiation
	Electrospinning + laser cutting system	Cell type: SMCs <ul style="list-style-type: none"> • Migration • Angiogenesis
MULTISCALE	Freeze-drying	Cell type: Bovine articular chondrocytes <ul style="list-style-type: none"> • Migration
	3D-painting + salt leaching	Cell type: hMSCs <ul style="list-style-type: none"> • Adhesion • Viability • Proliferation • ECM synthesis
	Electrohydrodynamic direct-jet printing (EHDP)	Cell type: MSCs <ul style="list-style-type: none"> • Adhesion • Viability
	Polymer foaming	Cell type: hMSCs <ul style="list-style-type: none"> • Adhesion • Viability
	3D-printing	Cell type: mBMSCs <ul style="list-style-type: none"> • Adhesion • Viability • Proliferation
	Stereolithography	Cell type: MLO-A5 <ul style="list-style-type: none"> • Proliferation • ECM synthesis
	Solvent casting within precisely patterned molds + photocuring	Cell type: HUVEC <ul style="list-style-type: none"> • Proliferation
	Extrusion deposition + porogen foaming	Cell type: C2C12s <ul style="list-style-type: none"> • Adhesion • Proliferation • Differentiation

3D bioprinting

3D bioprinting is a novel technique that permits to obtain a complex 3D model starting from biomaterials, hydrogels where it is possible to cultivate cells, or bioinks, composed by hydrogels and cells, that are deposited according to a computer-aided design (CAD). With this technique it is possible to reach high fidelity tissue architecture, to realize graded macroscale structures that mimic ECM, to integrate multiple cell types. As said before, there are two type of materials that can be used: biomaterial, like natural polymers, that are deposited layer by layer by 3D printer, in order to realize a scaffold; bioinks that are based on biomaterials plus cells, so they contain a hydrogel, cells, nutrients and growth factors. In both cases there are two factors to take in mind: physicochemical properties of bioinks/biomaterials influence bioprinting process, so they need to be controlled in terms of bioink's viscosity, bioink's cellular components concentration, material flow, printing time and printing head[18]; every printed construct undergoes to crosslinking process, essential to assure structure stability in physiological conditions.

Hydrogels should be biocompatible, should assure ECM structural and biological properties, gelation process should be controllable. Their viscosity influences printability and print fidelity, but also cells vitality, so it is important that the final bioink is shear thinning. Then, bioink should be crosslinkable, depending on the selected crosslinking method.

Crosslinking process can be realized with chemical, such as enzymatic crosslinking, or physical methods, like UV-crosslinking.

Bioprinting methods are classified, based on their deposition mechanism, into:

- Droplet based (fig. 14, A), where bioink is extruded as droplets using a source of energy, that can be sound, temperature, electricity;
- Extrusion based (fig. 14, B), where bioink is deposited as a continuous flow by the printhead, following a defined pattern, and the printhead can use different type of mechanical actuations;
- Laser based (fig. 14, C), where bioink is deposited thanks to the usage of laser. This method is nozzle free, so there are less problems about cells shear stress.

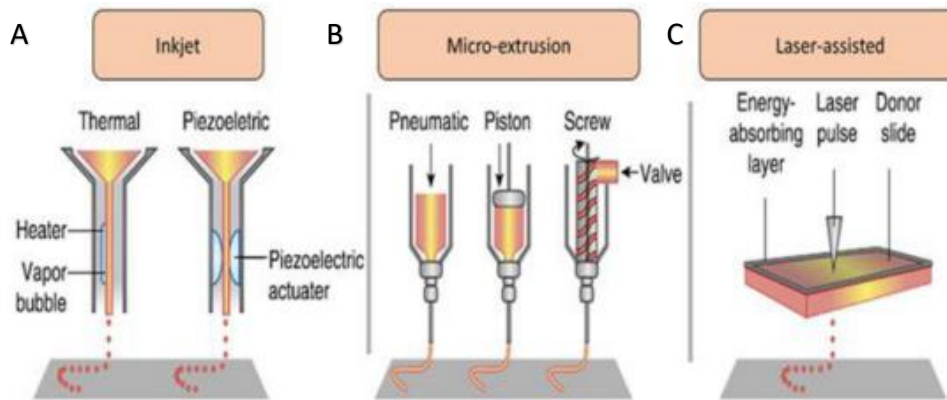


Figure 14 3D bioprinting techniques: A) inkjet bioprinting; B) micro-extrusion bioprinting; C) laser-assisted bioprinting[18]

Some disadvantages of 3D bioprinting are: the necessity of cell isolation for creating bioinks, maintenance of these cells and printing them, avoiding their damaging. There are other problems linked to resolution and to cells density control, that should be improved[16], [18].

Microfluidic devices

Microfluidic technology allows to process fluids in micrometrical channels. These chips are often made by polydimethylsiloxane (PDMS), in order to obtain a transparent surface to couple microscopic imaging techniques. Thanks to their microchannels, microfluidic chips permit to control flow rate and mimic shear stress conditions, in fact, these devices assure a dynamic laminar flow. It is also possible to integrate biosensors and devices for signals registration, to monitor chemical signals, together with the real time monitoring achieved with microscopy[23]. Some advantages of these devices are reduction of reagents volume used, because of channels small volume; possible devices large-scale manufacturing; production protocol easy to automatize; the use of a biocompatible and gas permeable material (PDMS)[24]. In conclusion, PDMS microfluidic devices are able to assure right cells spatial organization and dynamic flow to recapitulate in vivo-like environment[23].

3D Co-culture

As reported before for 2D cultures, it is possible to achieve 3D co-culture, both direct and indirect ones. For **direct 3D co-culture models**, there are mixed cell types cultured in synthetic or natural polymers, that act as support. It is possible to study cell interactions in a more physiological structure. Together with cell-cell interactions, in this co-culture models, the interaction between cells and ECM through cells adhesion can be also studied, and its influence on cellular behaviour, because matrix

properties, like geometry, elasticity, and the presence of mechanical signals, can regulate cell adhesion, migration, differentiation, reproduction, and apoptosis.

For **indirect 3D co-culture models**, instead, different cell lines are cultured together using hydrogel encapsulation. In this way, it is possible to reproduce native environment structure and benefit of cellular communication. The already mentioned pros and cons of co-cultures are still valid also for 3D co-cultures.

1.6 Organ-on-chip technology: a brief description

Microfluidic devices are used also to recreate the 3D multicellular organs architecture with the so called 'organ-on-a-chip (OOC)' technology[23]. Microfluidic chips have been chosen for OOCs because they allow also to study 3D cells migration, controlling them not only through flow rate but also establishing chemical gradients. OOCs couple microfluidic devices advantages to the possibility to culture multiple cell types in order to recapitulate physiological environment, both for biomechanical and biochemical features[23]. That is why there are many OOCs models nowadays, for lung, liver, gut, etc., but also for PDAC. For cancer models OOC technology can be useful to understand cell-cell interaction, and other characteristics of tumour microenvironment that influence therapeutic response, like hypoxia, dense matrix and tissue stiffness. OOCs can also overcome some limitations of previous models, like ethical problems of *in vivo* models, or reproducibility problems of organoids[23].

1.6.1 Fabrication techniques

In this thesis work, the following techniques have been used to fabricate the microfluidic chips, composed by three layers, bottom layer, top layer and reservoir, to realize the indirect co-culture. For bottom layer, SU-8 lithography has been used, while for the top and reservoir layers 3D printing technology has been used. All the techniques have been the starting point for replica molding, the techniques to realize the PDMS replicas.

Lithographic technique

There are many top-down approaches for nanofabrication that are included into the term “lithography”, because they all use an energy source to transfer a pattern on a substrate[25], covered by a photosensitive material called **resist**. Lithography techniques are organized in steps: first, the substrate is covered by the resist; second, there is the irradiation of the substrate; then, there is the development to remove the excess; in the end, there is the etching of the substrate. The energy source and the development method depend on the type of resist and the lithography technique. There are two types of resists: negative resist (fig. 15, A) or positive resist (fig. 15, B); both are photosensitive, but in the positive resist, internal bonds are broken by the irradiation, while in the negative one, the bonds become stronger with the exposure, due to a cross-linking phenomenon. The development solution for a negative resist removes the non-irradiated resist, while the one for a positive resist removes the irradiated resist.

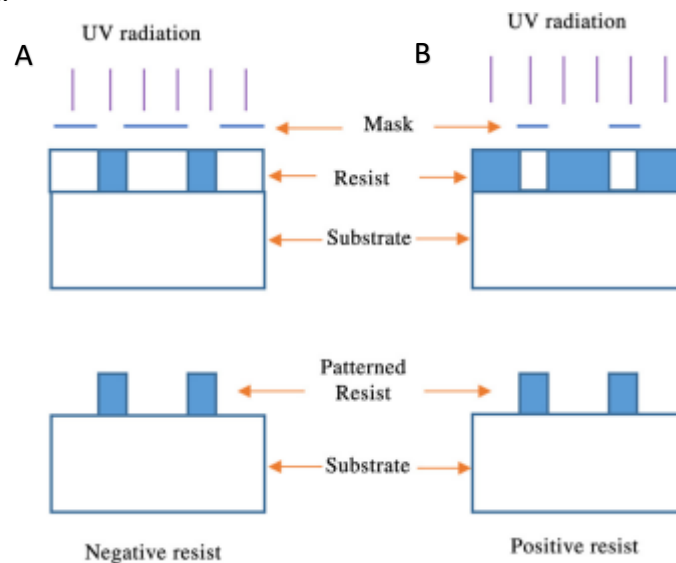


Figure 15 A) negative resist example, B) positive resist example[25]

Another principal element is how the resist and the substrate are irradiated. All the lithography techniques that rely on masks belong to **physical mask methods** or **mask lithography**, while when the pattern is drawn directly on the substrate are known as **software methods** or **direct write methods**. Differences between these two categories are mainly based on the speed and the resolution of the technique[25]. Between the huge number of lithography techniques there is the **soft lithography**, a set of processes to realize masters in PDMS from a mould (fig. 16). Mould can be

realized through photolithography techniques, and the support for the mould is a silica wafer[26].

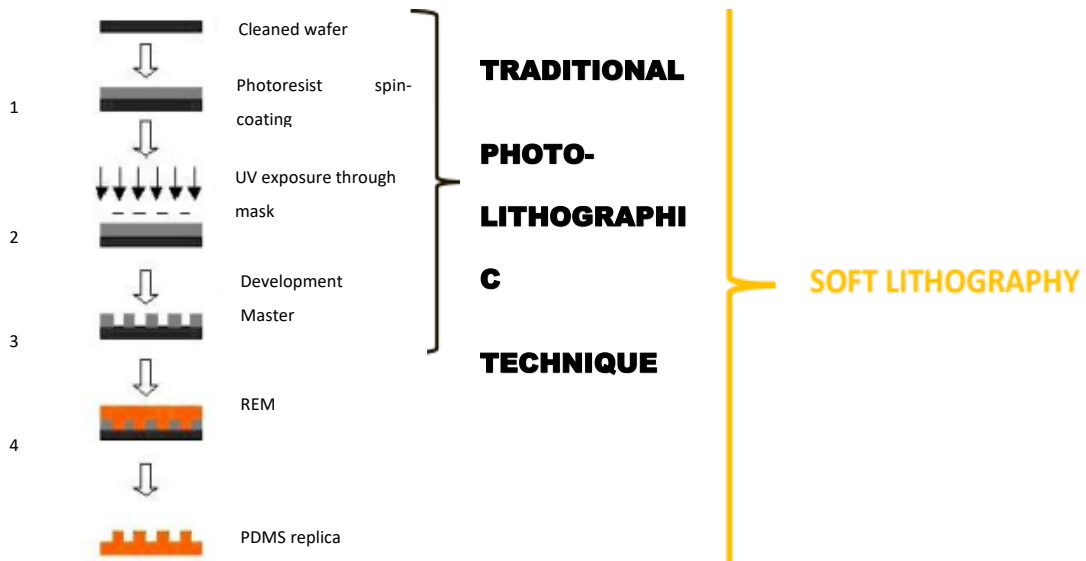


Figure 16 Soft lithography steps[26]

To fabricate the master on the wafer, the photoresist is spun on the support (fig. 16, 1), then the wafer is exposed to UV through the mask (fig. 16, 2). The resist is developed, and the geometry is obtained on the wafer (fig. 16, 3); the substrate is treated with hydrophobic solution to avoid that PDMS sticking. Then, PDMS is poured (fig. 16, 4) on the wafer[27].

Replica molding

Replica molding is a soft lithography technique to realize PDMS microfluidic devices duplicating a mould, which can be obtained through different processes. The PDMS prepolymer and the curing agent mixed in a proper mixing ratio are poured into the mould, then the whole is heated for a certain time, in order to obtain a solid PDMS structure; at the end, the replica is peeled away from the mould. Some advantages of this techniques are that moulds can be used many times to obtain replicas, reducing costs and time; these PDMS devices can be used with a lot of compounds; replica molding can be considered universal, because several patterns and shapes can be realized through it[27].

3D printing

3D printing is a rapid prototyping process to realize finite prototypes. This is an additive manufacturing layer by layer process, that minimizes time and costs. The 3D printing process is organized in several steps: first, a CAD model is created; then, it is

converted into a .stl file; at the end, the printer uses the file to print the object layer by layer[28]. The materials used in 3D printing are various, from plastics to metals; also, the 3D printer types are several. A 3D printer technology is PolyJet®, used to realize prototypes or parts that are accurate and smooth[29]. Thanks to this technique, it is possible to realize complex geometries, details and features, with different colours and materials, such as the sacrificial material and the structural one. In this thesis work, 3D printing is used for printing the mould for top and reservoir layers.

2 Materials and methods

2.1 Microfluidic devices

2.1.1 Materials: PDMS

Polydimethylsiloxane (PDMS) is one of the most common silicone polymers used for industrial applications, thanks to the possibility to produce chains of different length controlling its molecular weight[30] PDMS is an elastomer, with elastic and hyperplastic properties, that shows a thermoplastic behaviour; the transition from hard material to amorphous state is reversible[31]. Moreover, PDMS

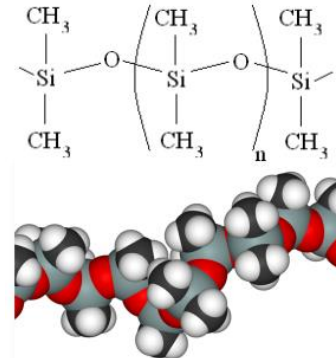


Figure 177 Structural formula and representation of PDMS[31]

properties can be tuned and optimized adding pendant groups, modifying the network and reinforcing it[30]. PDMS is very flexible, it shows low viscosity even at high molecular weight, so it is a non-Newtonian polymer; the polymer behaviour is influenced by chains orientation and the presence of fillers[30], (fig. 17). In the table 4 a summary of the main physical properties is reported. This material has been largely exploited in the microfluidic and tissue engineering fields too, because of its biocompatibility, its oxygen permeability, its easy fabrication[23].

Table 4 PDMS SYLGARD™ 184 Silicone Elastomer kit physical properties[32]

Color	Clear
Dielectric Constant at 100 Hz	2.72
Dielectric Constant at 100 kHz	2.68
Dielectric Strength	500 volts per mil v/mil
Durometer / Hardness	Medium Stiffness 20A-50A
Specific Gravity	1.03 @ 25°C
Viscosity / Flow	Controlled Flow 3000 - 10,000 cps

To obtain a well crosslinked solid structure, PDMS solution used for replica molding has been prepared using a polymeric base and a curing agent (both belonging to SYLGARD™ 184 Silicone Elastomer kit, fig 18A), with a ratio of 10:1 v/v (volume /

volume). The solution has been vigorously hand-mixed and then trapped air bubbles have been eliminated using a vacuum pump (fig 18B).[32]

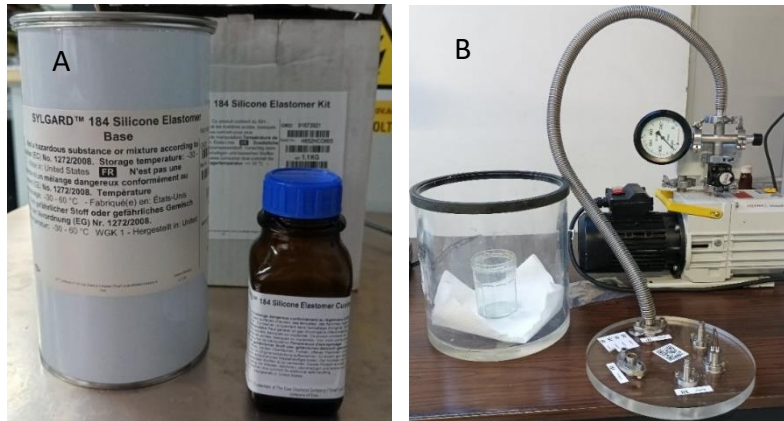


Figure 18 A) SYLGARD™ 184 Silicone kit, B) vacuum pump used to eliminate trapped air bubbles.

2.1.2 Bottom layer design

Bottom layer design has been developed starting from the protocols optimized by Beatrice Minervini during her master project (fig. 19)[32]. The new design preserves the division in three channels, whose dimensions are: 900 μ m in width, 6.4mm in length and 200 μ m in height for the central channel, 500 μ m in width, 6.4mm in length and 200 μ m in height for the lateral ones. To separate the central channel from the lateral ones, two rows of pillars are introduced, every pillar is 100 μ m in diameter and 200 μ m in height, while the pitch between pillars is 75 μ m.

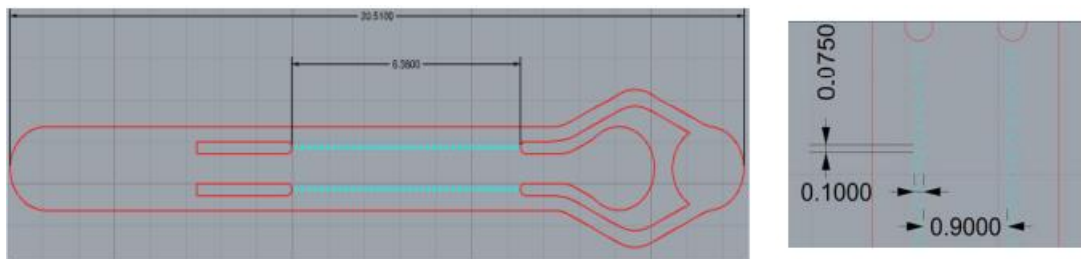


Figure 19 Beatrice Minervini's design for the pancreas on chip described[32]

The introduced innovation consists in two different inlets for the lateral channel, that allow to obtain specific inlets for each lateral channel for the culture media; every inlet has a diameter of 2mm, and they have been obtained through a biopsy puncher. The CAD has been designed with the software Rhinoceros, and it is shown in the fig. 20 below.

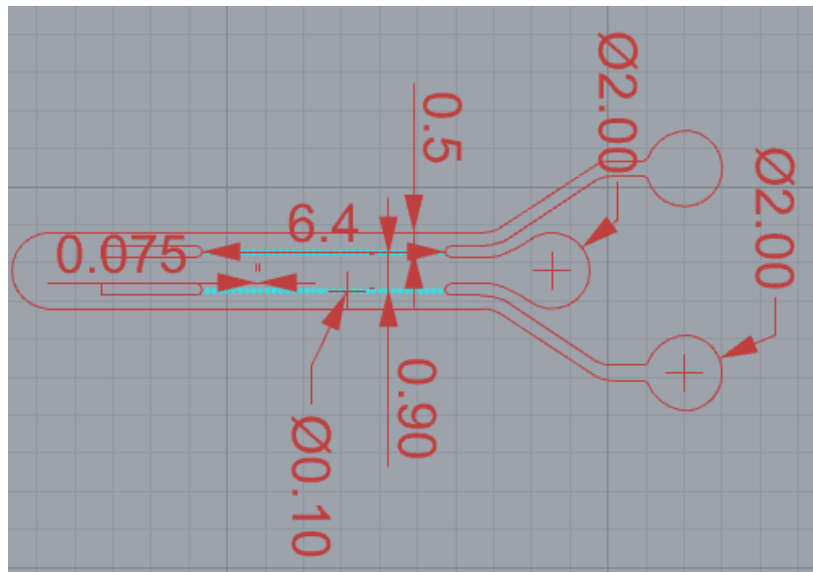


Figure 20 CAD bottom layer designed in Rhinoceros with measurements in mm

The modified bottom CAD layout takes inspiration from the literature, in particular from the work of *Drifka et al.*[8], that developed a microfluidic platform to create a heterotypic stroma-cancer microenvironment model. In this paper, they designed a three-inlet microfluidic device to achieve a trilayer co-culture, in order to mimic the multicellular complexity and the 3D spatially controlled ECM architecture observed into human PDAC microenvironment. The fig. 21 reports the scheme of the microfluidic chip.

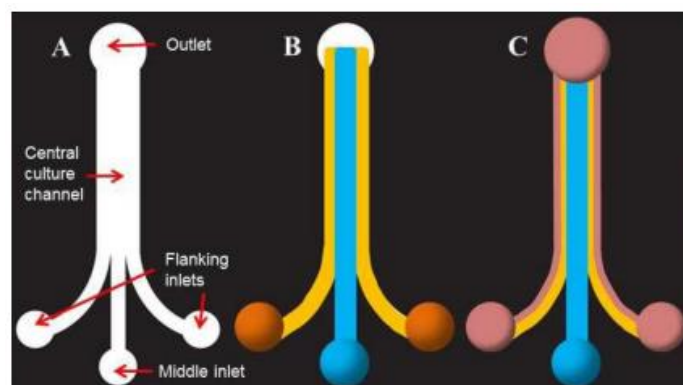


Figure 21 A) The empty device; B) the device after seeding (PSC in yellow, PANC-1 in blue); C) the contracted cellular trilayer and the media (pink)[8].

To reach the pillar small diameters, it has been chosen to resort to SU-8 soft lithographic technique after several tries with 3D printer, as reported in the addendum (pag. I).

2.1.3 Bottom layer mould realization method: mask realization



Figure 22 MICROTECH LaserWriter LW405 A71.

As explained before, a crucial element for photolithographic techniques is the mask, that has been realized through direct laser writing technique. The LaserWriter used is MICROTECH LASERWRITER LW405 A71 (fig. 22), that can pattern a planar geometry on surfaces covered by photoresist using a GaN laser beam at 405nm[33]. This technique is low cost and assures high performances, thanks to its resolution (down to 0.7 μ m).

The LaserWriter is composed by the following sections:

- The **write unit**, where the GaN laser is collocated, together with the substrate microtranslation system, the laser interferometer and the electro-optical components, to control the beam and the exposure energy. This unit permits the beam adjustment through specific optics, according to the wavelength, to write the desired pattern.
- The **cabinet**, that contains the write unit to protect laser beam from the clean room air flow, which might cause vibrations.
- The **control unit**, which controls the laser beam through several interconnections.

All the elements are made with top quality materials, which minimize wear and assure long-term stability. Best results can be obtained assuring microcontamination and microvibration control and working in a clean room[34].

In this work, the mask has been realized using a chromium/glass support (Cr/SiO₂), patterning by the LaserWriter, that follows the .CIF CAD showed in fig. 21 (the Rhinoceros CAD has been converted using CleWin, a layout editor). The writing process takes about 1 hour and then the mask has to be developed and etched.

The mask development/etching is organized in different steps, showed in fig. 23:

1. **Mask dipping** into a solution of water and AZ 400k Developer by Merck (with a ratio of 3:1), to remove the resist excess. This dipping phase last about 30s, then the mask is rinsed in deionised water (DI) and dried under a flux of hyperpure nitrogen.
2. **Chromium etch**, to eliminate the chromium layer exposed where the resist has been removed in the previous step. The mask is dipped into the chromium etchant (Chrome ETCH N°1, SIGMA-ALDRICH®) till the pattern is clearly visible, then the mask is rinsed with acetone and isopropyl alcohol (IPA), washed in DI and dried with nitrogen.
3. **Mask cleaning**, the mask is dipped into a pirañha solution for 30min to assure its cleanliness before the usage. The solution is composed by 3 parts of sulfuric acid 99% and 1 part of hydrogen peroxide 30%. After that, the mask is washed in DI and dried with nitrogen.

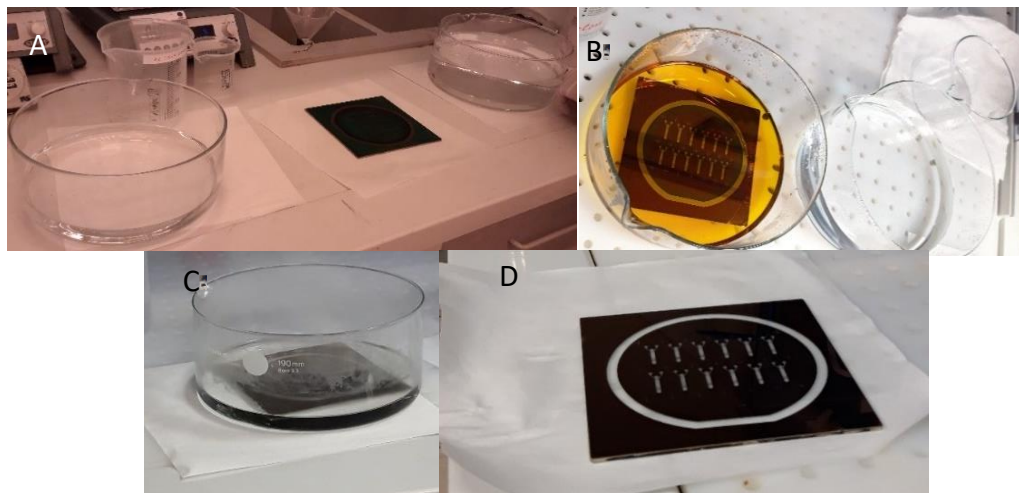


Figure 23 Images of mask development: A) just written mask before first dipping into developer; B) chromium etching; C) mask cleaning using pirañha solution; D) mask after cleaning.

2.1.4 Bottom layer mould realization method: SU-8 lithography

SU-8 is an epoxy-based negative resist used for soft lithography in micromachining and microelectronic applications, because of its characteristics, like a high aspect ratio, a wide range of film thickness in a single coat, near UV processing, high thermal stability[31]. It is composed by EPON resin (Bisphenol A Novolak epoxy oligomer) and photo acid generator (triarylsulfonium hexafluoroantimonate salt), dissolved in the

GBL (gamma-butyrolactone) organic solvent[32]. SU-8 photoresist can absorb light in the UV region, starting the photo acid generator dissociation and hexafluoroantimonic acid generation; that acid is able to protonate the epoxide groups that are on the oligomers[35]. After UV light exposure, the resist cross-linking starts, obtaining a mechanically and thermally stable resin, with the physical properties reported in the fig. 24.

In this work, SU-2150 photoresist by MicroCHEM (fig. 26A) has been used to realize a mould with photolithographic process, that has been optimized as described in the addendum (pag. IV).

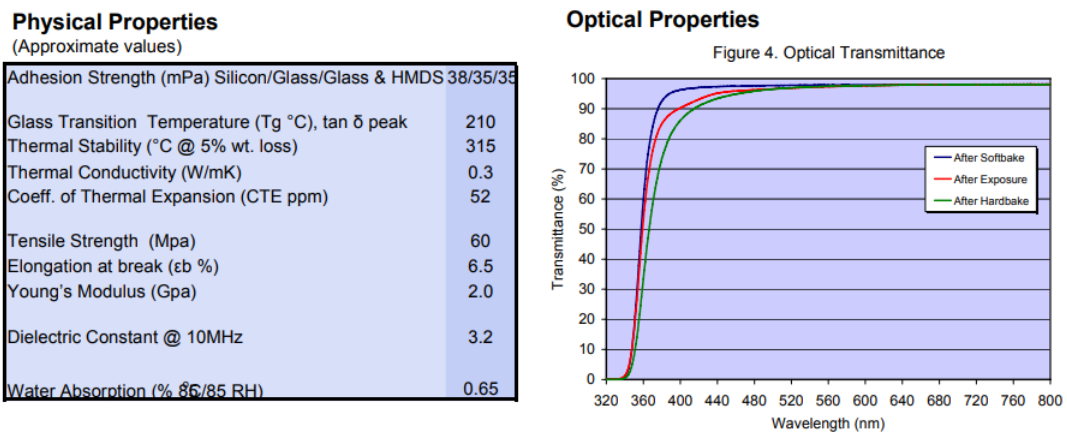


Figure 24 SU-8 2150 physical and optical properties[31]

As reported in fig. 25, different steps have been performed for the bottom layer mould manufacturing:

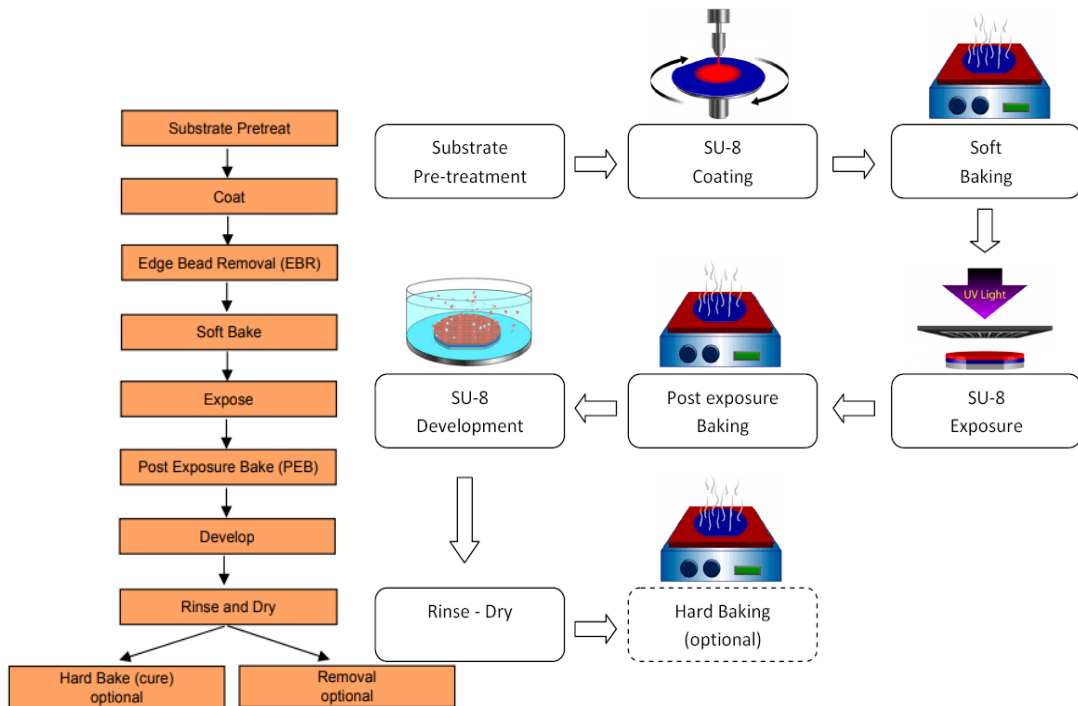


Figure 25 The photolithographic process for SU-8 soft lithography: A) the workflow[31]; B) a pictorial representation of each step[69]

Substrate pre-treatment: the substrate, a silicon/silicon oxide wafer, has been prepared before the process; during this phase, it is possible to use an adhesion promoter, like the Omniccoat, or a heating treatment or a plasma treatment. This step is helpful to promote SU-8 adhesion; in this work, the wafer has been pre-treated with a heating treatment at 200°C for 15min, then it has been treated with O₂ plasma, whose parameters are the same reported into the table 5 below.

Coat: after surface preparation, a photoresist layer has been deposited using a spin coater (fig. 26B), for a thin settled layer. Firstly, the wafer has been centred on the spin coater support, thanks to vacuum; then a drop of SU-8 2150 has been poured at wafer centre. After that, photoresist has been spin coated in two steps:

1. 500rpm for 10s with an acceleration of 300rpm/s, to allow SU-8 spreading;
2. 2000rpm for 60s with an acceleration of 300rpm/s, to reach the desired layer thickness.

Edge bead removal (EBR): in some protocols, there is the EBR step, where the external portion of SU-8 is removed using 2-Propanol Alcohol (IPA), but in this thesis work this step has been skipped since wafer edges never get into play.

Soft bake: this step is necessary to permit solvent evaporation (around 7% for a good exposure) and SU-8 solidification; it results in a photoresist layer's thickness variation before UV exposure. For a progressive solvent evaporation, soft bake requires a two temperature steps protocol, the first one at 65°C, the second one at 95°C, on the hot plate (fig. 26C). In this thesis work, the coated wafer has been kept at 65°C for 8min, then ramped at 95°C, and kept at this temperature plateau for 40min, in accordance with SU-8 2150 data sheet. At the end of soft bake, the wafer has been left resting on a flat surface for about 1h.

Exposure: photoresist exposure has been performed using a UV lamp, to achieve the cross linking in exposed regions of SU-8, inducing local properties changes. Indeed, after this step, the exposed resist becomes hard, while the unexposed one remains soluble and it will dissolve during the development phase, because SU-8 is a negative photoresist. To select which wafer part has to be irradiated, a mask is positioned above the coated substrate, and the UV light has to pass through it. In this thesis work, exposure has been performed using the mask aligner (fig. 26D), with a filter to remove radiation under 365nm. The resulting near UV radiation shows a surface power density of 3.5mW/cm², so the selected time of exposure is 50s, to assure the right energy for SU-8 absorption.

Post exposure bake (PEB): the next step is the PEB, whose goal is to give energy to exposed photoresist, that can finish the cross-linking process. A critical point is the mechanical stress induced in the resist during heating and cooling steps, so controlling the temperature increase and decrease is essential to assure stress release. The PEB temperatures are the same as for soft bake, while times for each temperature level are different; the exposed wafer has been kept at 65°C for 5min, then it has been ramped at 95°C, and it is kept at this temperature plateau for 20min, in accordance with SU-8 2150 datasheet. The cooling phase has been performed on hot plate, to reach a progressive reduction in temperature, and the wafer has been cooled at 25°C.

Development: this step involves a SU-8 developer, a solvent that dilute the non-cross-linked photoresist, showing the desired pattern on the wafer. The developer, by MicroCHEM, is mainly composed by PGMEA (Propylene glycol monomethyl ether acetate), but sometimes Ethyl-lactate or Di-acetone alcohol are also used instead of

it. During this phase, firstly the coated wafer has been submersed by SU-8 developer and the whole has been stirred for around 20min, then it has been washed with fresh SU-8 developer for 10s and rinsed with IPA. At the end, the wafer has been dried with nitrogen.

Hard bake: the last step is another baking step, whose aim is to suppress the residual mechanical stresses inside the SU-8 photoresist, because they can create surface cracks or layer delamination. The developed wafer has been heated at 150°C for 5min, then it has been cooled at 25°C on the hot plate. This step is skipped in some works.

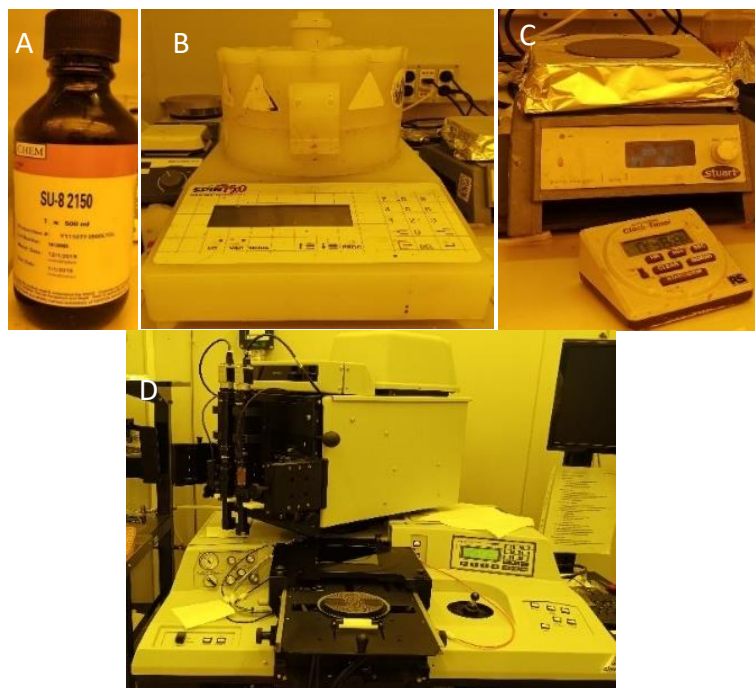


Figure 26 Set up used for soft lithography: A) SU-8 2150 by MicroCHEM; B) spin coater used for wafer coating; C) hot plate; D) mask aligner used for exposure step

Before using the realized mould for replica molding, a silanization process has been performed on the wafer. This step produces a passivation layer that allows PDMS peeling off and preventing its adhesion to the master[36].

The followed procedure is:

- **Solution preparation:** a solution has been prepared pouring toluene and trichloromethylsilane into a Petri dish, with a ratio of 1:10.
- **Rest:** the wafer has been immersed into the solution and it has been left submerged for 3h.

- **Washing and baking:** the wafer has been washed with IPA and dried with nitrogen, then it has been baked for 15min at 160°C.

2.1.5 Top layer design

Top layer design has been realised starting from the bottom layer. The design presents a channel, whose dimensions are: 1mm in width, 5.5mm in length and 200µm in height. This channel reflects the central channel of bottom layer, and these two channels are separated by polycaprolactone (PCL)/gelatine electrospun membrane. There are four inlet holes, that are about 2mm in diameter, and two outlet holes, which have the same inlet holes' dimension. There is also a rectangular frame which surrounds the channel, that has to host the membrane. In the fig.27 below the top layer CAD realized in Rhinoceros is reported.

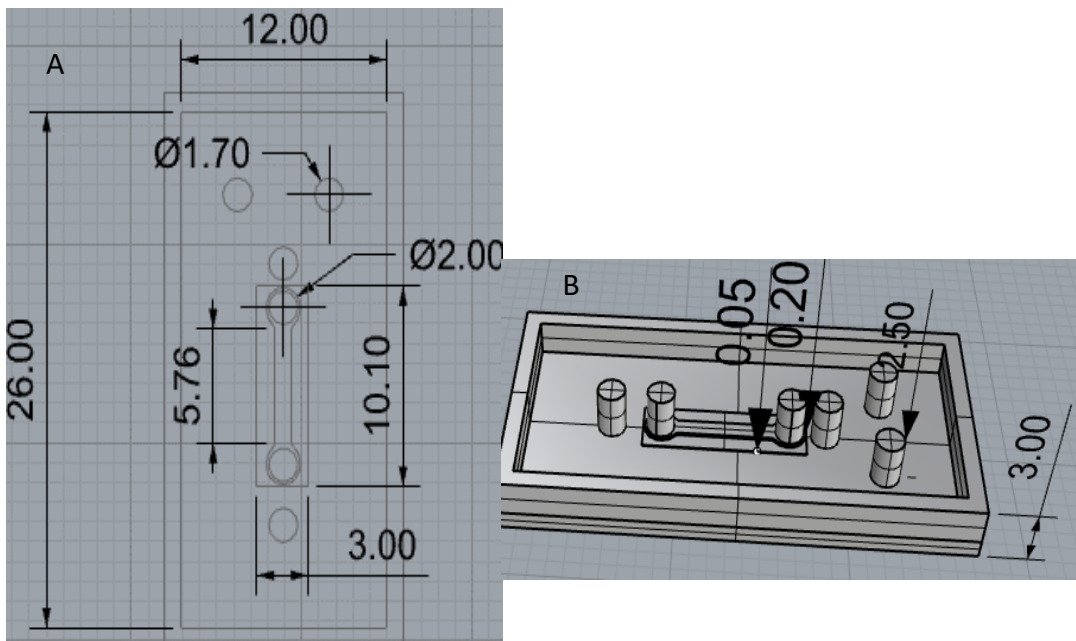


Figure 187 Top layer mould CAD in Rhinoceros; A) the 2D model; B) the solid model exported in .stl to print it

2.1.6 Reservoir design

On the top of the layers described above, this pancreas on chip model presents a third layer, the reservoirs, whose purpose is to store culture media for the cells seeded in the other layers. This layer is composed by two holes, one placed on the inlets (9.8mm in diameter) and one on the outlets (5.4mm in diameter). In the following fig. 28 the CAD realized in Rhinoceros.

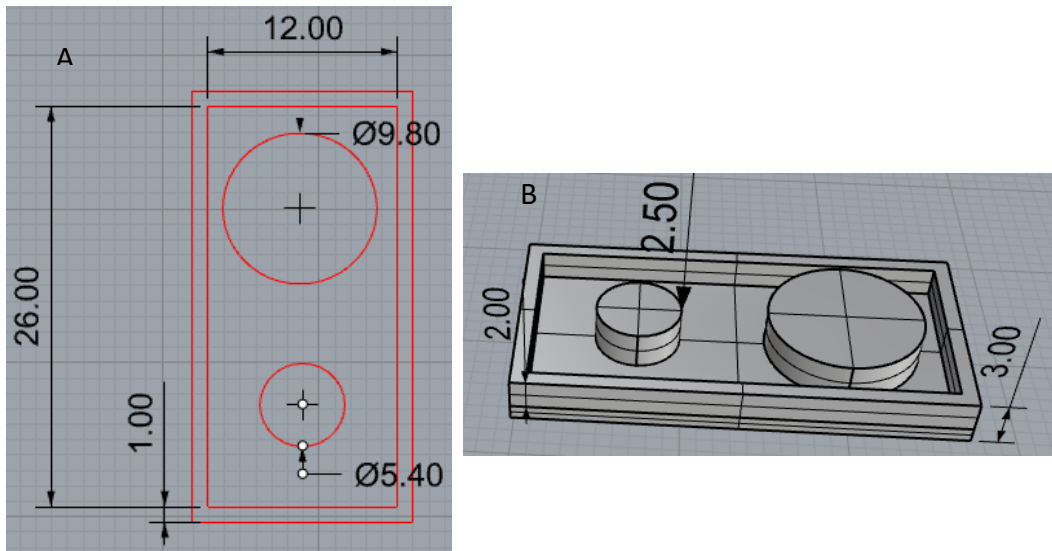


Figure 28 Reservoir mould CAD in Rhinoceros; A) the 2D model; B) the solid model exported in .stl to print it

2.1.7 Top layer and reservoir mould realization method: 3D printing

As mentioned in the first chapter, top and reservoir layers have been obtained through replica molding, and the moulds have been realized through 3D printing. The polyjet OBJET30 Stratasys is the 3D printer used in this thesis work, and it exploits a liquid UV photopolymer as resin (VeroWhite™, Stratasys, fig. 29).



Figure 29 OBJET30 Stratasys

Before starting the printing process, the exported .stl file is loaded into the 3D printer computer, using the Objet Studio software, which allows also to orientate the



Figure 30 Operating ultrasonic bath, with a falcon filled with acetone and the mould

elements in the tray of the printer. After that, the printing process begins, and the resin layer is deposited by the inkjet head, each layer is polymerized by the UV lamp, and then the tray steps down along Z axis, to restart with another deposition. Together with the mentioned photopolymeric resin, the printing head can deposit another material, the sacrificial supporting one,

that is SUP705. The printing process requires less than one hour, then it is possible to extract the moulds, which have to be washed with water and dried with air before the curing phase, where the moulds are left overnight in the oven at 150°C. This step is essential to guarantee the complete curing of the photoinitiator in the resin, in order to avoid any interference with the PDMS polymerization. At the end of the process, the moulds have been rewashed in acetone using an ultrasonic bath (fig. 30), with the following parameters: 5min, 59kHz, 20°C and 100% power.

2.1.8 Bottom, top, reservoir layers realization method: replica molding

As explained in the first chapter, replica molding (REM) is a technique to obtain microfluidic chips using a mould and liquid PDMS that is poured on it. In this thesis, REM is used to realize the three layers, whose moulds have been realized with different techniques. The already described non-crosslinked degassed PDMS is poured onto the moulds, then the whole is placed in the oven for 30min at 90°C, to favour PDMS solidification. Then, replicas are removed from the mould using ethanol, in the 3D printer moulds (fig. 31A), or isopropanol, in the SU-8 moulds (fig. 31B), to help the detachment.



Figure 31 A) Top and reservoir layer replicas after the thermal polymerisation ; B) bottom layer replica before the thermal polymerisation.

2.1.9 Microfluidic device assembly technique: plasma oxygen

To assembly top and bottom layers oxygen plasma bonding has been used. PDMS is

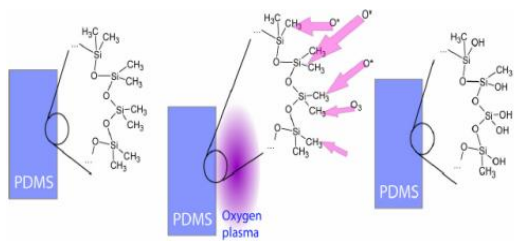


Figure 32 A schematic representation of PDMS surface chemical process that occurs during plasma treatment[31].

hydrophobic and inert because of its methyl groups but using plasma oxidation it is possible to obtain hydroxyl radicals, the silanol groups, on the surface. These exposed groups are able to generate irreversible covalent bonds (Si–O–Si) when they meet other free

radicals[30]. This technique can be used also to bond PDMS to glass, as it has been done in this work. In the figure 32 a representation of the corresponding chemical process.

Plasma is an ionized gas, obtained starting from a noble gas that is subjected to a high external electrical field, which is able to separate positive and negative charges. Starting gas (or gas mixture) is released into a sealed plasma chamber, where the pressure is low, and then gas (or gases) is energized through radiofrequency electric field. This results in the generation of free activated ions, that etch all the free surfaces in the chamber, breaking the material surface bonds and then substituting molecules/elements of the open radicals[37].

For this thesis work the Electronic Diener Plasma-Surface-Technology has been used (fig. 33), with the following parameters, reported in the table 5.



Figure 33 Electronic Diener Plasma at Chilab

Table 5 Plasma treatment parameters

Parameters	
Pumping down pressure	0.3mbar
Gas supply period	1min
O2 flow	100%
Plasma process duration	0.30s
Plasma power	22%
Venting time	1min

Before plasma treating, PDMS replicas have been washed in ethanol with ultrasonic bath, using the same parameters used to clean 3D printed moulds, then they have been dried on hot plate at 100°C for 5min. After the plasma treatment, a thermal

treatment has been performed on the bonded layers, using the hot plate at 80°C for 4min, to improve the bond.

2.1.10 Microfluidic device assembly technique: interlayer bonding

To assembly the reservoir layer and the top layer, interlayer bonding technique has been used. A thin layer of non-crosslinked PDMS is laid on the reservoir layer, then it is placed on the top layer. To stabilize the link, the whole is loaded into the oven at 90°C for 15min. Before this treating, PDMS replicas have been washed in ethanol with ultrasonic bath, using the same parameters used to clean 3D printed moulds, then they have been dried on hot plate at 100°C for 5min.



Figure 34 Top layers bonded with reservoir layers and membranes

The same technique has been used to place the PCL/gel membrane on the top layer, but in this case the top layer frame is filled with non-crosslinked PDMS, then it is loaded in the oven at 90°C for 2min, to obtain a pre crosslinked PDMS. Then, the membrane is positioned into the frame and the whole is placed on the hot plate at 35°C for 10min to complete the PDMS solidification.



Figure 35 Leica digital microscope

2.2 Microfluidic devices characterization

2.2.1 Digital microscope analysis

Digital microscopy is an imaging technique that relies on optics and a digital camera to obtain a digital image on a monitor. It is based on a light source, as LED light, and a digital circuit that is used to focus the image. This technology is low price and

simple to use, so it is quite common today[38]. In this thesis work, the used digital

microscope is Leica VZ80C (fig. 35), that belongs to DVM2500 series; their characteristics are: 2.11Mpixel CCD digital camera, lens' zoom range from 50 to 400x, visual field from 6.1 to 0.78mm, depth of field from 13.3 to 0.25mm[39].

Thanks to this technology, images and videos of assembled chips have been captured and measurements have been acquired to demonstrate the replica consistency as compared to Rhinoceros CAD, as reported in the next chapter.

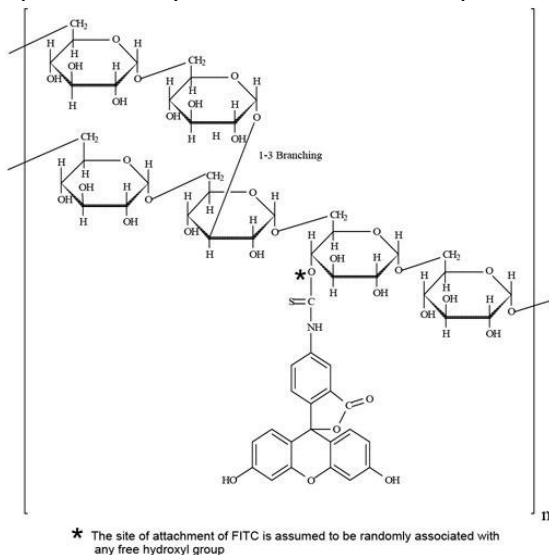
2.2.2 Microfluidic test

The assembled device has been undergone to a leakage test in static condition, using a solution of water and food dye, injected through a micropipette. Digital microscope Leica DVM 2500 has been used to observe the solution path in the device's channels. This test has been useful for evaluation of pillars fluid separation capability, the endurance assured by bonding processes.

The test has been also replicated on the bottom layer only, using collagen hydrogel instead of dyed water, to verify the correct pillar fluid separation with a different fluid viscosity.

2.2.3 Permeability test

Permeability test has been performed on the assembled chip to verify the membrane permeability; the test has been performed using a fluorescent solution 1mg/mL,



made by fluorescein isothiocyanate–dextran (FITC-dextran) and phosphate buffered saline (PBS). Dextran is a polymer, composed by glucose molecules linked together through α -D glycosidic bond mostly (fig. 36). Dextran shows a wide range of molecular weight: lower molecular weight Dextran (between 9 million and 10 million) presents few branches; increasing the molecular

Figure 36 Dextran formula[40].

weight, there is an increase in the number of branches, that implies a behavioural change in the molecule. In high molecular weight Dextran, the molecules assume a

greater symmetry, their properties are the same of expandable coils and are more rod-like.

The FICT- dextran (Sigma-Aldrich), shown in fig. 37, has fluorescent properties, in particular the excitation peak is at 490nm, while the emission peak is at 520nm; the fluorescent properties are influenced by solution pH, with the optimal one being around 8[40].



Figure 37 FICT-dextran used at DIMEAS laboratory

The test has been prepared inserting collagen into bottom central channel, and, after 60min at room temperature, the FICT-dextran solution has been inserted into the chip. To test the permeability in both directions (from the bottom to the top, from the top to the bottom), in some devices the solution has been inserted into the two bottom lateral channels, while in other devices it has been inserted into the top channel. In the other channels, where there no collagen or the solution, PBS has been used. Five time steps have been chosen to perform the test: 30min, 1h, 1h 30min, 2h, 2h 30min, and at every time step, the PBS inserted has been collected and analysed using the plate reader. The resulting data has been examined using Excel.

2.3 Membrane

2.3.1 Materials: PCL

Polycaprolactone (PCL) is a hydrophobic, linear (fig. 38), synthetic and semicrystalline polymer[41], easy to process and solubilize in common solvents, with high mechanical strength. Its melting point is around 60°C, while its vitreous transition temperature is around -60°C. PCL shows a high molecular weight, good adhesion to different substrates, excellent flexibility and toughness, good stability, and low viscosity[42].

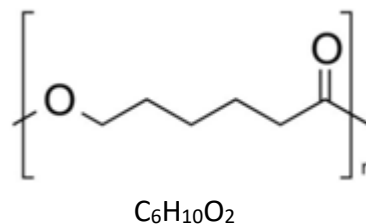


Figure 38 Chemical formula of PCL[42].

This polymer is often used to realize scaffolds for tissue engineering, bioabsorbable device or bioprinting, thanks to its biocompatibility and its ester bonds, that can be simply break through a slow hydrolytic degradation (around 2-3 years, because of its

crystallinity). It is often used in combination with other polymers to realize mixture or copolymer blends, to improve their properties, as degradation rate, for different applications[43]. In this work, PCL has been used in combination with gelatin to realize an electrospun membrane where PSC cells can adhere and proliferate, maintaining the communication with PDAC cells.

2.3.2 Materials: gelatin

Gelatin is a water-soluble protein, derived from different collagen sources, one of the most widespread protein in animals. To obtain gelatin, collagen is denatured, so tertiary and secondary structure of collagen are destroyed through hydrolytic processes. These processes involve a thermal denaturation in mild conditions, around 40°C, and then enzymes, acid or alkali, to break intramolecular bonds. Gelatin can be classified into type A and type B, depending on the implemented collagen treatment; the two processes are the acid process and the basic process, which differ in the substances used to pre-treat collagen before heating it. In the acid process, the resulting gelatin has an isotonic point between 7 and 9, while in the basic one, the resulting gelatin has an isotonic point between 4 and 6.

Gelatin has a high molecular weight, its primary structure and aminoacidic composition follow the primary structure and composition of collagen, as shown in the fig. 39 below.

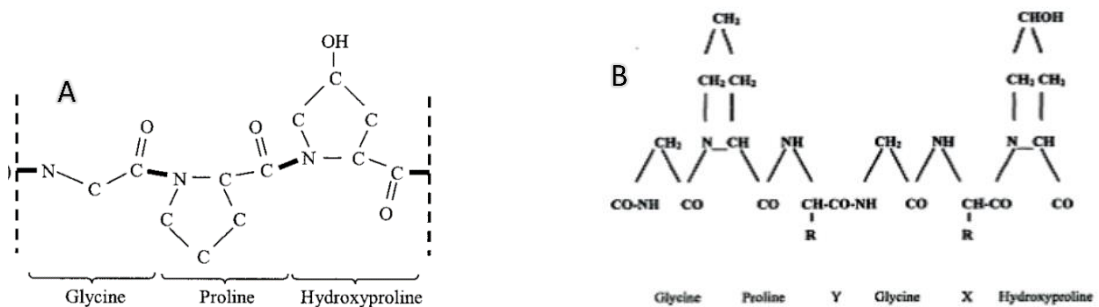


Figure 39 Comparison between collagen and gelatin primary structure: A) collagen primary structure, with the three amino acids which composed it; B) gelatin primary structure, with the amino acids which composed it and their organization[44].

In contact with cold water, gelatin tends to swell, and it goes into solution increasing the temperature above gelatin's melting point, while it forms a gel if it is cooled[44].

2.3.3 PCL/gelatin solution

PCL and gelatin have been used to realize a solution that has been electrospun; the solution has been obtained as explained in the following:

the two polymers, PCL pellet and gelatin powder, have been mixed in a ratio 80:20 weight/weight (w/w), and they have been added to a mixture of acetic acid and formic acid (in the ratio 1:1 volume/volume), to obtain a solution at 15% weight/volume (w/v). Then, the solution was stirred for 24h at room temperature at 250rpm, in order to obtain compact and well-mixed fibres. After that, a 3.68% volume/volume (v/v) of gelatin crosslinker, GPTMS, has been added to the solution, to avoid gelatin degradation. The final solution has been stirred for further 30min, to assure chains tangles formation, and to obtain a transparent solution.

2.3.4 Membrane realization methods: electrospinning

The PCL/gelatin membrane used in this thesis work has been realized through a spinning technique that relies on electric potential, electrospinning. Thanks to electric potential, the surface tension of a solution is overcome by the high electric field and an ultra-thin solution filament is ejected towards a collector, that can be a flat surface or a rotating mandrel; the fibre elongates and solidifies while it travels across the electric field[45]. This technique is frequently used for tissue engineering applications, to mimic ECM structure and properties, both chemical and mechanical ones[46]. Even if the process is simple, the complex physics behind is regulated by many parameters, divided into solution parameters, process parameters and ambient parameters; to govern all the variables of the process it is essential to regulate polymer chemistry, electric field, and environmental conditions. The process parameters are resumed in the table 6 below.

Table 6 Electrospinning process parameters divided into three categories[45].

Solution parameters	Process parameters	Ambient parameters
Material selection	Electromagnetic fields	Humidity
Solvent selection	(strength and orientation)	Temperature
Concentration	Spinning distance	Atmosphere
Viscosity	Solution flow rate	Air movement
Dielectric constant	Spinneret morphology	
Conductivity	Collector morphology	
Surface tension		
Elasticity		

The importance of these variables is tightly tied to the fibres' morphology and the final constructs' defects, as reported into the table 7.

Table 7 Electrospinning parameters influence on the fibre's morphology[47].

Parameters	Effect on fiber morphology
<i>Solution parameters</i>	
Viscosity	Low-beads generation, high-increase in fiber diameter , disappearance of beads.
Polymer concentration	Increase in fiber diameter with increase of concentration.
Molecular weight of polymer	Reduction in the number of beads and droplets with increase of molecular weight.
Conductivity	Decrease in fiber diameter with increase in conductivity.
Surface tension	No conclusive link with fiber morphology, high surface tension results in instability of jets.
<i>Processing parameters</i>	
Applied voltage	Decrease in fiber diameter with increase in voltage.
Distance between tip and collector	Generation of beads with too small and too large distance, minimum distance required for uniform fibers.
Feed rate/Flow rate	Decrease in fiber diameter with decrease in flow rate, generation of beads with too high flow rate.
<i>Ambient parameters</i>	
Humidity	High humidity results in circular pores on the fibers.
Temperature	Increase in temperature results in decrease in fiber diameter.

Therefore, there are some issues to consider:

1. the electric potential, and consequently the applied voltage, has to be high, in order to overcome the solution's surface tension, and to decrease the fibres diameter;
2. the solidification time affects the uniformity and the defect generation, and it depends on the distance between collector and needle and on the evaporation rate of the solvent;
3. the time and the space the polymer jet has to cross influence the fibres dimension, because when it travels droplets tend to elongate and to produce thinner fibres, but they can elongate only at a certain solution fluidity[45].

In this work, the chosen parameters to electrospin the membrane are resumed in the table 8 below, while in the fig. 40 is reported the electrospinner employed for this work (NovaSpider instrument).

Table 8 electrospinning parameters

PCL/gel	parameters
Voltage (kV)	+ 16/-4
Z distance (mm)	160
Flow rate (μl/h)	500
Volume (ml)	5
Stroke (mm)	measured

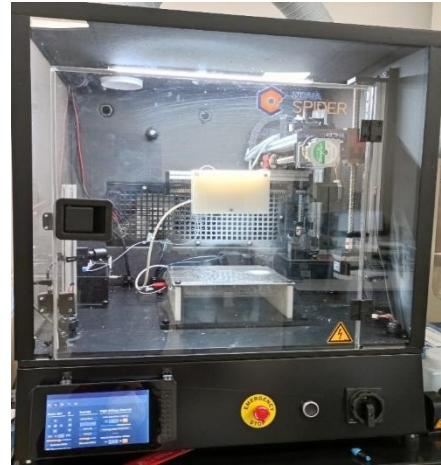


Figure 40 Electrospinner used

This electrospinner presents different sub-systems, such as a **glass syringe**, where the PCL/gel solution is loaded, and whose volume is 5 mL; then the **volumetric pump**, which imposes a continuous pressure on the syringe to extrude the solution, assuring a constant flow rate. There is a **voltage generator**, that forces the selected potential at the **flat collector**, covered by an aluminium foil where nanofibers are deposited, and at the **nozzle** connected to the syringe by a tube.

2.4 Membrane characterization

2.4.1 Scanning Electron Microscope (SEM)

Scanning electron microscopy (SEM) is an imaging technique to study the materials' surface morphology. As other field emission microscopy techniques, this technology is based on the phenomenon of a field emission, in particular an electrons' flux, to obtain the images of metal covered samples (mainly gold covered samples). The metallic surface interacts with electrons, that return on their trajectory, and they are detected by sensors, which convert them into electric signals, used to display the images. All these events happen in ultrahigh vacuum[48]. In this thesis work, SEM has been used to analyse membrane surface after interlayer bonding, to verify if the PDMS layer has spread on all the surfaces or it remained confined into the support realized on the top layer. The membrane samples have been detached from the device, then they have been placed on the stubs, and they have been coated with a thin layer of gold, to obtain the necessary conductive surface for FESEM.

2.5 Cellular components

2.5.1 Material: collagen

Collagen is the most important and abundant animal protein; it represents the 30% of proteins in animals. Its basic unit is called tropocollagen, and it is a rod-shaped



Figure 41 Collagen triple helix with the Gly-X-Y triplets[49]

molecule made by three polypeptide chains, each one contains 1000 amino acids, where the sequence glycine – hydroxyproline – proline (Gly-X-Y) is repeated (fig. 41). Many collagen types consist in two α -1 chains and one α -2 chain, twisted together into a right-handed super helical structure, where hydrogen bonds link the chains[49]. Tropocollagen molecules join together to form fibrils, where the various triple helixes assume parallel staggered positions, in order to assure an overlapping between molecules for $\frac{3}{4}$ of their length. Then, fibrils organize themselves in wavy or parallel arrangement to form fibres, that can reorganize in turn in fibres bundles[50]. In our body there are almost than 28 collagen types, each of them is synthesized by a different set of genes; all the collagen types present the same primary structure, but a different arrangement and different type of tropocollagen α -helix, together with the ability of collagen to assemble itself into different supramolecular structures, because collagen presents two main types of domains: triple helical and globular[49].

Among the most relevant collagen physical and mechanical properties we can mention a high tensile strength, minimal extensibility, the transmission of tensile and compressive force. This protein works in the ECM in cooperation with other ECM molecules, such as glycosaminoglycans and fibronectin, during many physiological pathways, like wound healing, thanks to its chemotactic properties and its promotion of cellular adhesion. Collagen chemical properties, instead, rely on its covalent peptidic bonds, and their comprehend biodegradability, low immunogenicity, controllable stability, solubility[49].

In this thesis work, type I collagen solution Advanced BioMatrix Fibrinol[®] (fig. 42) has been used to realize a hydrogel solution for suspending Human Foreskin Fibroblast 1 (HFF-1). Fibrinol[®] contains 97% of Type I collagen and 3% of Type III collagen, the collagen concentration is 10mg/mL. In the following table 9 there are summarized Fibrinol[®] properties.

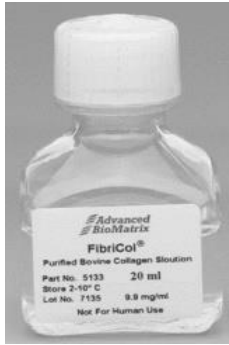


Figure 42 Fibrinol[®] used for HFF1 hydrogel solution[32]

Table 9 Fibrinol[®] physical-chemical properties[32]

Form	Solution
Storage Temperature	2-10°C
Collagen Concentration - Biuret	9.0-11.5 mg/mL
Collagen Purity - Silver	≥99.9%
Staining	
pH	1.9-2.1
Source	Bovine Hide

The collagen hydrogel solution has been prepared mixing together 1 part of PBS 10X and 8 parts of collagen at low temperature, then the whole has been stirred for few minutes at 230rpm. The aim is to obtain a solution with a pH around 7.8, so solution pH has been monitored using a pH paper and sterile 0.1M NaOH has been added when the pH was too low. After NaOH adding, the solution has been stirred again, and, in the end, 1 part of sterile distilled water has been added. All the process has been executed using an ice filled beaker place on the stirrer, to assure the maintenance of collagen at low temperature, to avoid solution reticulation.

2.5.2 Human Foreskin Fibroblasts cells

The Human Foreskin Fibroblast (HFF-1) cell line has been used for mimicking PDAC stroma into bottom layer only; these cells have been suspended into collagen hydrogel to seed them into the bottom layer bonded on a microscope glass. As explained in the first chapter, fibroblasts are connective tissue cells, and they are responsible for ECM components production, so they are useful to study the role of PDAC stroma.

HFF-1 have been purchased from the American type culture collection (ATCC), and they have been grown into DMEM/F-12 (Dulbecco's Modified Eagle Medium/Nutrient Mixture F-12, Gibco, ThermoFisher scientific). It contains glucose

and phenol red in high concentration, to assure a source of energy for cell and a pH indicator for cellular metabolic activities. It is a 1:1 solution of DMEM and Ham's F-12, combining high concentration DMEM with F-12's wide range of components, like vitamins, but the whole doesn't contain proteins, lipids, or growth factors[51].

In this work, DMEM has been enriched with:

- Fetal bovine serum (FBS, Gibco ThermoFisher scientific), 15%, because it is a source of embryonic growth promoting factors, hormones, inorganic minerals, and vitamins, necessary for cell vitality and maintenance;
- Penicillin/streptomycin (P/S, Gibco, ThermoFisher scientific), 1%, an antibiotic to avoid gram-positive/gram-negative contamination;
- L-glutamine (Gibco, ThermoFisher scientific), an aminoacid.

When cultured into flask, HFF-1 assume an elongated shape, but to seed them they have to be detached. For cell splitting, 0.05% trypsin has been used, following the protocol:

- 1- Culture medium removal;
- 2- Cells wash out with Dulbecco's phosphate-buffered saline (DPBS, Gibco), to avoid alteration of trypsin action with the residual serum;
- 3- Trypsin addition, with the consequent flask incubation at 37°C for 3min, to promote trypsin bind with intracellular amino acid sequences and cell-to-substrate proteins and their interruption;
- 4- Observation of cells morphology, if they are round shaped the trypsin has detached them;
- 5- Medium adding, to stop trypsin;
- 6- Aspiration of cell suspension, to place it into a falcon.

After that, cells have to be seeded into bottom layer, resuspending them into collagen; firstly, cells have to be counted, to select the correct volume of cellular suspension to centrifuge and resuspend, because the seeding protocol establishes a certain number of cells for each chip suspended into 3µL of collagen hydrogel. To count cells, 10µL of cell suspension have been dropped into Burker chamber, covered by a microscope glass, to observe it by optical microscopy. The chamber presents two cells, divided into 9 squares with a 1mm sides, and each of them is divided into 16 squares whose dimensions are 0.2x0.2mm. There are other 9 smaller squares with a

0.05mm side and 24 rectangles whose area is 1/100mm², placed between the 1mm side squares[52]. Cells considered are in the four-square grid; the total number of cells is calculated as follow:

$$N^{\circ} \text{ cells} = \frac{\text{count}}{4} * 10000 * \text{suspension Volume}$$

Thereafter, the volume to centrifugate has been calculated with the proportion:

$$N^{\circ} \text{ cell: suspension Volume} = N^{\circ} \text{ cell to seed: Volume to centrifugate}$$

where the N° cell to seed has been calculated as *number of chips * number of cells desired for each chip*. Then, the calculated volume has been centrifuged at 1000rpm for 8min, to separate the solid pellet, that contains cells, from the liquid phase, that has been eliminated. Cells have been resuspended into collagen together with a small quantity of fresh media, to destroy the cellular aggregates. At the end, a small volume of this suspension has been inserted into every chip, while another volume has been poured into transwell plate as control. After seeding, chips and controls have been incubated at 37°C at 5% CO₂ humidity saturated atmosphere, for 30min. Then, culture medium has been added into the two lateral channels thanks to the reservoirs, and it has been replaced every day. In the table 10 below, a summary of the cell quantity used for each experiment.

Table 10 Experiment performed on the bottom layer only with HFF-1: number of cells chosen for each chip, counted cells with Burker chamber, number of chips analysed, centrifuged volume to obtain the right number of cells to resuspend

	Num. cell for chip	Count. Cells	Num. chip	V to centr. (µl)
1° exp	100000	1925000	15	857
2° exp	10000	1627500	12	4200

The microfluidic chips seeded with HFF-1 have been analysed at three different time steps, 24h, 48h, 72h, and for each time step two tests have been performed: live/dead assay and fluorescence imaging.

2.5.3 Human Pancreatic Duct Epithelial cells

Human Pancreatic Duct Epithelial (HPDE) cells are immortalized cell lines, obtained from normal human pancreatic duct cells, frequently used for studying pancreatic duct carcinogenesis[53]. In this thesis work, they have been seeded into top layer channel, in close contact with PCL/GEL membrane, to represent pancreatic epithelia.

The HPDE used cells were purchased from the American type culture collection (ATCC)[32]. These cells have been grown in RPMI media, Roswell Park Memorial Institute (Gibco, ThermoFisher scientific), that contains glutathione and high concentrations of vitamins (biotin, vitamin B12), conversely from other media like Eagle's Minimal Essential Medium or Dulbecco's Modified Eagle Medium[54]. It has been supplemented with:

- fetal bovine serum (FBS, Gibco ThermoFisher scientific), 5%, a source of embryonic growth promoting factors, hormones, inorganic minerals, for cell vitality and maintenance;
- Penicillin/streptomycin (P/S, Gibco, ThermoFisher scientific), 1%, an antibiotic to avoid gram-positive/gram-negative contamination;
- L-glutamine (Gibco, ThermoFisher scientific), an aminoacid.

To seed cells into top layer, they have been detached from the culture flask, and suspended into culture medium. For cell splitting, 0.05% trypsin has been used, following the protocol:

- 1- Culture medium removal;
- 2- Cells wash out with Dulbecco's phosphate-buffered saline (DPBS, Gibco), to avoid alteration of trypsin action with the residual serum;
- 3- Trypsin addition, with the consequent flask incubation at 37°C for 3min, to promote trypsin bind with intracellular amino acid sequences and cell-to-substrate proteins and their interruption;
- 4- Observation of cells morphology;
- 5- Medium adding, to stop trypsin;
- 6- Aspiration of cell suspension, to place it into a falcon.

After that, cells have been counted, to select the correct volume of cellular suspension to centrifugate and resuspend. The seeding protocol establishes 7000cell/ μ L for each device, and each channel's device presents a volume of 5 μ L. To count cells, 10 μ L of cell suspension have been dropped into Burker chamber, covered by a microscope glass, to observe it with optical microscopy. The total number of cells is calculated as follow:

$$N^{\circ} \text{ cells} = \frac{\text{count}}{4} * 10000 * \text{suspension Volume}$$

Thereafter, the volume to centrifugate has been calculated with the proportion:

$$N^{\circ} \text{ cell: suspension Volume} = N^{\circ} \text{ cell to seed: Volume to centrifugate}$$

where the N° cell to seed has been calculated as *number of chips * number of cells desired for each chip*. Then, the calculated volume has been centrifugated at 1000rpm for 5min, to separate the solid pellet, that contains cells, from the liquid phase, that has been eliminated. The solid pellet has been resuspended into culture media, and the cited volume of cells- media solution has been inserted into top layer's channel. In the table 11 below, a summary of the cell quantity used for each experiment.

Table 11 Experiment performed on the top layer only with HPDE: number of cells chosen for each chip, counted cells with Burker chamber, number of chips analysed, centrifugated volume to obtain the right number of cells to resuspend

	Num. cell for chip	Count. Cells	Num. chip	V to centr. (μ l)
1° exp	35000	16975000	12	450
2° exp	140000	950000	8	737

The microfluidic chips seeded with HPDE have been analysed at different time steps, 24h, 48h, 72h, 96h, and for each time step fluorescence imaging has been performed.

2.5.4 Assembled device

Assembled devices have been used for co-culturing HPDE and HFF-1 cells. Firstly, collagen hydrogel has been prepared, UV sterilized and then it has been used for HFF-1 cell seeding. The preparation method has been described in the 2.5.1 paragraph, while the seeding technique has been explained in the 2.5.2 one. After the HFF-1 cell seeding in the bottom layer central channel, the top layer channel has been used for HPDE cell seeding, using the same procedure described in the previous paragraph. In the table 12 below, a summary of cell quantities used for each layer.

Table 12 Experiment performed on assembled device with HFF-1 and HPDE: for each layer cell's density, counted cells with Burker chamber, suspension volume for each channel.

Exper.	Layer	C. density(cell/mL)	Count. Cells	V (μ l)
1° exper.	Bottom	$3.3 \cdot 10^6$	$2.2 \cdot 10^6$	240
	Top	$7 \cdot 10^6$	$3.5 \cdot 10^6$	60
2° exper.	Bottom	$3 \cdot 10^6$	$0,84 \cdot 10^6$	280
	Top	$7 \cdot 10^6$	$0,28 \cdot 10^6$	280

HFF-1 tracking

HFF-1 cells have been pre-treated with CellTracker™ Red CMTPX Dye (ThermoFisher Scientific), a fluorescent dye that allows to monitor cell movement and position. This dye can easily pass-through cells membrane, and it is transformed into a reaction product. It has some properties: it is non-toxic, it is well retained in cellular cytoplasm, it presents a fluorescent signal at physiological pH, that belongs to deep red spectra[55]. To treat cells with CellTracker™ Red CMTPX Dye, it has to be solubilized into dimethyl sulfoxide (DMSO), an organosulfur compound used as polar solvent both for polar and nonpolar compounds[56]. To obtain a 10nM solution, 50µg of CellTracker™ Red CMTPX Dye has been dissolved into 7.3µl of DMSO; then, this solution has been diluted with serum free medium (SFM), a balanced solutions without any supplements and with a defined composition[57], to reach a final concentration of 5µM. For dilution, the following formula has been used: $C_i * V_i = C_f * V_f$, so 4.5µl of first solution have been diluted into 9nL of SFM. At the end, this final solution has been added into the culture flask, where the culture media has been beforehand removed, and the whole has been incubated for 30min.

2.5.5 Fluorescence imaging

To perform fluorescence imaging, seeded cells have been subjected to this procedure:

- For each device, cells have been treated with paraformaldehyde for 40min, that guarantees cells fixation and a good conservation of cellular structures, due to its ability to bind free amino groups of amino acidic lateral chains[58];
- TritonX100 has been used to permeabilize cellular membrane, to facilitate phalloidin access. It is a surfactant and emulsifier, often used for protein solubilization, because it is a mild agent, non-denaturant, but also for living cell membrane permeabilization[59]. Cells have been treated with a solution of TritonX100 in PBS (0.5%) for 10min.
- Cellular proteins have been blocked using a blocking buffer, the bovine serum solution (BSA), that saturate the exceeding protein binding sites[60]. BSA has been diluted in PBS to obtain a 1% BSA solution for the cell treatment, that lasts for 1h.

- Cells have been incubated for 40min with a solution of phalloidin (1:60µl in BSA), (ThermoFisher Scientific), a fluorescent dye that is mainly used for labelling and identifying F-actin in cell cultures[61], [62].
- Then, cells have been incubated for 5min with a solution of 4',6-diamidino-2-phenylindole (DAPI) and PBS, because DAPI is a blue-fluorescent dye, it binds DNA's AT regions. It is used as a nuclear stain in fluorescence microscopy[63]. The final solution has been obtained from an intermediate one, made by 2µl of DAPI in 100µl of PBS; 1µl of this intermediate solution has been diluted into 1ml of PBS.

2.5.6 Live/Dead (L/D) assay for cell viability

This assay is performed using a mixture of two fluorescent dyes, ethidium homodimer (EthD-1) and calcein AM, which differentiate live cells from dead cells. Live cells are died with green dye, the calcein, that is a membrane permeant molecule, because it interacts with intracellular esterase, that enzymatically converts non fluorescent calcein into fluorescent. Fluorescent calcein release a uniform green fluorescence signal between 495nm and 515nm. Dead cells are died with red dye, the ethidium homodimer, which is membrane impermeant; it binds with DNA released by dead cells, increasing its fluorescence 30-fold. The bonded ethidium releases a uniform red fluorescence between 528nm and 635nm[52]. In this work, LIVE/DEAD™ Viability/Cytotoxicity Kit for mammalian cells by ThermoFischer has been used to evaluate HFF-1 viability in the bottom layer and in the controls. The followed protocol is reported above:

- In a PBS filled Eppendorf ethidium 2µL and calcein 0.5µL have been added using the proportion

$$20\mu L(EthD - 1): 10mL (V_{tot}) = x (EthD - 1): 1mL (PBS \text{ solution})$$

$$5\mu L(calcein): 10mL (V_{tot}) = x (calcein): 1mL (PBS \text{ solution})$$

- Culture medium has been removed, while a small volume of L/D solution has been added in each chip and control.
- The whole has been stirred for 20min on a wave plate, then they have been observed at microscope, and the captured green and red channel images have been merged with ImageJ software.

3 Results and discussion

3.1 Microfluidic devices characterization

3.1.1 Digital microscope analysis

The obtained PDMS replicas of bottom, top and reservoir layers have been observed with the digital microscope described in the previous chapter, in order to verify the design and the related measurements. In the following paragraphs a collection of the captured images for each layer (reported in the fig. 43).

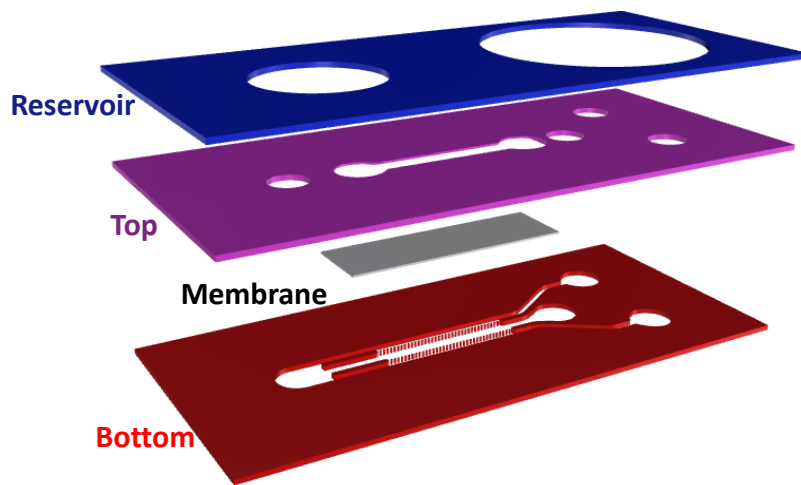
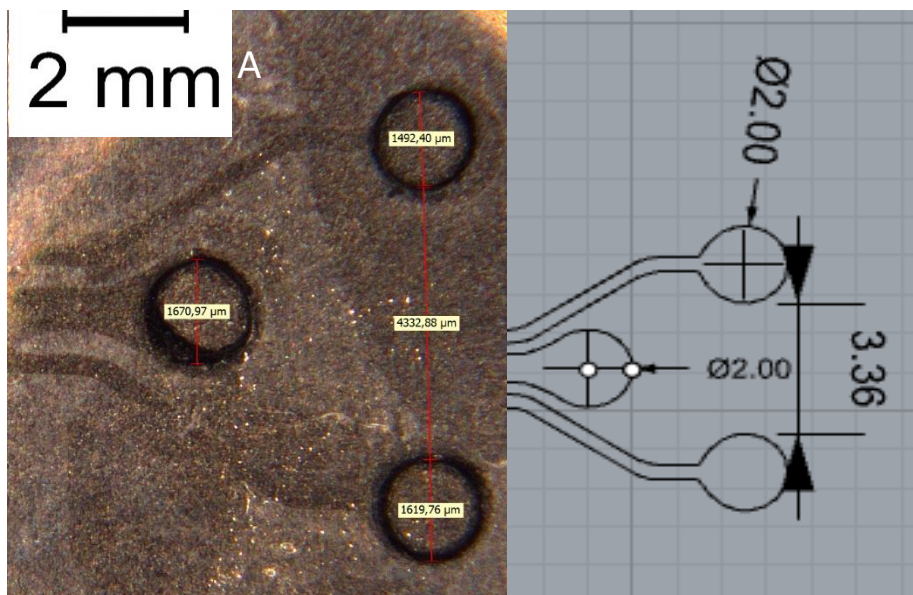


Figure 43 A scheme of the device, with the name of the layers

Bottom layer

In the fig. 44, the geometry dimensions of bottom layer features have been verified.



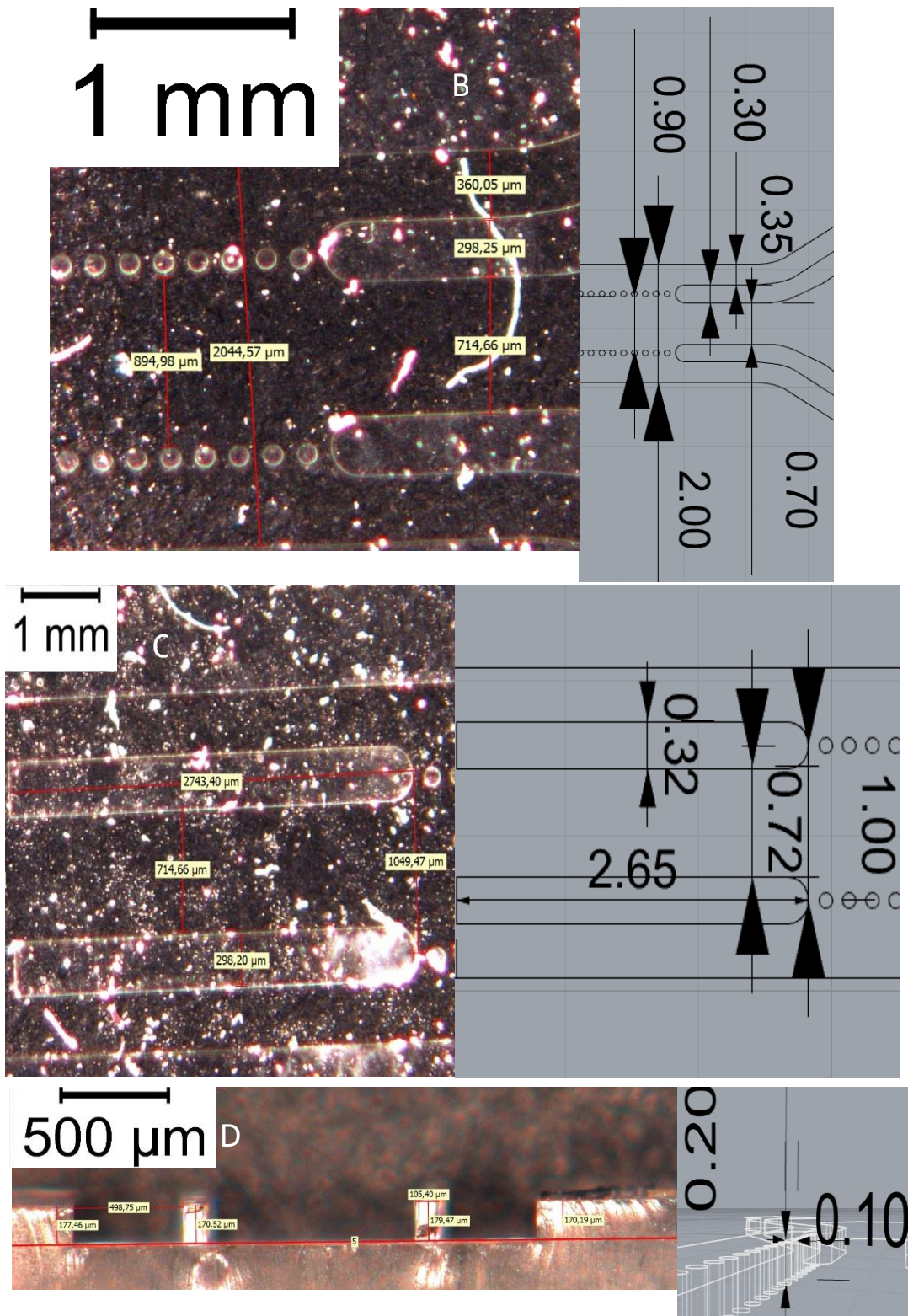
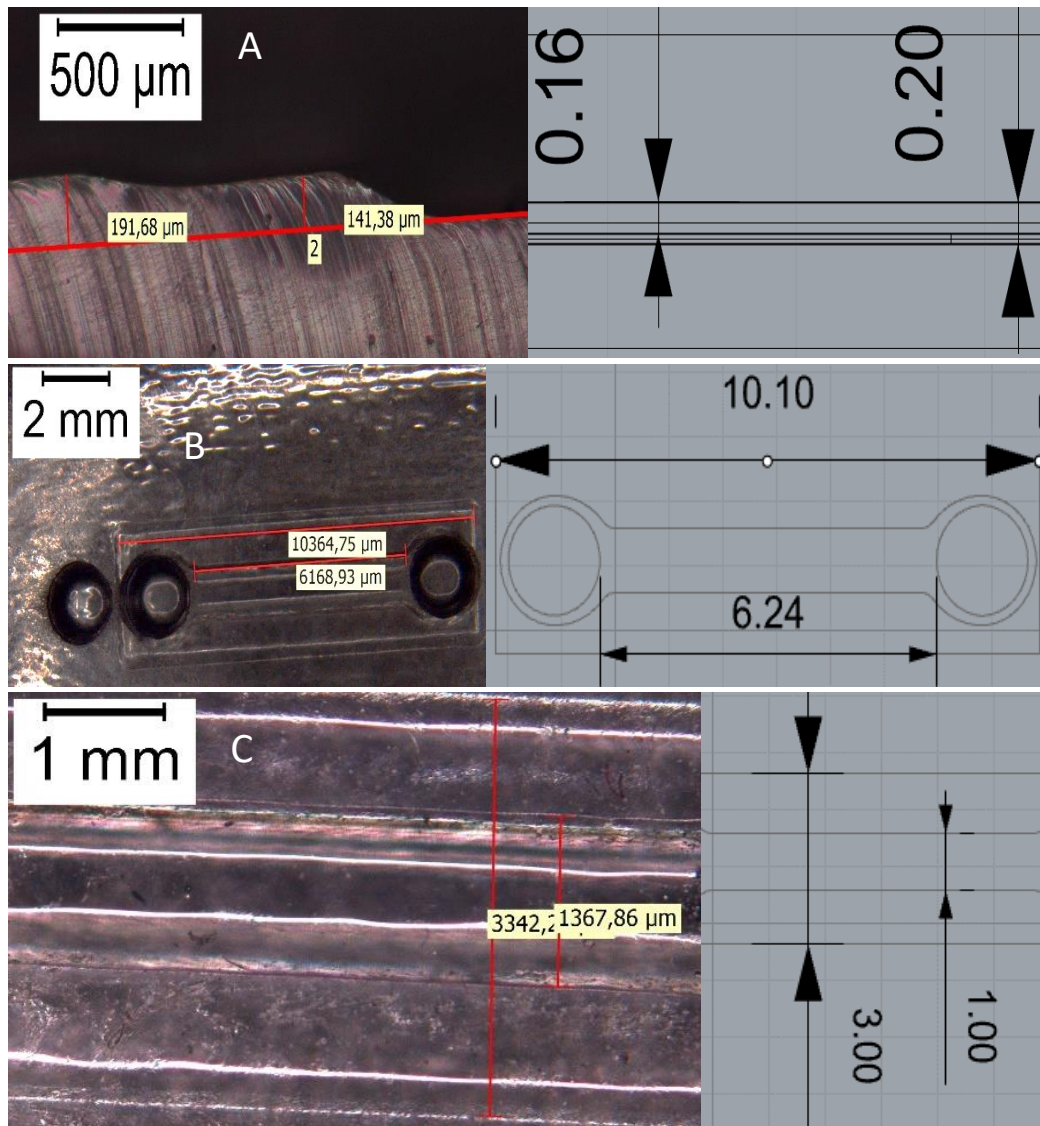


Figure 44 Digital microscope images with acquired measurements in mm: A) bottom layer upper view, with inlets diameter; B) bottom layer upper view, with central and lateral channels width; C) bottom layer upper view, with channels end width and length; D) bottom layer section view, with channels and pillars height and width.

The measurements reveal that the replicas (fig. 44, A-D, left side) present the desired CAD dimensions (fig. 44, A-D, right side), while pillars and lateral channels walls height, that derives from the used SU-8 resist, deviates slightly from the expected value showed in the CAD (fig.44, D, right side). This difference derives from the chosen variables (temperature and times) of the soft lithographic technique, but they are also linked to measurements' acquisition process, because it is largely operator-dependent, this implies that the starting and final acquisition points have been chosen manually; that is the reason why some replicas measurements appear different from CAD ones.

Top layer design

In the fig. 45, the geometry dimensions of top layer features have been verified.



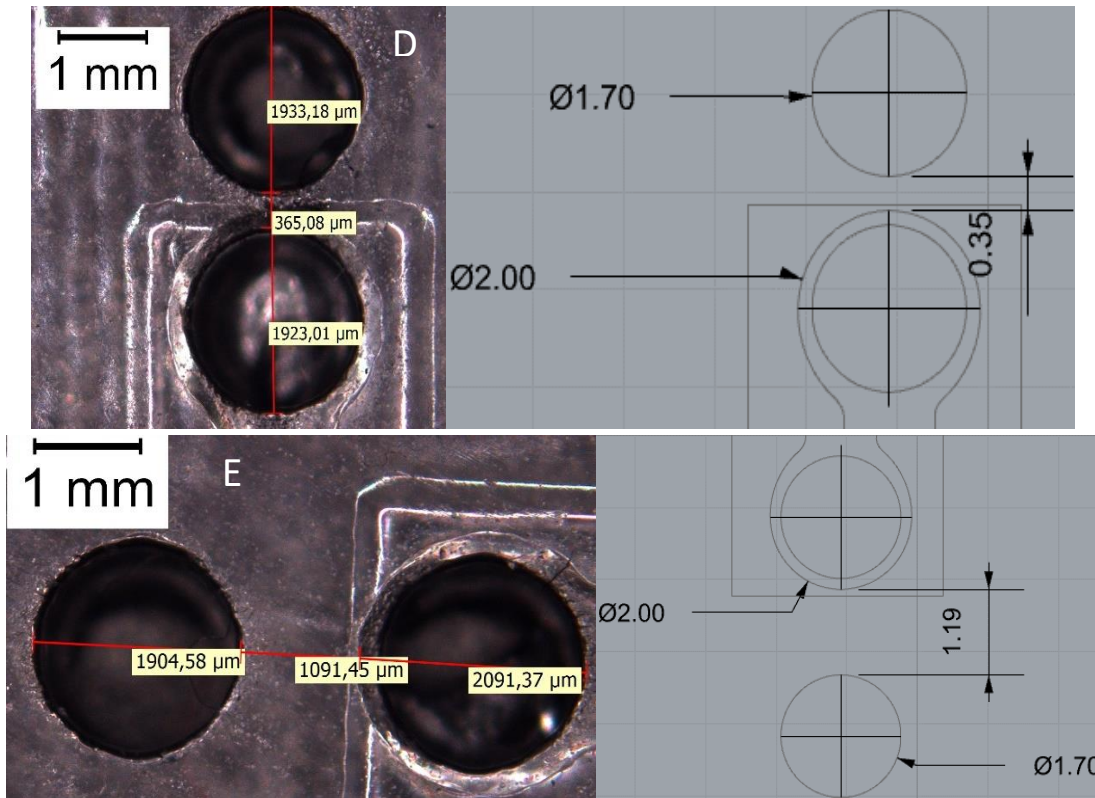


Figure 45 Digital microscope images with acquired measurements in mm: A) top layer section, with channel and membrane insert height; B) top layer upper view, with channel and membrane insert length; C) top layer upper view, with channel and membrane insert width; D) top layer upper view, with inlet holes diameter; E) top layer upper view, with outlet holes diameter

The measurements reveal that the replicas (fig. 45, A-E, left side) present the desired CAD dimensions (fig. 45, A-E, right side), it implies that 3D printing process has produced accurate moulds. The measurement acquisition process is largely operator-dependent, this implies that the starting and final acquisition points have been chosen manually, that is the reason why some replicas measurements appear different from CAD ones.

Assembled device

In the fig. 46 below, a group of assembled devices realized through the techniques described in the previous chapter. These chips have been used for permeability test, for cells seeding and cellular tests described above. These complete devices show the three layers, bonded together, and the membrane, that has been positioned between top and bottom layers.



Figure 46 Assembled devices realized to perform permeability test and for cells seeding

3.1.2 Microfluidic test

Microfluidic performed test shows that the bottom layer's pillar structure assures the desired fluid separation, both with dyed water and with collagen hydrogel, the bonding technique assures the absence of leakage phenomena. In the following fig. 47, a frame acquired with the digital microscope, that shows the test result.

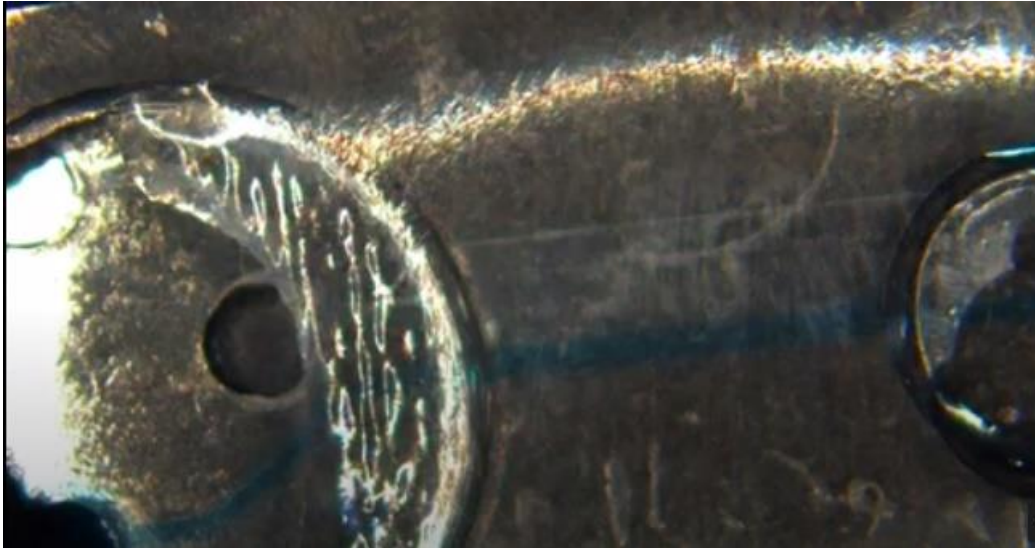


Figure 47 A frame of the video acquired with digital microscope; it shows the filling process of one of the bottom layer's lateral channel with dyed water. This image shows also how the pillar row assure fluid separation between the lateral channel and the central one.

3.1.3 Permeability test

Permeability test has been performed to study the membrane permeability and the interaction between the top layer channel and the bottom layer central channel. The test procedure has been already explained. In this paragraph the results are reported:

- in the table 13 there is fluorescence data obtained with the plate reader is reported. The letter "s" identifies the samples where Dextran has been introduced into the top layer's channel, the letter "g" identifies the samples where Dextran has been introduced into bottom layer's central channel;

Table 53 Fluorescence data obtained with plate reader

time (min)	s	s2	s3	g	g2	g3
0	536	536	536	536	536	536
30	117	231	95	46	125	21
60	22	4	59	51	26	8
90	12	24	7	19	9	14
120	4	4	3	1	4	31
150	4	4	8	14	4	2

- table 14 reports the fluorescence data statistical analysis, performed with Excel. The samples' fluorescence values have been used to calculate the average for each time step and condition, together with the correspondent standard deviation;

Table 14 Fluorescence data statistical analysis

time (min)	s(%)	s2(%)	s3(%)	Avera ge(%)	Std Dev	g (%)	g2(%)	g3(%)	Avera ge(%)	Std Dev
0	100	100	100	100	0	100	100	100	100	0
30	21,83	43,10	17,72	28	0,14	8,58	23,32	3,92	12	0,10
60	4,10	0,75	11,01	5	0,05	9,51	4,85	1,49	5	0,04
90	2,24	4,48	1,31	3	0,02	3,54	1,68	2,61	3	0,01
120	0,75	0,75	0,56	1	0,00	0,19	0,75	5,78	2	0,03
150	0,75	0,75	1,49	1	0,00	2,61	0,75	0,37	1	0,01

- Fig. 48 there is the graphical representation of statistical analysis results, performed with Excel. “Top” is referred to the samples where Dextran has been introduced into top layer’s channel, while “Bottom” identifies the samples where Dextran has been introduced into bottom layer’s central channel.

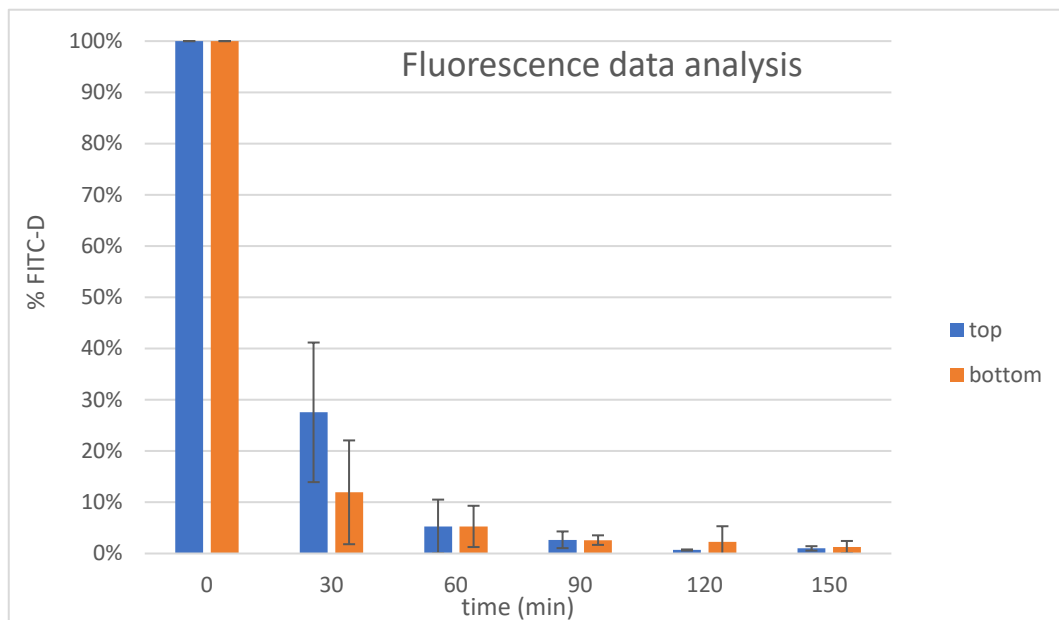


Figure 48 Bar graph of average values, with the related standard deviation values.

The data show that most of the Dextran passes through the membrane in the first thirty minutes, as the first two blue columns (0 and 30) explains; these rapid passages of dextran molecules happen in both cases (from up to down, from down to up), because the blue columns data trend is the same for first two orange columns. Then, dextran molecules flow decreases more and more, and becomes almost absent (less than 10%) in the last two columns, for both blue and orange ones. As the graph shows, the data presents a big standard deviation. These evidence suggest that permeability through the membrane occurs rapidly, in the first few minutes, due to the membrane porosity. This is essential to simulate cells communication between two compartments, as in the PDAC microenvironment, where pancreatic cancer cells release some factors, which stimulate PSC proliferation[12]

3.2 Membrane characterization

3.2.1 Scanning Electron Microscope (SEM)

SEM technique has been used to study the membrane morphology, and to assure the absence of defects, after the interlayer bonding. In fig. 49 below, the obtained images are shown.

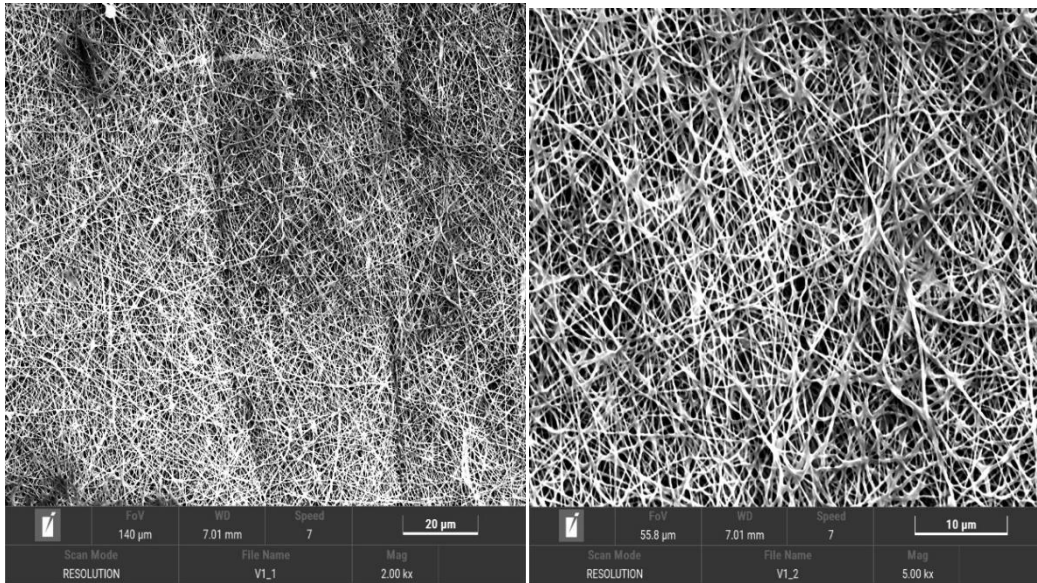


Figure 49 Membrane SEM images at different magnifications. In the first figure, on the right, the scale bar is 20µm, while in the left one is 10µm

The SEM images show that the PDMS has not damaged and imbibed the membrane, and there are not defects. The fibres diameter is in the nanometres order(100-150 nm), and the bonding process temperature has not impaired them (Fig. 49).

3.3 Cellular components

3.3.1 Fluorescence imaging

Cells treated with DAPI/Phalloidin have been observed through fluorescence microscopy, and the collected images have been reported in the following fig. 50-53.

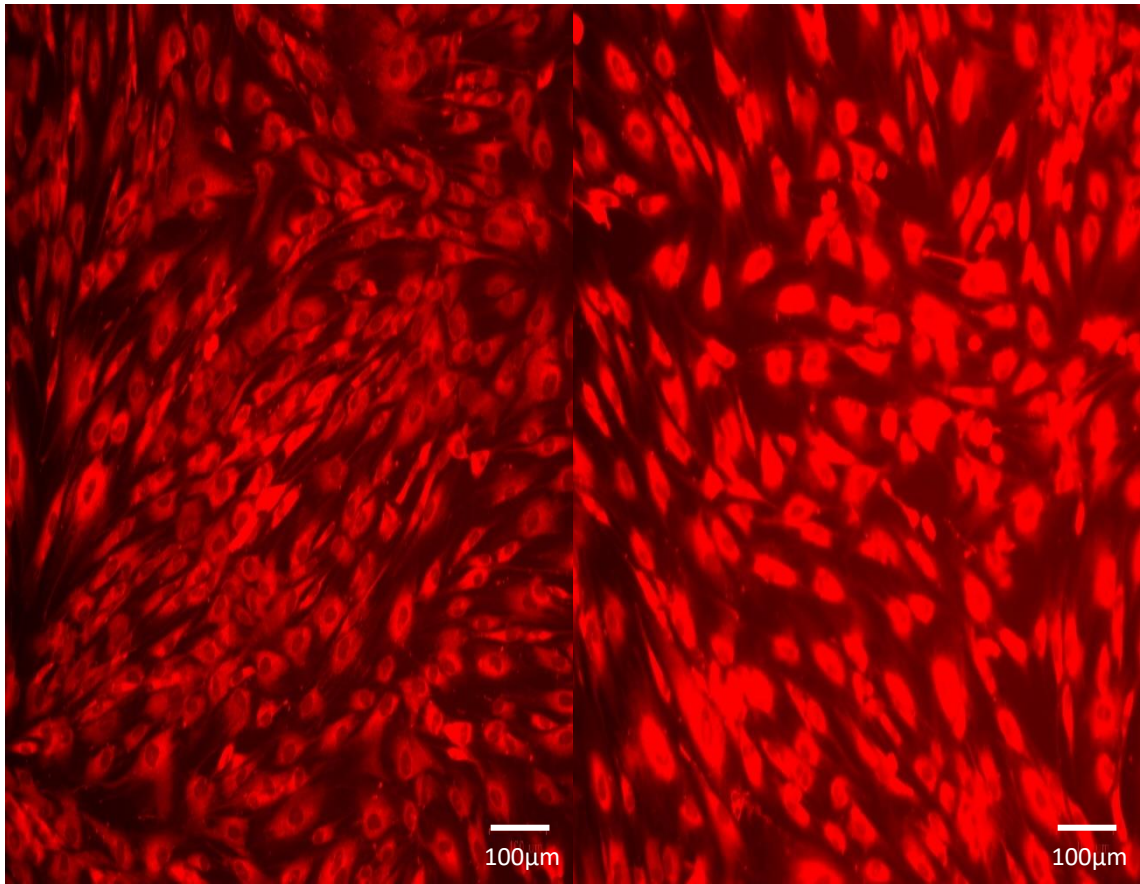


Figure 50 HFF-1 treated cells during the culture time on the flask. The scale bar is 100µm

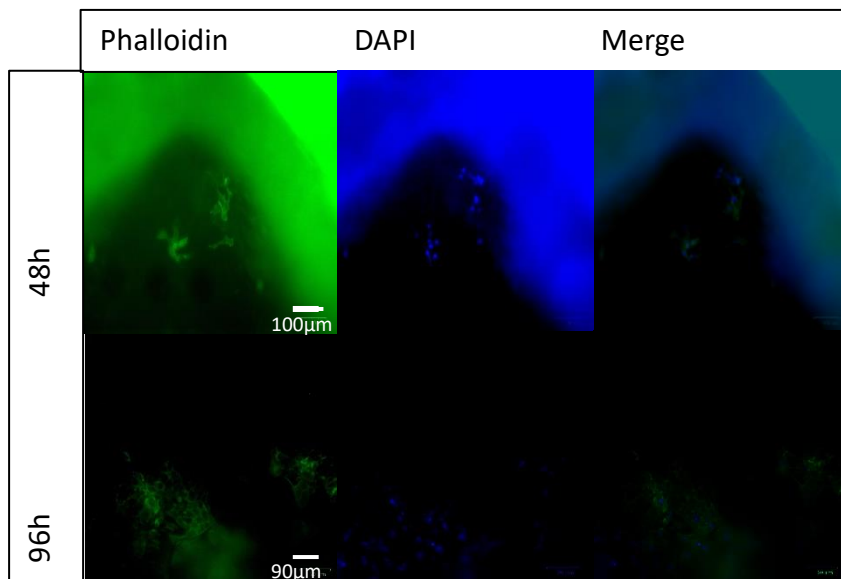


Figure 51 HPDE cells adhered to the membrane of the assembled device, at 48h and 96h.

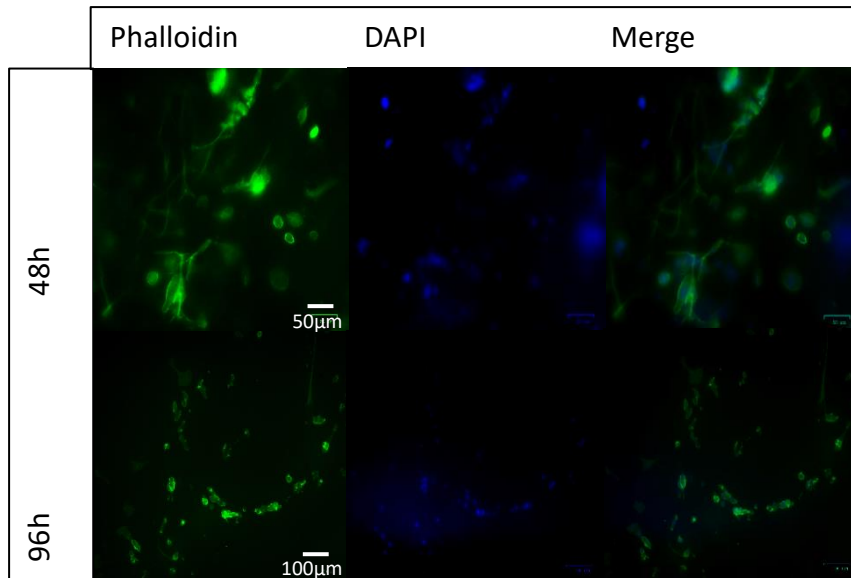


Figure 52 HFF-1 and HPDE cells adhered on the assembled device, at 48h and 96h.

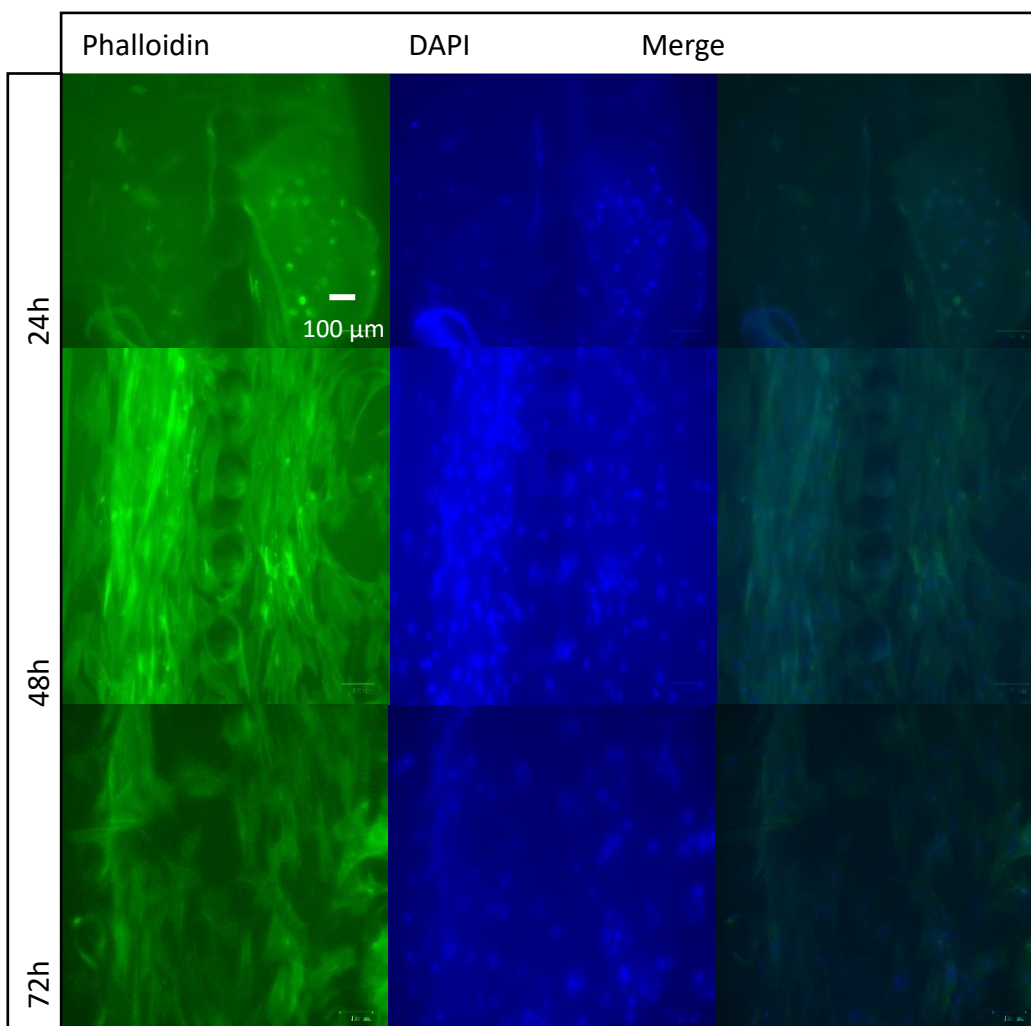


Figure 53 HFF-1 cells seeded in the bottom layer alone, at 24h, 48h and 72h.

The images show that HFF-1 cells can survive and spread in the bottom layer, both when it is bonded with microscope glass (fig. 53) and when it is bounded with top layer (fig. 52). During HFF-1 seeding in the assembled device, the membrane has shown resistance to the collagen hydrogel passage, making the seeding phase difficult and impairing HFF-1 adhesion in the bottom layer of assembled device. To solve this problem, membrane positioning technique should be improved in the handling phase, to avoid that PDMS imbibe the membrane. Alternatively, soft lithographic process should be further optimized in the exposure and baking time, following SU-8 datasheet suggestions [64] to reach thicker features for the bottom layer mould, and consequently deeper channels for the bottom layer channels. HPDE cells can adhere to the membrane in the assembled device, as fig. 52 shows, and they are able also to create connections with HFF-1 cells during coculture (fig. 51). These connections have been constructed in the bottom layer, because HPDE cells came across the membrane, probably following HFF-1's released signals; this phenomenon has been already observed in the Minervini's thesis, between pancreatic stellate cells and HPDE [32]. However, the cell number at 48h and 96h is little, many membrane areas are cell-free, maybe because of the seeding process or the fluorescence imaging process. Seeding process results impaired by the membrane, if it is imbibed by PDMS, that alters membrane wettability; for the directly observation of cell culture, it is necessary to open the assembled device and to handle the membrane, because it obstacles cells examination with microscope. As for the previous work [32], HPDE adhere to the membrane and they assume the characteristic cuboidal shape, so they are still alive at 96h in coculture.

3.3.2 Live/Dead (L/D) assay for cell viability

Live and dead viability assay has been used to assure cells survival on bottom layer alone. In figures 54 a collection of images divided in time steps, 24h, 48h, 72h.

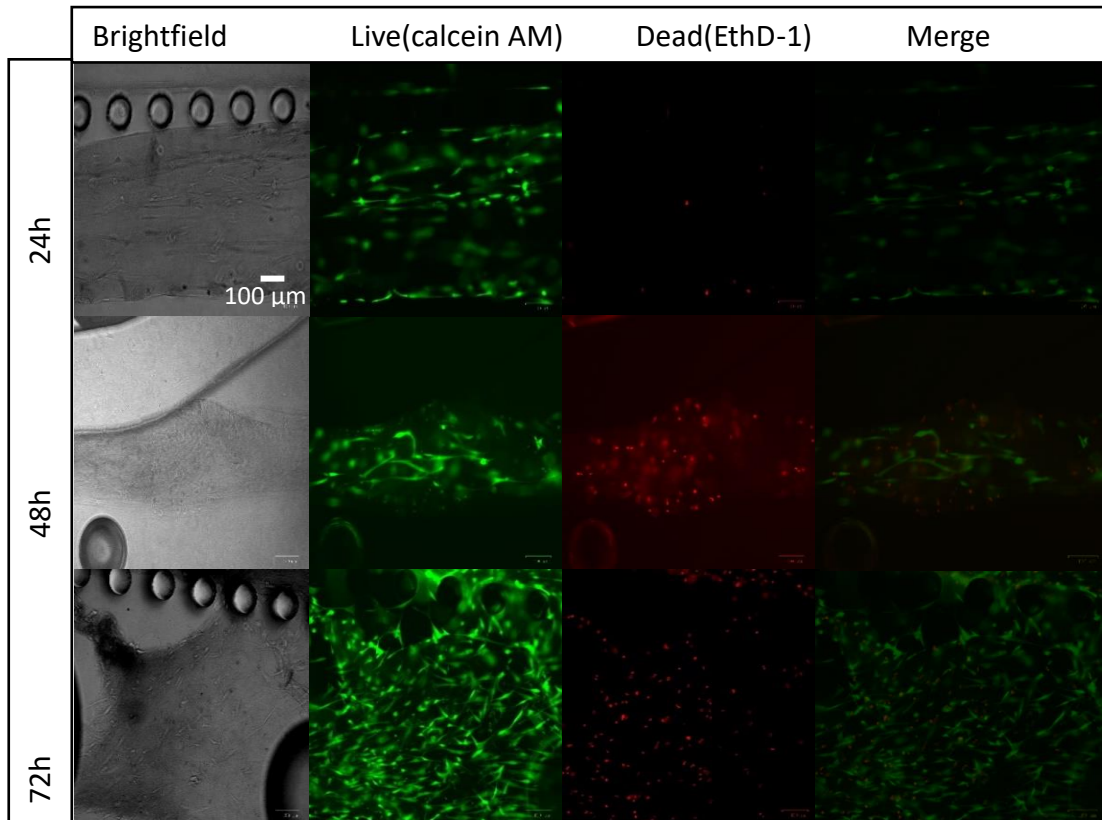


Figure 54 L/D assay performed on HFF-1 cells, seeded in the bottom layer alone, at 24h, 48h and 72h.

The images show that cells seeded into bottom layer are still viable after 72h, as shown by the live columns of fig. 54. The HFF-1 cells also show an elongated shape, suggesting that these cells are attached to the substrate, as explained in the previous chapter. In fig. 54, there is a huge number of HFF-1 cells, that suggest that they have found a good substrate for cellular expansion. In conclusion, this design assures HFF-1 vitality, adhesion and replication. Comparing the HFF-1 cells L/D outcomes with the previous work[32], it is clear that the change in the inlet number has not brought any major variations in the cell culture. The presence of two different inlets for each lateral channel has also guaranteed the possibility to fill every channel with culture media independently, instead of the one inlet solution applied by the previous work[32], that did not assure the filling of both channels. Pillars has not impaired the HFF-1 confluency, as the previous work [32] have already demonstrated; they can also pass through the pillars row, if the seeding procedure is not accurate. Cells can adhere and survive on the PDMS substrate, as expected, because it is a biocompatible

and oxygen permeable materials [24]. These observations suggest that material and geometry are optimal solution for device's bottom layer fabrication.

4 Conclusion and future perspectives

Nowadays, the pancreatic adenocarcinoma is one of the major leading causes of cancer-related death, because of its low survival rate, the difficulties of early diagnosis, its high resistance to treatments. These traits are correlated to its biological features, like the dense stroma and the cellular crosstalk that take place in it. Studying those physiological characteristics through an *in vitro* model, that recapitulates PDAC cellular 3D organization and the tumour microenvironment, it is possible to understand deeply how to treat this pathology and to achieve the early diagnosis. In this scenario, microfluidic devices represent a useful and a powerful tool to fulfil an *in vitro* organ model, whose cellular composition and microenvironment can be controlled. This technology was chosen for its many advantages, as its reduction of reagents volume, the usage of biocompatible and gas permeable materials. A microfluidic chip offers a series of microchannels, that allow to organise the cellular components position and the culture media distribution, to accurately create an *in vivo* like environment. The aim of the work of this thesis project is to develop an organ-on-chip model that recapitulate the acino-ductal unit structure. The developed microfluidic device is composed of three PDMS layer, a bottom layer, a top layer and a reservoir layer; these three layers have been fabricated using replica moulding techniques, and top and bottom layer are divided by a PCL/Gel electrospun microporous membrane. Every single layer replicates a different part of the acino-ductal unit: the bottom layer shows three channels separated by two micropillars rows, used for fibroblast seeding; seeded cells were previously embedded into a collagen hydrogel, to simulate the fibroblast *in vivo* ECM. Bottom layer mould was optimized starting from Beatrice Minervini's project [32] and the Drifka et al. work [8], introducing two separate inlets for lateral channels, and then it was fabricated using SU-8 soft lithographic process, optimized for obtaining a long-term mould to use for REM. The top layer shows one channel epithelial cells seeding; the channel is in communication with the bottom layer's central one through the membrane, that was positioned in a frame on the top layer. The reservoir layer shows two holes to store culture media; reservoir and top layers moulds were fabricated with 3D printing technique. Obtained replicas of bottom and top layer were checked with optical

microscope, to verify their fidelity to designed CAD, and it was found that the CAD dimensions were reproduced successfully, every layer assure that there is not liquid leakage, the pillars' bottom layer can confine fluids in the central channel. Electrospun membrane was observed at SEM to evaluate the presence of defects after positioning process, but no damage was observed after bonding procedure. Then, a permeability test was performed to evaluate the permeability through the membrane: using a fluorescent molecule, it was found that molecules pass through the micropores in few minutes. Moreover, the microfluidic device was tested with cellular components: in the bottom layer, HFF-1 cells were seeded, while in the top layer, HPDE cells were seeded. Cells vitality was verified using Live/Dead assay in the bottom layer alone, and it revealed that cells can survive till 72h, they appear elongated and adherent to the substrate, suggesting that they have found a good substrate for cellular expansion. The channel geometry has not impaired confluency, and the pillars assure the liquid separation. Cell morphology was verified using a combination of DAPI and Phalloidin both on top-bottom layer alone and on assembled device. The test shows that HFF-1 cells spread all over the bottom layer, even during co culturing period, while HPDE are not able to reach the confluency, but they assumed the active shape and they migrated through the membrane, to form physiological-like structure with the HFF-1 cells. The introduced innovation in bottom layer CAD has not affected cells adherence and growth, and the top layer's frame has assured a better way to position electrospun membrane, compared to previous work [32]. Possible future evolution of this device can be the automatization of culture media substitution, the improvement of membrane bonding process, identifying a technique to monitor cells in the assembled device. Furthermore, the crosstalk between cells on top and bottom layer should be evaluated using cell signals, maybe using tumoral cells instead of HPDE wild type. In conclusion, this model of acino-ductal unit can be a starting point for investigating PDAC pathophysiological characteristics, in order to develop new drugs and targeted therapies, and to identify new methodologies for early detection.

5 Bibliography

- [1] “<https://columbiasurgery.org/pancreas/pancreas-and-its-functions>.”
- [2] “<https://www.pinterest.com.au/pin/145522631696314347/>.”
- [3] “<https://www.ncbi.nlm.nih.gov/books/NBK54134/>.”
- [4] P. Sarantis, E. Koustas, A. Papadimitropoulou, A. G. Papavassiliou, and M. v. Karamouzis, “Pancreatic ductal adenocarcinoma: Treatment hurdles, tumor microenvironment and immunotherapy,” *World Journal of Gastrointestinal Oncology*, vol. 12, no. 2. Baishideng Publishing Group Co, pp. 173–181, Feb. 15, 2020. doi: 10.4251/wjgo.v12.i2.173.
- [5] P. Gupta, P. A. Pérez-Mancera, H. Kocher, A. Nisbet, G. Schettino, and E. G. Velliou, “A Novel Scaffold-Based Hybrid Multicellular Model for Pancreatic Ductal Adenocarcinoma—Toward a Better Mimicry of the in vivo Tumor Microenvironment,” *Frontiers in Bioengineering and Biotechnology*, vol. 8, Apr. 2020, doi: 10.3389/fbioe.2020.00290.
- [6] A. McGuigan, P. Kelly, R. C. Turkington, C. Jones, H. G. Coleman, and R. S. McCain, “Pancreatic cancer: A review of clinical diagnosis, epidemiology, treatment and outcomes,” *World Journal of Gastroenterology*, vol. 24, no. 43. Baishideng Publishing Group Co, pp. 4846–4861, Nov. 21, 2018. doi: 10.3748/wjg.v24.i43.4846.
- [7] C. S. Yabar and J. M. Winter, “Pancreatic Cancer: A Review,” *Gastroenterology Clinics of North America*, vol. 45, no. 3. W.B. Saunders, pp. 429–445, Sep. 01, 2016. doi: 10.1016/j.gtc.2016.04.003.
- [8] C. R. Drifka, K. W. Eliceiri, S. M. Weber, and W. J. Kao, “A bioengineered heterotypic stroma-cancer microenvironment

- model to study pancreatic ductal adenocarcinoma,” *Lab on a Chip*, vol. 13, no. 19, pp. 3965–3975, Oct. 2013, doi: 10.1039/c3lc50487e.
- [9] S. R. Nelson and N. Walsh, “Genetic alterations featuring biological models to tailor clinical management of pancreatic cancer patients,” *Cancers*, vol. 12, no. 5. MDPI AG, May 01, 2020. doi: 10.3390/cancers12051233.
- [10] C. D. Logsdon, T. Arumugam, and V. Ramachandran, “Animal models of gastrointestinal and liver diseases. the difficulty of animal modeling of pancreatic cancer for preclinical evaluation of therapeutics,” *American Journal of Physiology - Gastrointestinal and Liver Physiology*, vol. 309, no. 5, pp. G283–G291, Sep. 2015, doi: 10.1152/ajpgi.00169.2015.
- [11] R. W. Cowan and A. Maitra, “Genetic Progression of Pancreatic Cancer,” 2014. [Online]. Available: www.journalppo.com
- [12] R. R. Bynigeri *et al.*, “Pancreatic stellate cell: Pandora’s box for pancreatic disease biology,” *World Journal of Gastroenterology*, vol. 23, no. 3. Baishideng Publishing Group Co, pp. 382–405, Jan. 21, 2017. doi: 10.3748/wjg.v23.i3.382.
- [13] R. Suri, J. W. Zimmerman, and R. A. Burkhart, “Modeling human pancreatic ductal adenocarcinoma for translational research: Current options, challenges, and prospective directions,” *Annals of Pancreatic Cancer*, vol. 3. AME Publishing Company, Dec. 01, 2020. doi: 10.21037/apc-20-29.
- [14] D. Caballero, S. Kaushik, V. M. Correlo, J. M. Oliveira, R. L. Reis, and S. C. Kundu, “Organ-on-chip models of cancer metastasis for future personalized medicine: From chip to the patient,” *Biomaterials*, vol. 149. Elsevier Ltd, pp. 98–115, Dec. 01, 2017. doi: 10.1016/j.biomaterials.2017.10.005.

- [15] C. Ricci, L. Moroni, and S. Danti, "Cancer tissue engineering-new perspectives in understanding the biology of solid tumours-a critical review," *OA Tissue Engineering*, vol. 1, no. 1, Apr. 2013, doi: 10.13172/2052-9643-1-1-607.
- [16] G. Kaushik, M. P. Ponnusamy, and S. K. Batra, "Concise Review: Current Status of Three-Dimensional Organoids as Preclinical Models," *Stem Cells*, vol. 36, no. 9. Wiley-Blackwell, pp. 1329–1340, Sep. 01, 2018. doi: 10.1002/stem.2852.
- [17] M. Kapałczyńska *et al.*, "2D and 3D cell cultures – a comparison of different types of cancer cell cultures," *Archives of Medical Science*, vol. 14, no. 4, pp. 910–919, 2018, doi: 10.5114/aoms.2016.63743.
- [18] R. Augustine *et al.*, "3D Bioprinted cancer models: Revolutionizing personalized cancer therapy," *Translational Oncology*, vol. 14, no. 4. Neoplasia Press, Inc., Apr. 01, 2021. doi: 10.1016/j.tranon.2021.101015.
- [19] N. K. Paschos, W. E. Brown, R. Eswaramoorthy, J. C. Hu, and K. A. Athanasiou, "Advances in tissue engineering through stem cell-based co-culture," *Journal of Tissue Engineering and Regenerative Medicine*, vol. 9, no. 5. John Wiley and Sons Ltd, pp. 488–503, May 01, 2015. doi: 10.1002/term.1870.
- [20] M. Beer *et al.*, "A novel microfluidic 3D platform for culturing pancreatic ductal adenocarcinoma cells: Comparison with in vitro cultures and in vivo xenografts," *Scientific Reports*, vol. 7, no. 1, Dec. 2017, doi: 10.1038/s41598-017-01256-8.
- [21] B. F. L. Lai *et al.*, "Recapitulating Pancreatic Tumor Microenvironment through Synergistic Use of Patient Organoids and Organ-on-a-Chip Vasculature," *Advanced Functional Materials*, vol. 30, no. 48, Nov. 2020, doi: 10.1002/adfm.202000545.

- [22] V. Sgarminato, C. Tonda-Turo, and G. Ciardelli, "Reviewing recently developed technologies to direct cell activity through the control of pore size: From the macro- to the nanoscale," *Journal of Biomedical Materials Research - Part B Applied Biomaterials*, vol. 108, no. 4. John Wiley and Sons Inc., pp. 1176–1185, May 01, 2020. doi: 10.1002/jbm.b.34467.
- [23] M. R. Haque, T. H. Rempert, T. A. Al-Hilal, C. Wang, A. Bhushan, and F. Bishehsari, "Organ-chip models: Opportunities for precision medicine in pancreatic cancer," *Cancers*, vol. 13, no. 17. MDPI, Sep. 01, 2021. doi: 10.3390/cancers13174487.
- [24] S. L. Marasso *et al.*, "Optimized design and fabrication of a microfluidic platform to study single cells and multicellular aggregates in 3D," *Microfluidics and Nanofluidics*, vol. 21, no. 2, Feb. 2017, doi: 10.1007/s10404-017-1872-0.
- [25] O. Nur and M. Willander, "Conventional nanofabrication methods," in *Low Temperature Chemical Nanofabrication*, Elsevier, 2020, pp. 49–86. doi: 10.1016/b978-0-12-813345-3.00003-4.
- [26] G. Ciardelli, "Lezione 5-6-7-8 Tecniche di Micro e Nanofabbricazione top down." 2020.
- [27] "[https://openwetware.org/wiki/Replica_molding_\(REM\)_-_Adam_Selsman](https://openwetware.org/wiki/Replica_molding_(REM)_-_Adam_Selsman)."
- [28] "<http://www.3dprinterscanada.com/3d-printing.php>."
- [29] "<https://www.stratasys.com/it/3d-printers/objet30-pro>."
- [30] F. O. Stark, J. R. Falender, and A. P. Wright, "Silicones," 1982. doi: 10.1016/B978-008046518-0.00016-7.
- [31] "DESIGN E PROGETTAZIONE DI DISPOSITIVI Polymer-Material & Technologies." [Online]. Available: www.microchem.com

- [32] Beatrice Minervini, "In vitro microfluidic 3D platform as a pathological model of the pancreatic acino-ductal unit," Master of Science in biomedical engineering, Politecnico di Torino, Torino, 2021.
- [33] "<https://microtechweb.com/2d/2d.htm>."
- [34] "www.microtechweb.com."
- [35] A. del Campo and C. Greiner, "SU-8: A photoresist for high-aspect-ratio and 3D submicron lithography," *Journal of Micromechanics and Microengineering*, vol. 17, no. 6, Jun. 2007, doi: 10.1088/0960-1317/17/6/R01.
- [36] C. Saenz, "Microfluidics/Microfabrication Facility, HMS PROCEDURE FOR SILANIZATION OF SU-8/SILICON MASTER Microfabrication Core Facility, Harvard Medical School."
- [37] I. Carmagnola, "Modifiche superficiali-Tecnica Layer by Layer." Torino, 2021.
- [38] "https://en.wikipedia.org/wiki/Digital_microscope#mw-head."
- [39] "<https://www.tecnolabor.it/Prodotti.aspx?menuId=100&id=249>."
- [40] "<https://www.sigmaaldrich.com/IT/it/technical-documents/technical-article/cell-culture-and-cell-culture-analysis/cell-based-assays/fluorescein-isothiocyanate-dextran>."
- [41] M. Dehghan, M. K. Mehrizi, and H. Nikukar, "Modeling and optimizing a polycaprolactone/gelatin/polydimethylsiloxane nanofiber scaffold for tissue engineering: using response surface methodology," *Journal of the Textile Institute*, vol. 112, no. 3, pp. 482–493, 2021, doi: 10.1080/00405000.2020.1766317.
- [42] "<https://www.xpolymers.it/pcl.html>."

- [43] S. Doppalapudi, A. Jain, W. Khan, and A. J. Domb, "Biodegradable polymers-an overview," *Polymers for Advanced Technologies*, vol. 25, no. 5. John Wiley and Sons Ltd, pp. 427–435, 2014. doi: 10.1002/pat.3305.
- [44] A. Mariod, "Characterization of a thermostable mannitol dehydrogenase from hyperthermophilic *Thermotoga neapolitana* DSM 4359 with potential application in mannitol production View project Unconventional sources of vegetable oils View project," 2013. [Online]. Available: <https://www.researchgate.net/publication/236735648>
- [45] B. Robb and B. Lennox, "The electrospinning process, conditions and control," in *Electrospinning for Tissue Regeneration*, Elsevier, 2011, pp. 51–66. doi: 10.1533/9780857092915.1.51.
- [46] R. Sahay *et al.*, "Electrospun composite nanofibers and their multifaceted applications," *Journal of Materials Chemistry*, vol. 22, no. 26, pp. 12953–12971, Jul. 2012, doi: 10.1039/c2jm30966a.
- [47] N. Bhardwaj and S. C. Kundu, "Electrospinning: A fascinating fiber fabrication technique," *Biotechnology Advances*, vol. 28, no. 3. pp. 325–347, May 2010. doi: 10.1016/j.biotechadv.2010.01.004.
- [48] "https://en.wikipedia.org/wiki/Field-emission_microscopy#mw-head."
- [49] "https://journals.lww.com/implantdent/Fulltext/2002/07000/Collagen__An_Overview.14.aspx."
- [50] "<https://en.wikipedia.org/wiki/Collagen>."
- [51] "<https://www.thermofisher.com/order/catalog/product/11320033>."

- [52] “<https://www.abcam.com/live-and-dead-cell-assay-ab115347.html>.”
- [53] “Human Pancreatic Duct Epithelial Cell Line (H6c7) - Kerafast.”
<https://www.kerafast.com/productgroup/531/human-pancreatic-duct-epithelial-cell-line-h6c7> (accessed May 24, 2022).
- [54] “RPMI 1640 Media | Thermo Fisher Scientific - IT.”
https://www.thermofisher.com/it/en/home/life-science/cell-culture/mammalian-cell-culture/classical-media/rpmi.html?s_kwcid=AL!3652!3!596365170860!p!!g!!rpmi&ef_id=EAlalQobChMlir--1tD49wIV6e3mCh0ERAqlEAAAYASAAEgI4DPD_BwE:G:s&s_kwcid=AL!3652!3!596365170860!p!!g!!rpmi&cid=bid_clb_cce_r01_co_cp0000_pjt0000_bid00000_0se_gaw_nt_pur_con&gclid=EAlalQobChMlir--1tD49wIV6e3mCh0ERAqlEAAAYASAAEgI4DPD_BwE (accessed May 24, 2022).
- [55] “CellTracker™ Red CMTPX Dye.”
<https://www.thermofisher.com/order/catalog/product/cn/en/C34552> (accessed Jun. 03, 2022).
- [56] “Dimethyl sulfoxide - Wikipedia.”
https://en.wikipedia.org/wiki/Dimethyl_sulfoxide (accessed Jun. 03, 2022).
- [57] “Serum-free Cell Culture Media.”
<https://www.westburg.eu/blog/serum-free-cell-culture-media> (accessed Jun. 03, 2022).
- [58] asimone, “METODI DI FISSAZIONE CELLULARE.” Accessed: Jun. 05, 2022. [Online]. Available: <https://doc.studenti.it/dispense/genetica/metodi-fissazione-cellulare-appunti-genetica.html>

- [59] "Triton X-100 Sigma-Aldrich CAS No.9036-19-5."
<https://www.sigmaaldrich.com/IT/it/product/sial/x100>
(accessed Jun. 05, 2022).
- [60] "Blocking buffer, Blocker™ BSA (10X) in PBS or TBS | VWR."
<https://it.vwr.com/store/product/18524237/blocking-buffer-blockertm-bsa-10x-in-pbs-or-tbs> (accessed Jun. 05, 2022).
- [61] "Phalloidin Conjugates for Actin Staining | Thermo Fisher Scientific - IT." <https://www.thermofisher.com/it/en/home/life-science/cell-analysis/cell-structure/cytoskeleton/phalloidin-and-phalloidin-conjugates-for-staining-actin.html> (accessed Jun. 05, 2022).
- [62] PromoKine, "General Phalloidin Staining Protocol." 2018. [Online]. Available: www.promocell.com
- [63] "DAPI (4',6-Diamidino-2-Phenylindole, Dihydrochloride)."
<https://www.thermofisher.com/order/catalog/product/D1306>
(accessed Jun. 05, 2022).
- [64] "SU-8 2000 Permanent Epoxy Negative Photoresist PROCESSING GUIDELINES FOR." [Online]. Available: www.atgc.co.jp
- [65] "Kapton - Wikipedia." <https://en.wikipedia.org/wiki/Kapton>
(accessed Jun. 22, 2022).
- [66] "The multiple uses of Kapton™ tape |."
<http://alltapesdepot.com/los-multiples-usos-de-la-cinta-kapton/> (accessed Jun. 22, 2022).
- [67] "The 6 main properties of Kapton® polyimide films | ADDEV Materials." <https://www.addevmaterials.us/en/actualite/6-main-properties-kapton-polyimide-films> (accessed Jun. 22, 2022).
- [68] R. Jose Varghese, E. H. M. Sakho, S. Parani, S. Thomas, O. S. Oluwafemi, and J. Wu, "Introduction to nanomaterials: Synthesis

and applications,” in *Nanomaterials for Solar Cell Applications*, Elsevier, 2019, pp. 75–95. doi: 10.1016/B978-0-12-813337-8.00003-5.

- [69] “<https://www.elveflow.com/microfluidic-reviews/soft-lithography-microfabrication/su-8-mold-lithography/>.”
- [70] “Microla Optoelectronics s.r.l. - Marcaturo laser stand-alone LASER Slider.” <https://www.micro-la.com/open/product/7/marcaturo-laser-standalone-laser-slider> (accessed Jun. 22, 2022).

6 Addendum

6.1 CAD bottom layer

As mentioned in the chapter 2, some tests have been performed in order to fabricate the bottom layer mould through the 3D printer. The equipment presents a limit in the features minimum dimension, so the previous bottom CAD (Beatrice Minervini's one[32]) has been modified to overcome the problem. In particular, to obtain holes large and deep enough for the pillars, a pillars diameter of 350 μm has been chosen (fig. 6-1).

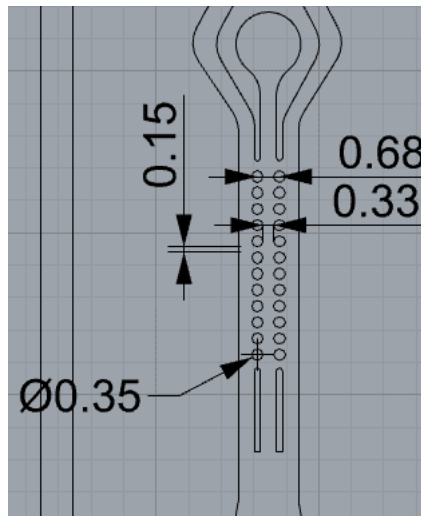


Figure 6-1 CAD realized for 3D printer with pillars diameter of 350 μm

The resulting mould has been used to obtain some replicas, all of them have shown a wrong diameter and a small height (fig. 6-2), a signal that there is another problem to consider, the features aspect ratio.

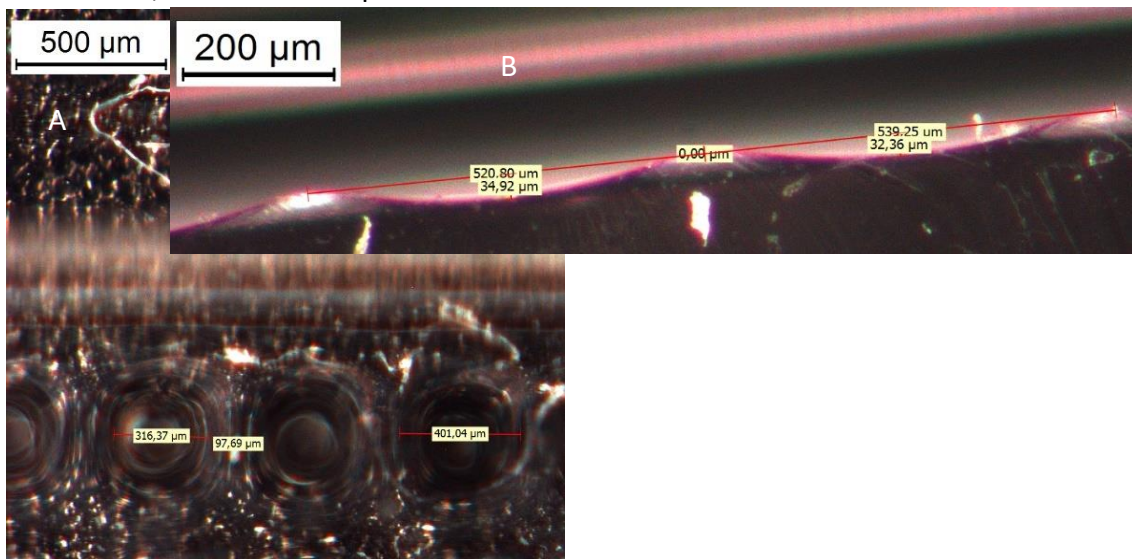


Figure 6-2 digital microscope images of pillars diameters (A) and their height (B)

To solve this new problem, the CAD has been modified again, increasing pillars' diameter ($500\mu\text{m}$), the gap between the holes ($180\mu\text{m}$), and their height ($350\mu\text{m}$). The obtained replicas have shown that this is not the right solution to 3D print the masters, as reported in the fig. 6-3.

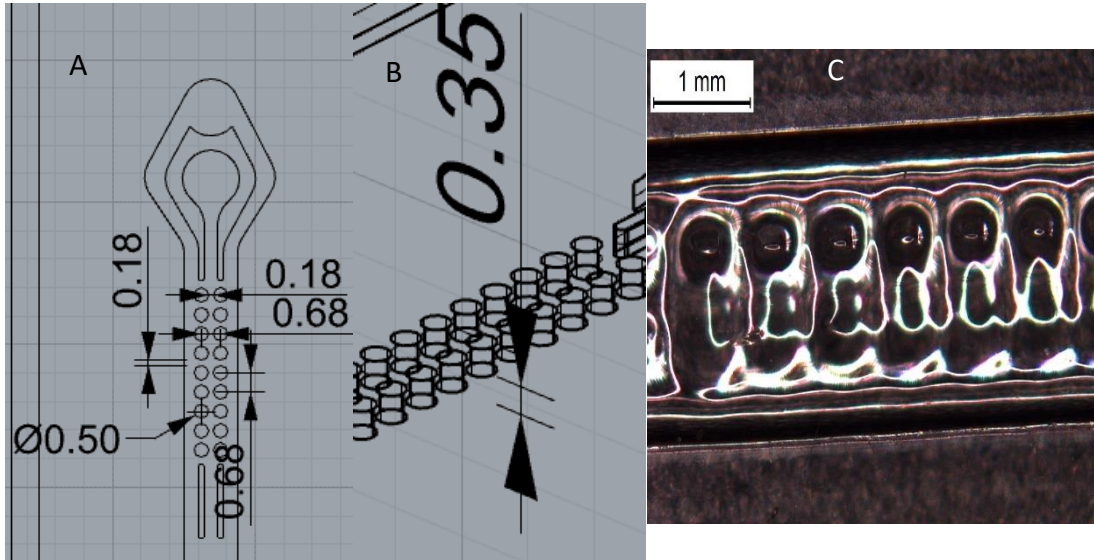


Figure 6-3 CAD and replica of the bottom layer second version: A) upper CAD view, B) prospected CAD view, C) upper replica view, that shows the lack of pillars.

In the last 3D printed version, pillars have been substituted by three segments (length = 1.35mm , width = $350\mu\text{m}$, height = $350\mu\text{m}$), as shown in the fig. 6-4. They have to divide the central channel from the lateral ones, and to sustain the membrane. Ideally, these segments permit to bypass the arisen critical issues, assuring the same pillars' microfluidic function intact.

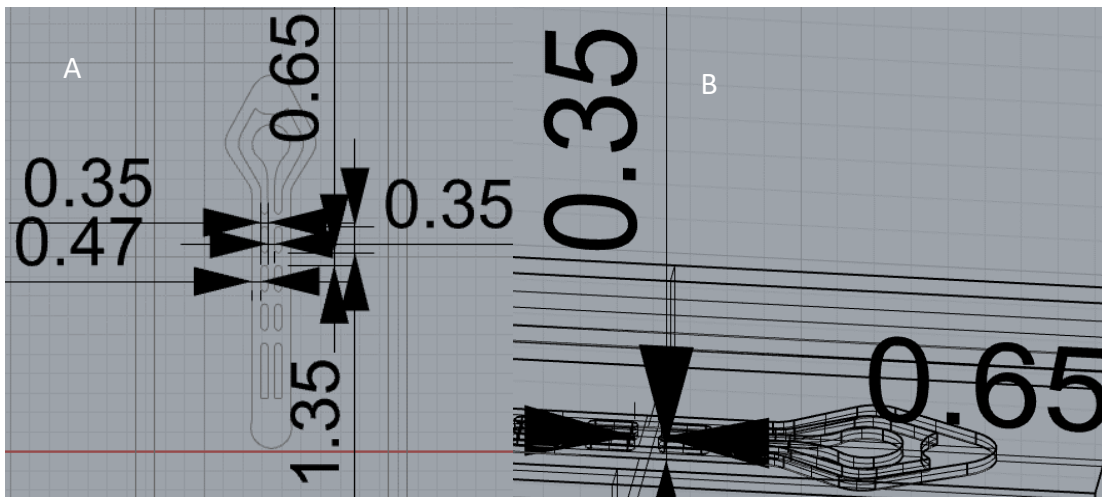


Figure 6-4 Bottom layer CAD where pillars have been replaced with segments: A) upper CAD view, B) lateral view.

The replicas in the fig. 5-5 show the desired geometry, but a functional problem has appeared during microfluidic tests, the fluid in the central channel is not confined by the segments. This could have been a problem for HFF1 seeding, because the collagen hydrogel has to be confined to assure the right cell seed in the central channel.

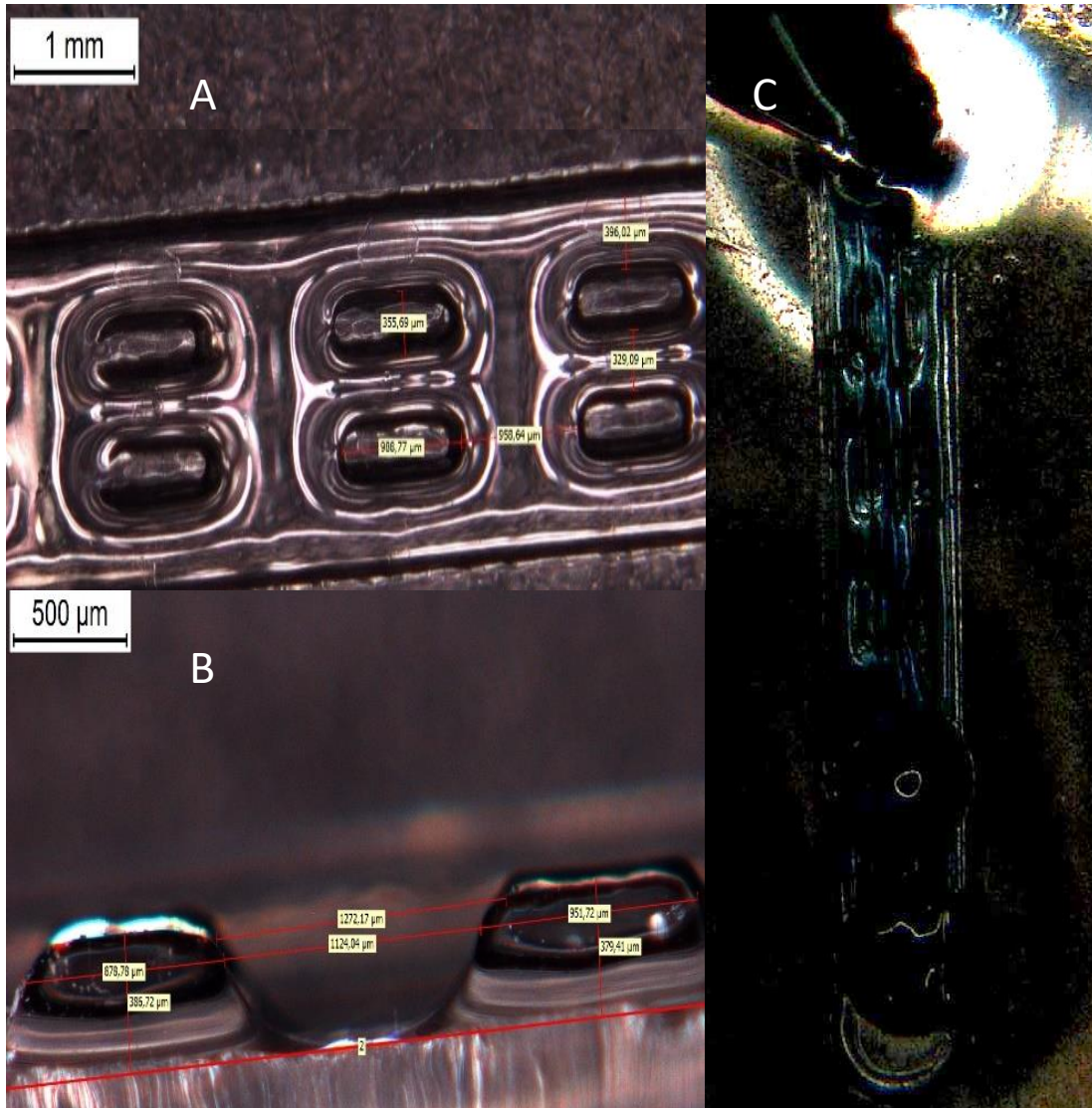


Figure 6-5 Digital microscope images of bottom layer replicas with segments: A) upper view with measurements; B) a section realized to measure segments height, C) a frame to show the lack of fluid confinement in the central channel.

At the end of these tests, the chosen fabrication technique has been the SU-8 soft lithographic process.

6.2 SU-8 soft lithographic process optimization

Soft lithographic process used in this thesis work has been optimized through many tests, whose aim is to reach the best conditions for a long-standing SU-8 master. In the tables 1-3 below, there is a collection of the various parameters used for this optimization.

Table 6-1 Mask for 4 inches Si wafer (fig. 5-6)

n. test	Soft bake	PEB	Exposure	Method	Result
1	8min@65°C, 40min@95°C	5min@65°C, 20min@95°C	50s	T* ramp up, no pre-treat, ramp down	Failed during development
2	8min@65°C, 40min@95°C	5min@65°C, 20min@95°C	50s	T* ramp up SB, no pre-treat, ramp down SB-PEB-HB	Failed after PDMS pouring
3	8min@65°C, 60min@95°C	5min@65°C, 20min@95°C	50s	T* ramp up, no pre-treat, ramp down SB-PEB-HB	Failed after PDMS pouring
4	8min@65°C, 40min@95°C	5min@65°C, 20min@95°C	50s	T* ramp up, Omnicoat pre-treat, no ramp down	Failed during development
5	8min@65°C, 40min@95°C	5min@65°C, 20min@95°C	90s	T* ramp up, no pre-treat, ramp down SB-PEB-HB	Failed after HB
6	8min@65°C, 30min@95°C	5min@65°C, 20min@95°C	50s	T* ramp up, no pre-treat, ramp down SB-PEB-HB	Failed after silanization

*T = abbrev. For temperature

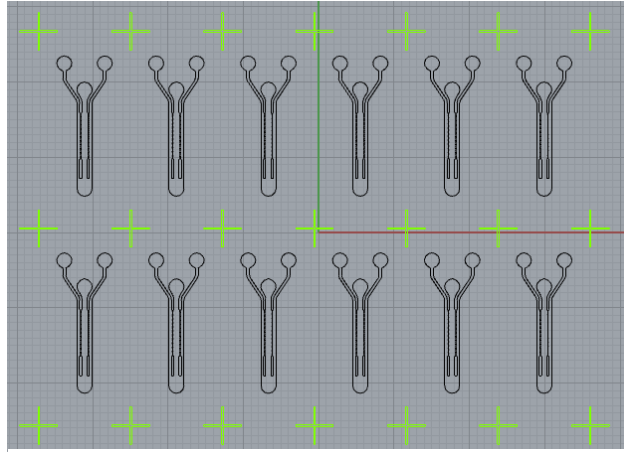


Figure 6-6 CAD realized for the 4 inches wafer's mask

Table 6-2 New mask for 2 inches wafer (fig. 6-7)

n. test	Soft bake	PEB	Exposure	Method	Result
1	8min@65°C, 40min@95°C	5min@65°C, 20min@95°C	140s	T* ramp up, pre-treat 15min@200°C, ramp down PEB-HB	Failed during development
2	8min@65°C, 30min@95°C	5min@65°C, 20min@95°C	50s	T* ramp up, pre-treat 15min@200°C, ramp down PEB-HB	Failed after HB
3	8min@65°C, 35min@95°C	5min@65°C, 20min@95°C	50s	T* ramp up, pre-treat 15min@200°C, ramp down PEB-HB	Failed during development
4	8min@65°C, 20min@95°C	5min@65°C, 20min@95°C	50s	T* ramp up, pre-treat 15min@200°C, ramp down PEB-HB	Failed during development

*T = abbrev. For temperature

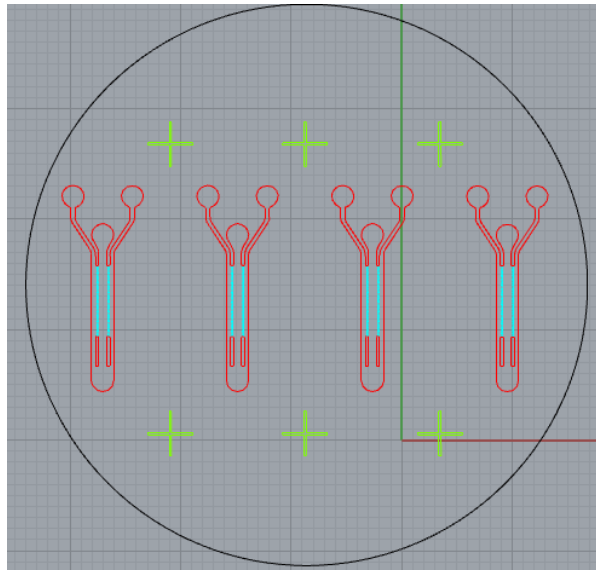


Figure 6-7 CAD realized for the 2 inches wafer's mask

Table 6-3 New mask for 2 inches SiO₂ wafer (fig. 6-8)

n. test	Soft bake	PEB	Exposure	Method	Result
1	8min@65°C, 40min@95°C	5min@65°C, 20min@95°C	50s	T* ramp up, pre-treat 15min@200°C, no ramp down	Failed during development
2	8min@65°C, 40min@95°C	5min@65°C, 20min@95°C	150s	T* ramp up, pre-treat 15min@200°C, no ramp down	Failed after HB
3	8min@65°C, 40min@95°C	5min@65°C, 20min@95°C	50s	T* ramp up, pre-treat 15min@200°C, no ramp down	Failed after HB
4	8min@65°C, 40min@95°C	5min@65°C, 20min@95°C	50s	T* ramp up, pre-treat 15min@200°C, ramp down PEB- HB	stable

*T = abbrev. For temperature

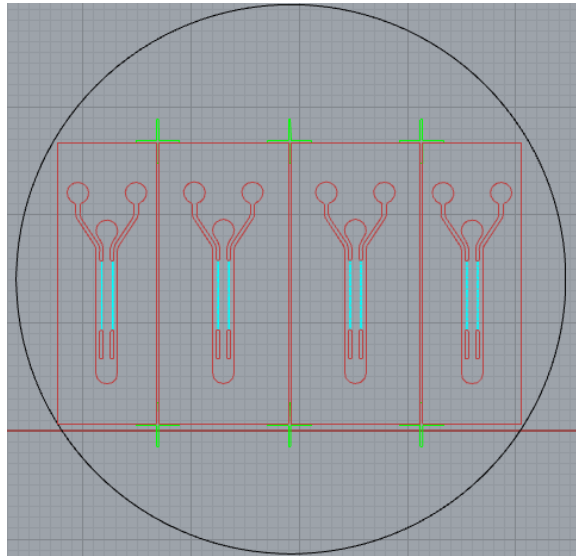


Figure 6-8 CAD realized for the 2 inches SiO₂ wafer's mask

The 6-3.4 (table 6-3, 4) recipe has been repeated on 4 inches SiO₂ wafer, using the first realized mask (fig. 6-6), and it proved to be repeatable, it assured a long-term stable master for PDMS.

6.3 Bottom layer PDMS master

Using the described 3.4 SU-8 soft lithography recipe on a 2 inches wafer, a PDMS master for bottom layer has been realized, using the geometry reported in the fig. 6-8 as mask. The lithographic process has been used for obtaining a geometry negative in PDMS, that has been silanized and then used for replica molding. The silanization method used is the following:

- **Solution preparation:** a solution has been prepared pouring toluene and trichloromethylsilane into a Petri dish, with a ratio of 1:10.
- **Rest:** the PDMS master has been immersed into the solution and it has been left submerged for 3h.
- **Submersion:** the PDMS master has been immersed into IPA and it has been left submerged for 1h.
- **Washing and baking:** the wafer has been washed with IPA and dried with nitrogen, then it has been baked at 80°C overnight into the oven.

The master has been used to realize some replicas, together with the SU-8 master obtained with 4 inches SiO₂ wafer.

6.4 Kapton

Before the insertion of a frame to position the membrane, the first idea has been the usage of a Kapton tape element for keeping the membrane in place and in line.

Kapton tape is a polyimide adhesive tape, obtained by the in-step polymerization of pyromellitic dianhydride (PMDA) and 4,4'-oxydiphenylamine (ODA) (fig.6-9).[65]

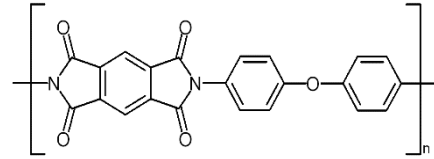


Figure 6-9 Chemical structure of Kapton[65]

Kapton tape has been introduced by DuPont Corporation in the 1960s, and it has a wide range of applications, from flexible printed circuits (flexible electronics) to satellites[66], thanks to its properties:

- Thermal stability, from -269 to 400°C[66], so it offers a great heat resistance and a reduced thermal expansion coefficient[65];
- Mechanical resistance, because of its elastic modulus, from 2,5GPa (at 23°C) to 2,0GPa (at 200°C), that assures tear resistance, resistance to frictional mechanical abrasion[67];
- Resistance to chemicals, like organic solvents and acids[67].

The Kapton tape has been cut through laser ablation technique, using the LASER Slider Marker System by Microla (fig. 6-10). Laser ablation is a process that permits



Figure 6-10 LASER Slider Marker System by Microla[70]

to cut with high precision different materials, using the appropriate parameters; the CO₂ laser, that work at 25-50W, is driven by a galvanometric head, and it can penetrate the sample surface[32], [68]. The sample is positioned on a slider, while the head orients the laser on the surface following the loaded CAD design (fig. 6-11).

The areas touched by the laser are subjected to a high electric field, that removes electrons and leads to the heating and vaporization of the surface. This process happens in vacuum or gaseous atmosphere[68].

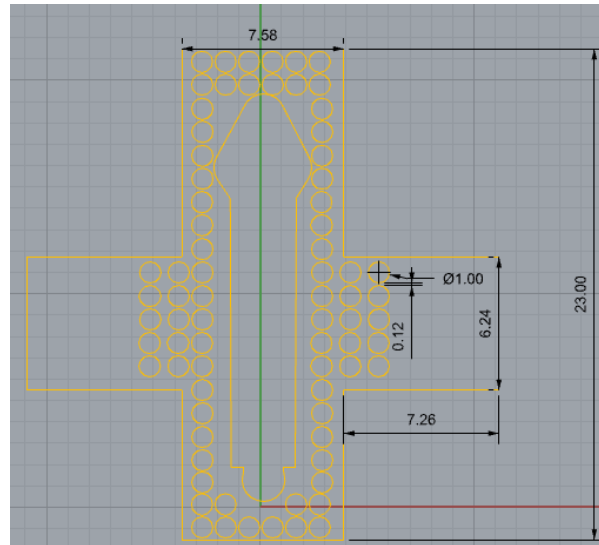


Figure 6-11 CAD design realized for Kapton laser ablation. The design has been developed using the previous bottom design (from Beatrice Minervini's thesis[32]).

The CAD has been used for Kapton tape's cut, but the tape is so thin that, after the laser ablation, the detachment from the slider has turned out to be too difficult. As result, the cut tape broke in more points; the left Kapton tape has been bonded using the plasma bonding technique between top and bottom layers, as shown in the fig. 6-12.

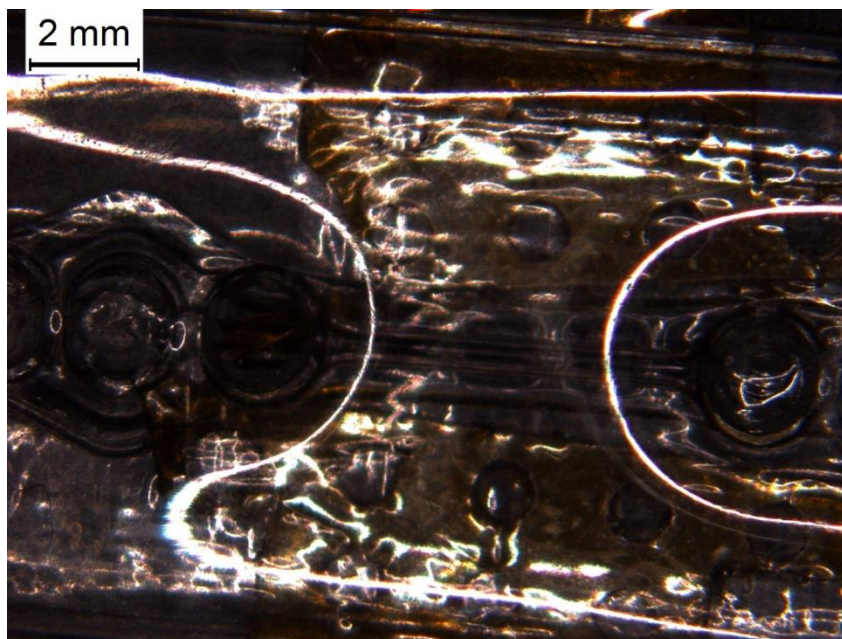


Figure 6-12 Kapton tape between top and bottom layer.

This idea has been left because of the difficulties encountered during the detachment, and because of the low-quality results of microfluidic test, there have been many leakages due to the folded edges caused by the cut Kapton breaking points.